INAUGURAL DISSERTATION
for
obtaining the degree of doctor
from the
Combined Faculties for
Natural Sciences and Mathematics
of the
Ruprecht Karl University of
Heidelberg

submitted by
Graduate physicist Thomas Bortfeld
from Hannover

New methods for solving the
inverse problem of radiotherapy planning

Reviewer: Prof. Dr. Josef Bille

                               Priv.-Doz. (*Privatdozent* [Associate Professor]) Dr. Bernd Jähne

My girlfriend Ina

Table of Contents

I Introduction

Radiation therapy is still one of the most important forms of treatment for tumor diseases. Of all newly diseased patients, about one in two is assigned to radiation treatment. Radiotherapy is used as primary therapy, palliative or supportive to other forms of therapy (H. Kuttig in: zum Winkel 1987). Most irradiations today are performed with high-energy photons (energies greater than 1 MeV). The investigations carried out in the present work are therefore limited to this type of radiation. Furthermore, only percutaneous irradiations are considered.

The goal of radiotherapy of localized tumors is to deliver a high dose of radiation to the *target volume,* which contains the tumor. It is generally accepted doctrine that the prognosis of treatment improves if the dose in the target volume can be increased without exceeding the tolerance limit in surrounding healthy tissues and organs (Airds 1989). Through a series of technical developments in recent decades, this has been achieved in many cases. Here, the availability of high-energy photon beams through medical linear accelerators and the introduction of *conformation therapy* by Takahashi (1961) are particularly noteworthy. Furthermore, the rapid development of modern imaging techniques such as computed tomography (CT) or magnetic resonance imaging (NMR) has made it possible to determine the target volume more precisely.

For more than 50 years, many tumors have been treated with standardized procedures that have proven to be particularly suitable due to long clinical experience. In many other cases, however, the radiation therapist must determine a well-suited radiation plan through time-consuming "trial and error" procedures. For this purpose, different configurations of the radiation fields with different field sizes and shapes are tried out, a dose calculation is performed in each case, the dose distributions are compared, and the best field configuration is finally selected. This process naturally becomes more complex the more complicated the irradiation technique and the greater the number of degrees of freedom. For this reason, a computer-aided determination of the irradiation parameters is desirable.

However, even with the most elaborate techniques, such as the exact adaptation of the beam fields to the projection of the target volume in today's approach to conformation therapy, adequate dose distributions cannot be achieved in all cases. Such situations exist when the cross-section of the target volume is not convex. For the treatment of arbitrarily shaped target volumes, a new technique has recently been presented independently by A. Cormack (1987) and A. Brahme (1988) in which the intensity is varied within the radiation field. It has been shown that non-convex target volumes can also be treated in this way. However, because of the enormously large number of degrees of freedom, it is in no way possible to use the conventional "trial and error" method for determining the irradiation

parameters, i.e. the intensity modulation, with this new method. The problem of automatically determining appropriate modulation profiles based on a given target dose distribution matched to the target volume is referred to as the *inverse problem* of radiotherapy planning. Chapter II/1. of this thesis deals with this subject area in more detail.

Since the introduction of modulation technology in 1987/88, methods for determining modulation profiles have been developed by a number of authors (Cormack 1987, Brahme 1988, Webb 1989, Barth 1990). However, the methods described therein are subject to significant shortcomings:

1. Strongly simplified algorithms for dose calculation are used, which do not meet the accuracy requirements of radiation therapy.

2. No optimization criteria are included in the calculations, or important medical criteria such as the special protection of certain organs at risk are not adequately taken into account.

3. So far, only slice-by-slice 2-D calculations are possible.

The aim of the present work is to develop new methods to compute the modulation profiles and thus to solve the inverse problem, which are not associated with these shortcomings.

II Methodology

1. Conformation therapy with modulated radiation fields and the inverse problem of therapy planning

In this chapter, the principle of *tumor conformal irradiation* or *conformation therapy* introduced by Takahashi (1961) is first discussed. Due to the great technical effort required for this irradiation technique, it has only become established on a larger scale at clinics in recent years. Different realizations of this technique are described, which are used in practice today.

However, in certain cases where the volume to be irradiated contains concave regions, tumor-conforming irradiation is not possible even with these currently available approaches. Here, a new approach recently presented by A. Cormack (1987) and A. Brahme (1988) seems promising, using *modulated radiation fields*. This new approach is briefly described. It is shown how the *beam modulation* is realized *in practice.*

The inverse problem of radiotherapy planning is then described. When using beam modulation techniques, this problem boils down to determining the modulation profiles. It is shown that this problem has a lot of similarity with *image reconstruction problems* known e.g. from computed tomography (CT). This similarity forms the basis for the correspondence of the methods described in Chapters II/2. and II/4. for calculating the modulation functions with calculation methods known from image processing.

1.1 Conformation therapy

The aim of any radiation treatment of tumors is to destroy the malignant cells while largely sparing or maintaining the function of normal tissues and organs. This goal can generally only be achieved to a satisfactory degree if the radiation doses required for tumor destruction are in a range in which damage to normal tissues and organs does not occur or is unlikely to occur. Holthusen clearly formulated and illustrated these boundary conditions as early as 1936 (Fig. 1.1): The further apart the two dose-response relationships (tumor destruction and tolerance exceedance), the higher the cure rate. Conversely, the cure rate decreases if tumor destruction only occurs at radiation doses that lead to a significant tolerance excess in normal tissue.
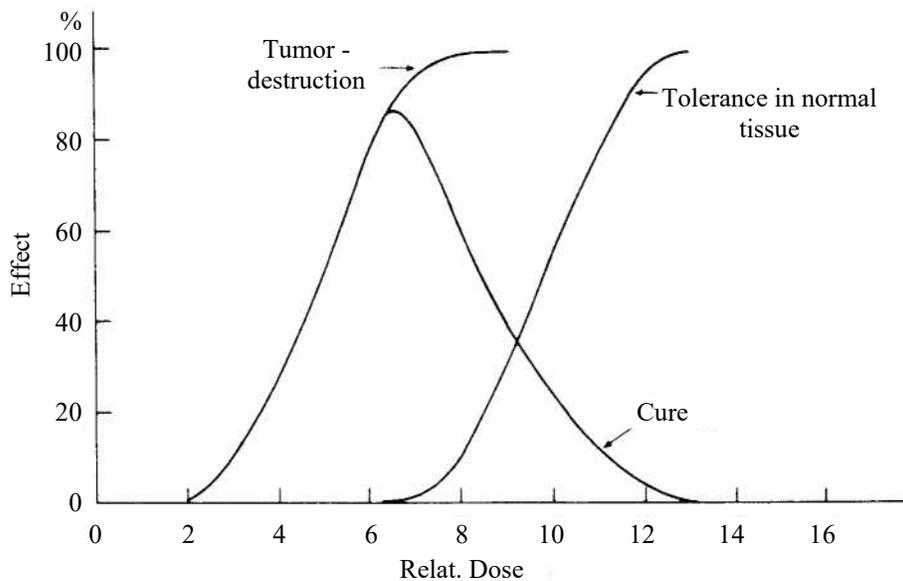
Fig. 1.1: *Tumor cure rate as a function of radiation dose, shown as a resultant between the dose dependence of tumor destruction and the tolerance of healthy tissue (Holthusen 1936).*

Now, there are a number of very radiosensitive tumors in which the curves of tumor destruction and tolerance of normal tissue shown in Figure 1.1 diverge significantly. Hodgkin's lymphoma may be mentioned as an example (Becker 1990). Such cases do not place high demands on radiation therapy and good cure rates can be achieved with relatively simple large-area irradiation techniques ("mantle fields"). In most cases, however, the conditions are not so favorable, and the two curves in Figure 1.1 lie close together or even interchange their positions, i.e. the healthy tissue reacts more sensitively to radiation than the tumor. In these cases, radiation treatment can only be carried out sensibly if suitable radiation techniques are used to ensure that the tumor is irradiated with a significantly higher dose than the healthy

tissue.

The requirement to concentrate the dose on the tumor is the starting point for the introduction of *conformational radiotherapy.* This term was coined by S. Takahashi in 1961. Today, this is understood to be a treatment technique in which the *irradiation volume* is adapted to the *target volume.* The irradiation volume is the volume in which the therapeutic dose, i.e. the dose required to destroy the malignant cells, is administered. The target volume includes, in addition to the actual tumor volume, the infiltration zones and lymphatic drainage paths to be irradiated according to medical prescription, as well as a safety margin that takes into account possible positioning errors and movements of the patient during irradiation (e.g. due to breathing).

Today, conformation therapy is usually realized with high-energy photons or electrons. As already mentioned in the introduction, this work is limited to the consideration of high-energy photons (energies > 1 MeV). The adaptation of the spatial dose distribution to the target volume is usually achieved by irradiating from several directions (multi-field technique) or with a rotating irradiator (pendulum technique). At each position of the irradiator *(gantry).* i.e. for each irradiation direction, the collimators limiting the beam are opened just as far as the projection of the target volume in this direction dictates. By superimposing the dose from different directions, the goal of conformation therapy can then be achieved. Figure 1.2 shows a schematic sketch of this. Shown is a two-dimensional section through the target volume perpendicular to the axis of rotation of the gantry. It can be seen that the irradiation volume can be adapted quite well to the target volume even with three fields.

Since its introduction in 1961, conformation therapy has been slow to gain acceptance in clinical practice due to the high technical effort involved. Today, however, this technique is established at almost all larger clinics. The irregular field shapes are realized by individually cast collimators or, as at the DKFZ (*Deutsches Krebsforschungszentrum* [German Cancer Research Center]), by so-called *multi-leaf collimators*. These collimators are composed of many narrow absorber sheets which can be shifted against each other as desired (see Fig. 1.3).

Irradiation volume

Target volume

Collimator

Tumor
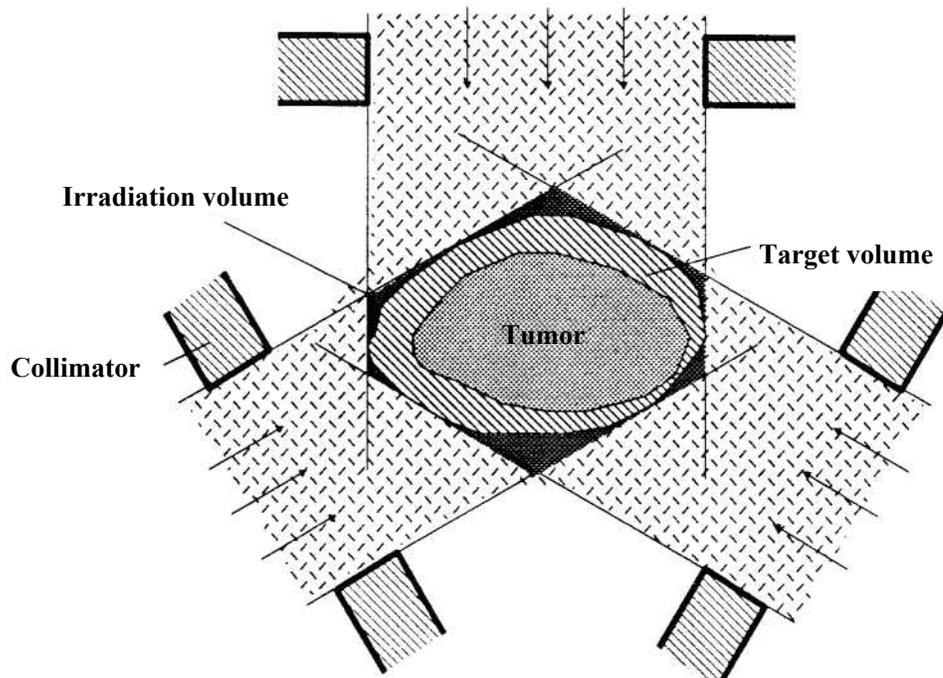
Fig. 1.2: Principle of conformation therapy realized by a three-field technique. The field boundaries are matched to the target volume boundary by suitable collimators for each irradiation direction.

Fig. 1.3: The Multi-Leaf collimator

The individual adjustment of the leaves is currently done by hand. However, an electrically powered multi-leaf collimator has been completed and is nearing clinical use (Pastyr et al. 1987).

As the above example shows, in many cases conformation therapy can be realized with only a few irregular fields. However, there are also situations in which, in principle, tumor-conforming irradiation cannot be achieved with the technique described above. They are always present when the target volume has concave indentations in planes perpendicular to the axis of rotation of the gantry. Examples are the irradiation of collum carcinoma (Morita et al. 1974) or the paraaortic lymph nodes (Nemeth and Schlegel 1989). Two-dimensional sections through these target volumes are largely horseshoe-shaped. Figure 1.4 makes it clear why the technique described above fails here. The result is always a convex irradiation volume. The marked particularly radiation-sensitive *at-risk organ* (this can be the spinal cord, for example) is also irradiated with the full therapeutic dose, and harmful side effects are therefore very likely.
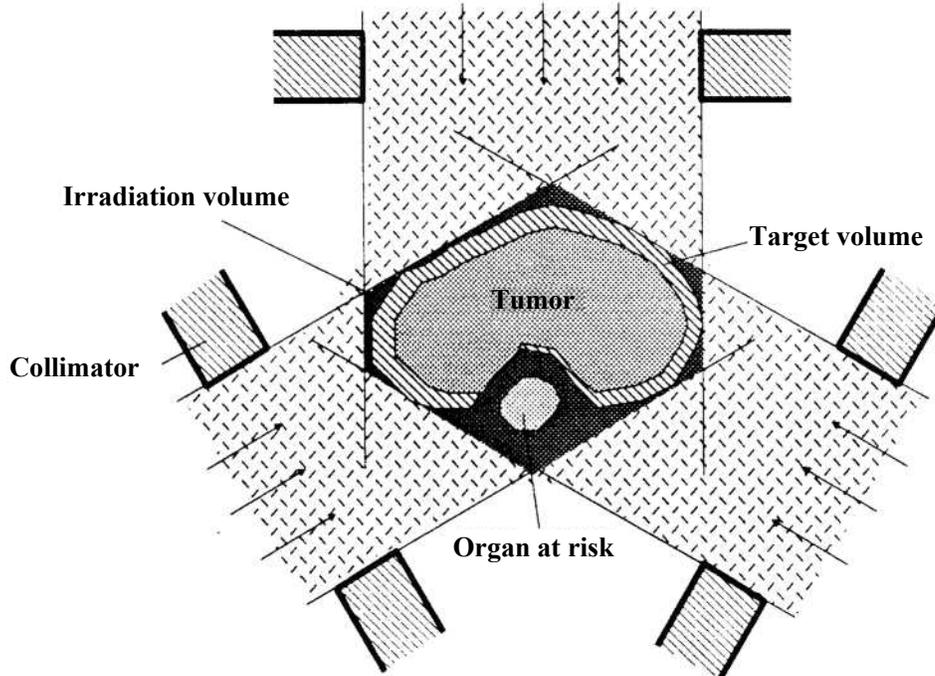
Fig. 1.4: *Irradiation of a horseshoe-shaped target volume. The irradiation volume cannot be adjusted to the target volume in this case.*

1.2   Approach with modulated fields

The conformation therapy method described in the previous section generally fails for target volumes with concave regions. For this reason, in 1987/88 a more flexible, albeit still more complex method was proposed, in which not only the shape of the beam fields is adapted to the target volume, but also the intensity within the beam is modulated (Cormack 1987, Brahme 1988). With a suitable choice of this modulation, any dose distributions can be generated, including horseshoe-shaped ones (Fig. 1.5).
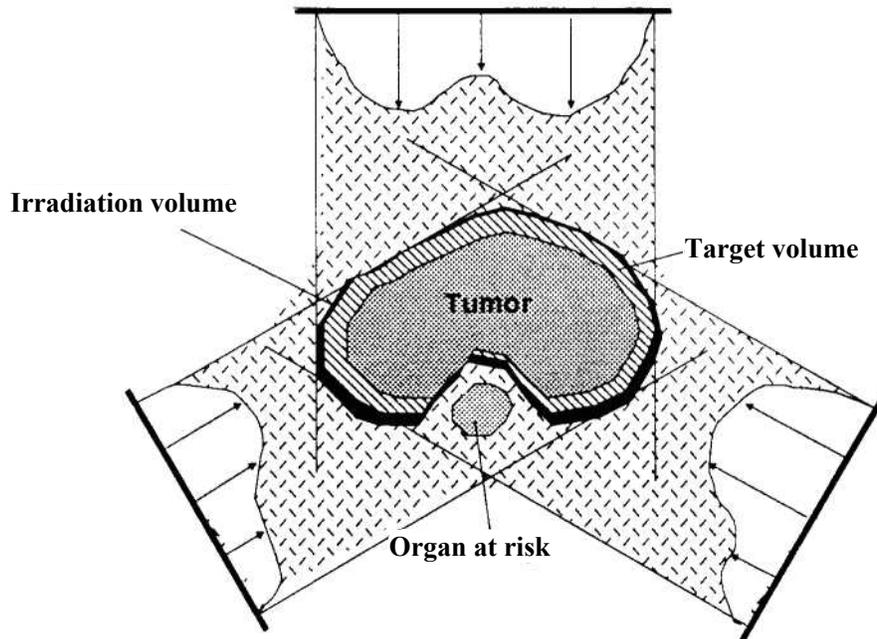
Fig. 1.5: Irradiation of the horseshoe-shaped target volume from Fig. 1.4 with modulated fields. This method allows the irradiation volume to be adjusted to the target volume.

In addition to the method introduced by Cormack and Brahme, there are a number of other techniques that can also be used to produce concave dose distributions. As important examples the *biaxial rotation* and the *tangential shell irradiation* are to be mentioned. In biaxial rotation (see e.g. H. Kuttig in: Scherer 1987), two rotations are performed around different parallel axes. The resulting dose distribution generally has the shape of an "8", but horseshoe-shaped distributions can also be obtained (Becker 1989). The tangential shell irradiation goes back to Rossmann (1955). The beam is not directed to the *isocenter,* i.e. to the axis of rotation, but is deflected laterally by a certain amount (Fig. 1.6). The resulting dose distribution has the shape of a cylindrical shell. This technique is particularly well suited for the irradiation of extensive superficial target volumes such as the thoracic wall.
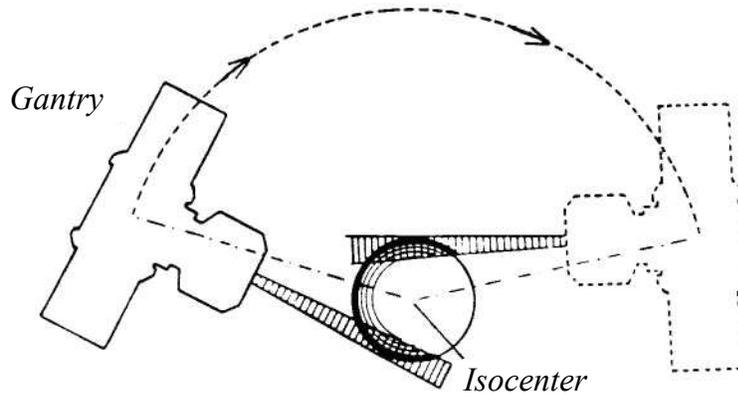
Fig. 1.6: *The principle of tangential shell irradiation*

Thus, although concavely indented irradiation volumes can also be produced by other simpler techniques, the modulation method has recently been favored by many authors (Airds 1989, Barth 1989, Kooy et al. 1989, Webb 1989, Webb 1990). The reason for this is the high flexibility that this method offers. There is justified hope that all conceivable target volumes can be treated with this method in the sense of conformation therapy. This makes the method particularly interesting for solving the so-called *inverse problem*. However, before the inverse problem is discussed in more detail, various possibilities for realizing intensity modulation will be briefly described.

1.3 Realization of the modulation

Since irradiation with intensity modulated fields is a completely new method of therapy, the techniques for intensity modulation are not yet very mature. Of the techniques described below, some are already quite well tested, while others are still in the development phase.

1.3.1   Use of compensators

Compensators are made of highly-effective radiation absorbing material with different thicknesses from point to point d. Thus, according to $I = I_0 e^{-\mu d}$ the intensity I can be adjusted, where μ is the attenuation coefficient characteristic of the absorber material and I_0 is the incident intensity. Such compensators are already widely used in clinics to compensate for inhomogeneities, which explains the name "compensator" (Quast 1978). Today, compensators are usually manufactured by first cutting the desired shape into a *Styrodur [foam] mold*, which is then filled with the liquefied compensator material (alloys with a low melting point are therefore used).

The use of compensators to modulate the fields has already been described by some authors (Bürkelbach 1990, Lind 1990). However, it can be assumed that this technique will not become established in daily clinical practice due to the extremely high personnel expenditure (approx. 7 compensators have to be manufactured per patient).

1.3.2   Use of a multi-leaf collimator

The use of the already described multi-leaf collimator for field modulation was proposed by Brahme (1988). This can be done in a number of ways. One possibility is to hold two opposing blades at a certain distance apart and to "scan" the target volume with the narrow gap thus formed at a variable speed. Thus, the intensity is not varied directly, but the irradiation time at each position of the gap is varied.

Another possibility is to superimpose different irregular field shapes formed with the multi-leaf collimator *from one irradiation direction*. However, since a large number of such superpositions are generally necessary, this technique requires a multi-leaf collimator with a very short setting time.

1.3.3   Scanning accelerator

This is perhaps the most elegant method of realizing modulated radiation fields; however, it is also the furthest from realization. First drafts for the construction of such a scanning accelerator are available (Brahme 1987). The electron beam generated in the accelerator must therefore be deflected by two magnets, similar to picture tubes, before it hits the target, where the photon beam is generated by bremsstrahlung.

1.4   The inverse problem of radiotherapy planning

The inverse problem of radiotherapy planning is understood as the task of directly calculating the required parameters of the irradiation based on the specification of a target dose distribution in the patient (Goitein 1990). This problem is not to be confused with well-known problems from mathematics, such as the inverse problem of the calculus of variations. Rather, the name "inverse problem" is explained in radiotherapy planning as follows: The process of radiotherapy planning today usually consists of the radiotherapist specifying the parameters of the irradiation, such as beam directions, apertures, etc., and then simulating the irradiation on the computer. The resulting dose distribution is then compared with the target dose distribution. In general, corrections to dose distributions will be required. Consequently, the radiotherapist must change the irradiation parameters accordingly and perform a simulation again. This process is carried out interactively until the dose distribution meets the requirements demanded by the radiation therapist. Conventional computer programs for radiotherapy planning are therefore designed to simulate radiation treatment. The essential component of these programs is an algorithm that calculates the dose resulting in the patient depending on the irradiation parameters. In the case of the inverse problem, the exact opposite approach must be taken.

Although the name "inverse problem" was coined only recently (Barth 1990, Goitein 1990), there are a number of older publications dealing with similar problems (Hope et al. 1967, Legras et al. 1986, McDonald and Rubin 1977, Redpath et al. 1976, Starkschall 1984). However, the approaches described there have not been able to establish themselves in practice. In these studies, only a few irradiation parameters are considered - mostly only the weighting factors of the individual fields - which, moreover, have only a minor influence on the shape of the dose distribution. In no way can arbitrary dose distribution shapes be generated in this way. It is rather a matter of modifying an already given set of parameters to improve the dose distributions.

Only with the introduction of modulation technology - due to the enormous increase in the number of degrees of freedom, i.e. the irradiation parameters - does a solution to the inverse problem seem to have become possible and feasible. However, it must be recognized that the dose distribution described by many authors as ideal, i.e., a constant dose value in the target volume sufficient to destroy the tumor and no dose outside the target volume, cannot be achieved even with this technique (Goitein 1990). This would require negative beam intensities and is therefore impossible for physical reasons. This relationship will be elaborated in the following chapters. Thus, since the ideal dose distribution cannot be achieved, the inverse problem in the present work is conceived as an optimization problem according to a proposal by Goitein (1990). It attempts to come as close as possible to the goal of ideal distribution according to certain criteria.

In the modulation technique, the irradiation parameters to be determined are the irradiation directions and the modulation profiles for each direction. The energy spectrum is usually determined by the type of accelerator used. With respect to the directions of irradiation, it has been shown that generally good results can be obtained with uniformly distributed beams in the angular range 0 - 2π (Webb 1989). Here, however, further investigations are necessary, which, however, shall not be the subject of the present work. Thus, this work is limited to the determination of the modulation profiles. The inverse problem can now be specified as follows:

The inverse problem of radiation therapy planning for modulated fields is the task of calculating the modulation profiles in such a way that an optimal conformation therapy can be realized with it according to given criteria.

1.5   Comparison of the inverse problem with image reconstruction problems

The problem of determining modulation profiles in conformation therapy has much in common with the problem of reconstructing an image from a series of projections taken at different angles, such as occurs in computed tomography (CT). The 2-D modulation profiles in conformation therapy correspond to the 2-D projection images in CT and the 3-D dose distribution corresponds to the 3-D density distribution in the patient (Fig. 1.7).

The main task in CT is to reconstruct the 3-D density distribution in the patient, i.e. the image, from the measured 2-D projections, so that pseudo-projections made in the computer match the measured projections. This is in fact the mirrored version of the inverse problem of treatment planning, which consists of determining the 2-D modulation functions from the given 3-D target dose distribution in such a way that the resulting 3-D dose distribution in the patient matches the given distribution as closely as possible. This similarity forms the basis for the transfer of methods from CT to conformation therapy planning performed in the present work.

Computer tomography Projection

Conformation therapy

Intensity
modulation

Radiation
source

Detectors

Radiation
source

Target
volume
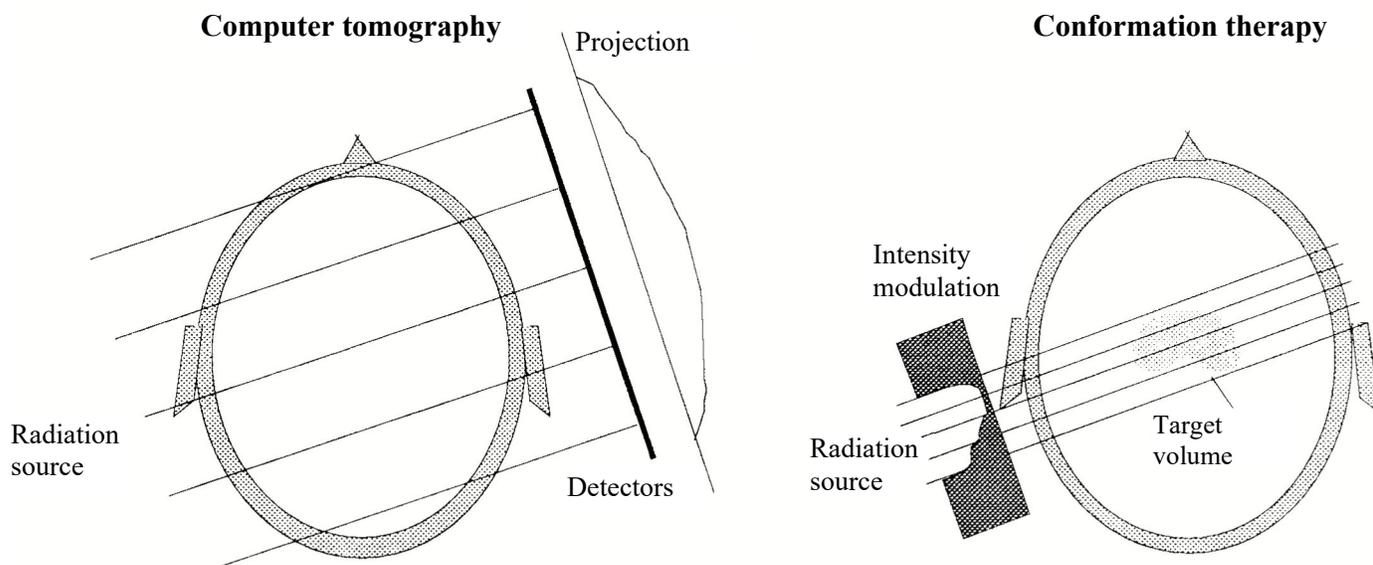
Fig. 1.7 Schematic sketch comparing computed tomography and conformation therapy with modulated fields for a 2-D slice. You have to think of the representation as being extended perpendicular to the plane of the paper, so that the projections and modulation profiles become two-dimensional and the target volume is a true 3-D volume. The beam geometry is assumed to be parallel. The modulation is indicated by a compensator.

The similarity between CT and conformation therapy with modulated fields has been recognized in a number of recent papers and notes (Brahme 1988, Webb 1989, see also Webb 1990). However, the methods proposed by these authors to calculate the modulation profiles are different from those commonly used in CT.

2. Approximate solution of the inverse problem based on a highly simplified dose calculation

In this chapter, a new direct, i.e. non-iterative, method for determining modulation profiles is described. It is based on the method of *filtered back projection,* which is widely used in computed tomography. First, however, the most important approach known from the literature for the direct determination of profiles is briefly presented (Brahme 1988). It is based on a slice-by-slice two-dimensional deconvolution of the 3-D target dose distribution with a point irradiation function. This approach is justified if the irradiation is carried out with very many (in principle infinitely many) fields from different directions. In practice, however, one must limit oneself to a few directions, and in this case the Brahme approach presents some problems. These include the non-existent location invariance of the point radiation function, the zeros of its Fourier transform, and the lack of optimization criteria.

The similarity of conformation therapy with computed tomography (see II/1.) suggests that the computational methods known there should also be applied to conformation therapy. In the second section of this chapter, the method of *filtered backprojection* is examined for this purpose. First, we justify in more detail why this method, which should better be called *filtered projection* in conformation therapy, can be usefully employed in this new application. The determination of the filter function is described with special consideration of the boundary conditions in conformation therapy (including the small number of fields). Although, in contrast to CT, for physical reasons no negative values of the *filtered* projections, i.e. the modulation profiles, can be realized, the method yields quite good results. Particularly advantageous is the low time requirement, since, in contrast to Brahme's method, only 1-D filtering or convolutions have to be performed. The filtered projection is therefore preferable to the Brahme approach.

However, the filtered projection also does not take into account any medically justified optimization criteria, and is also based on a highly simplified dose calculation. Therefore, the modulation profiles found with this method can only be considered as a first approximation to solve the inverse problem, and further optimization is needed, which is described in II/4.

2.1   An approach by A. Brahme

In 1988, a method for the non-iterative computation of modulation profiles was presented by A. Brahme, which is not restricted to the simplest geometries of the target volume, as the methods known until then (Cormack 1987). The principle is to first determine an adequate irradiation technique for a point-shaped target volume. This is, for example, a rotational irradiation with a narrow *needle beam.* The resulting dose distribution, which in this case is confined to a plane perpendicular to the axis of rotation, is called the point irradiation dose distribution ("point irradiation function") $\delta_p(\mathbf{r})$. It has similarities with the "point spread function", which is known from image processing. The irradiation of extended target volumes is realized by a weighted superposition of such point irradiations.

The mathematical problem consists in a calculation of the spatial density function $\varphi(\mathbf{r})$ of the point irradiances. If this function is known, the total dose distribution in the different slices A' of the target volume is obtained by a superposition of the $\delta_p(\mathbf{r})$ according to the following convolution integral:

$$D(\mathbf{r}) = \iint_{A'} \varphi(\mathbf{r}')\delta_p(\mathbf{r} - \mathbf{r}')dA'$$

For a given target dose distribution $D(\mathbf{r})$ this equation must be solved for $\varphi(\mathbf{r})$. To do this, a Fourier transform is performed, taking advantage of the fact that a convolution integral thereby becomes a multiplication (Brigham 1987):

$$\vec{D}(\mathbf{s}) = \tilde{\varphi}(\mathbf{s}) \cdot \tilde{\delta}_p(\mathbf{s})$$

Assuming that $\tilde{\delta}_p(\mathbf{s})$ has no zeros, $\varphi(\mathbf{r})$ can then be determined by dividing by $\tilde{\delta}_p(\mathbf{s})$ and then transforming back. Finally, the modulation profiles for each irradiation direction are obtained by projections of $\varphi(\mathbf{r})$ at the corresponding angles. If negative values occur, these are "truncated", i.e. the modulation profiles are set to zero at these points.

In practice, this approach of Brahme is associated with some difficulties. First of all, it is not yet possible to perform rotational irradiations with dynamically variable modulation. At present, only multi-field techniques can be implemented.
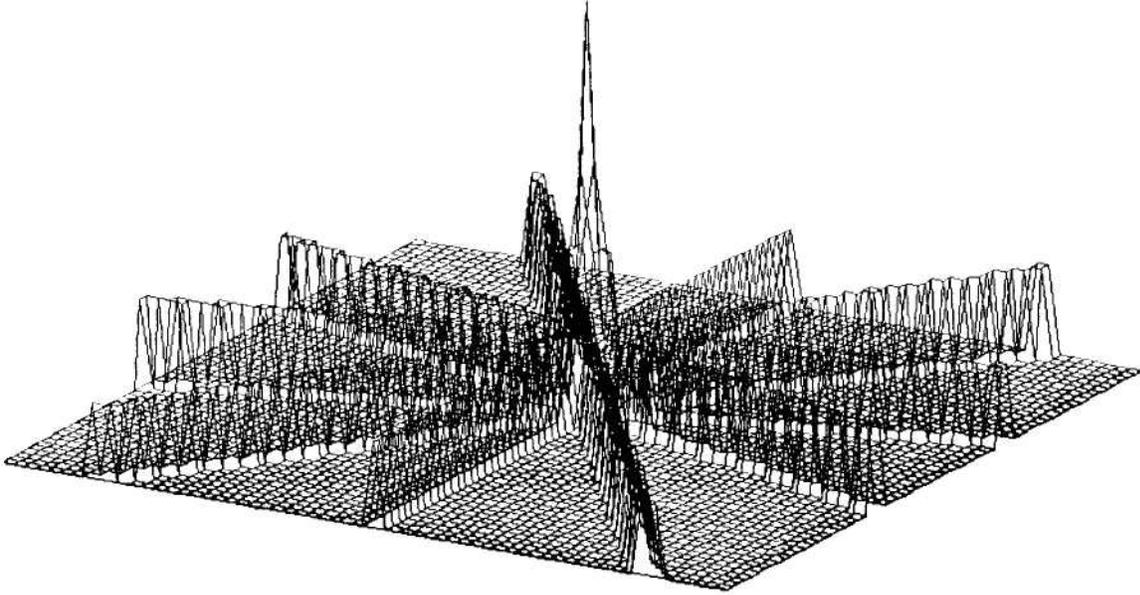
Fig. 2.1: *The point irradiation function $\delta_p(\mathbf{r})$ for 5 directions of irradiation*

The point irradiation function $\delta_{\mathbf{p}}(\mathbf{r})$ results in this case from superposition of the needle beam depth dose curves for the respective irradiation directions (Bürkelbach 1990). Figure 2.1 shows $\delta_p(\mathbf{r})$ for an irradiation with 5 fields.

Now, implicit in the convolution approach is the assumption that $\delta_p(\mathbf{r})$ is locationally invariant. This is fulfilled to a good approximation for rotational irradiations (Brahme 1988); however, when relatively few fields are used, errors can arise due to the different relative positions of the skin entry points as well as due to inhomogeneities. The assumption of spatial invariance is equivalent to disregarding beam attenuation.

Another major problem related to the small number of fields are zeros of $\tilde{\delta}_p(\mathbf{s})$, which, in contrast to rotational irradiations, occur already at relatively small frequencies $\|s\|$. The deconvolution in the frequency domain for the determination of $\varphi(\mathbf{r})$ can therefore only be performed in a rough approximation, neglecting a large part of the frequency spectrum. The optimization criteria demanded by Goitein (1990) have not yet been included in the calculation.

2.2 Filtered projection

2.2.1 Filtered projection and filtered rear projection

Due to the mirror image correspondence of the image reconstruction problem in computed tomography with the inverse problem of conformation therapy (see II/1.5), it is obvious to apply the methods already established in CT also in conformation therapy. In CT, there are two main reconstruction methods: *filtered backprojection* and *iterative reconstruction* (Brooks and Di Chiro 1976). Both methods are investigated in this paper. This section discusses the filtered back projection. This method should be referred to as *filtered projection* with respect to conformation therapy, because the projections (i.e. the modulation profiles) are calculated and not the superposition of the back projections (i.e. the image), as in CT.

In order to justify the applicability of the filtered projection method in conformation therapy, some properties of high-energy photon beams must first be anticipated. More detailed explanations on this subject are given in II/3. The photon beams used in conformation therapy today are usually generated by linearly accelerated electrons with an energy of ≥ 6 MeV in a bremsstrahlung process. Consequently, the photons have similar high energies and thus they acquire the following properties:

1. The attenuation coefficient in the tissue is very small (≤ 0.05/cm). This makes the depth dose profile relatively flat (see e.g. Fig. 3.2). (The so-called "build-up effect" (see II/3.1) is not taken into account).
2. The beam expansion caused by scattering is small (Webb 1989).
3. The dependence of the dose distribution on tissue inhomogeneities is generally relatively weak.

As a consequence of these properties, the dose distribution of a needle beam is very narrow. The attenuation can be neglected to a rough approximation in a relatively small area such as the target volume. Similarly, inhomogeneities are initially disregarded. Thus, the irradiation of a tissue with a modulated radiation field can be understood as a "smearing" of the intensity values along the beam direction. This is basically the same process as back projection in CT, where this "smearing" is applied to the filtered projections in the computer to get the image.

Image reconstruction
(filtered back projection)

Conformation therapy
(filtered projection)

**Density distribution
in the tissue**

**set of prescribed
2-D dose distribution slices**

**Slice-by-slice
projection on lines
(comp. tomograph)**

**Projection on lines at
different angles**

1-D filtering

1-D filtering

**Slice-by-slice
projection**

**Irradiation with
modulated fields**

Set of 2-D slice images

**3-D dose distribution in
tissue**
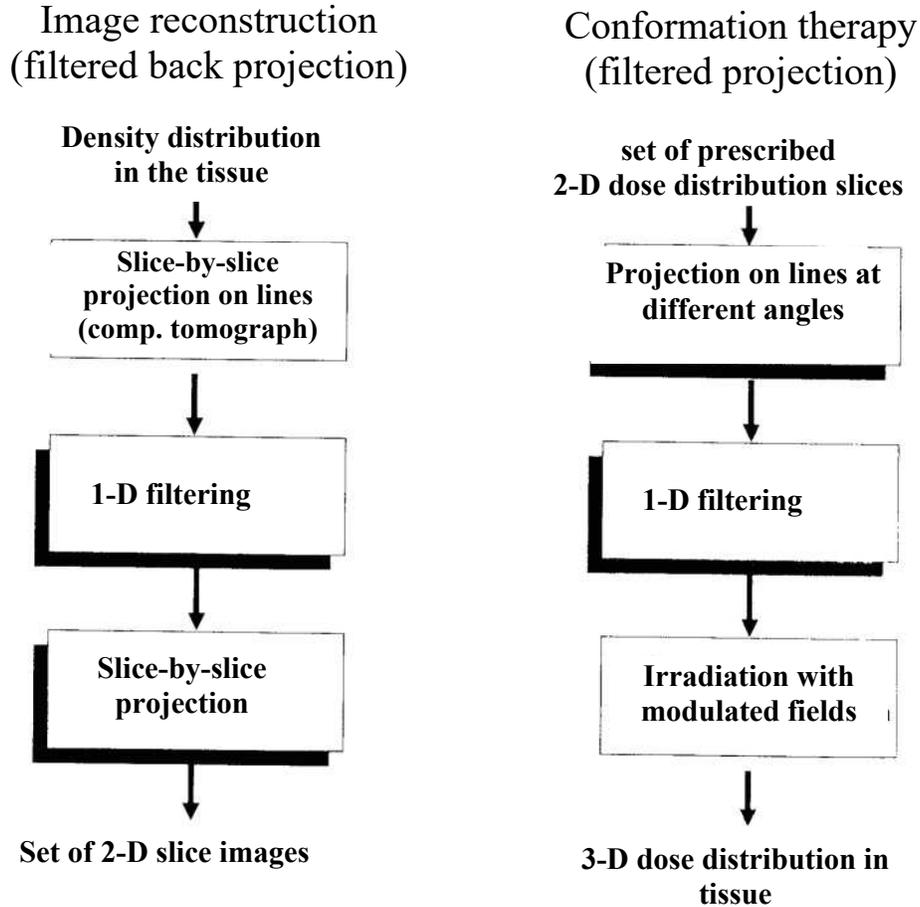
Fig. 2.2: *Comparison of the main processes of image reconstruction by filtered back projection and the corresponding processes in conformation therapy.*

The next logical step is now to transfer the other processes of image reconstruction to conformation therapy. Figure 2.2 shows an overview of the corresponding steps. Operations that are performed in the computer are shown with shadows. It was shown that irradiation with modulated fields is equivalent to CT back projection. The projection performed in the computer tomograph can be easily simulated in the case of conformation therapy. The remaining question is: Which filter function has to be chosen to achieve good results in conformation therapy? Before answering this question, we first briefly explain why filtering must be performed, and outline the derivation of the filter function in image reconstruction.

2.2.2   Determination of filter function

The filtered back projection method was first used in radio astronomy by Bracewell and Riddle (1967). It is based on the well-known *projection theorem* (Rosenfeld and Kak 1982): The 2-D Fourier transform of a 2-D function on a straight line at angle ϑ through the origin of frequency domain is identical to the 1-D Fourier transform of the projection of the 2-D function on a straight line at the same angle. The process of back-projection (irradiation) is now equivalent to "filling up" the frequency domain by superimposing such original lines at different angles. However, this method overemphasizes the small frequencies, since more straight lines contribute to small frequencies than to large ones. This results in a strongly low-pass filtered function. To avoid this, the projections must be filtered with a high-pass filter before the rear projection. The exact derivation of this fact is described in detail in the literature (see e.g. Rosenfeld and Kak 1982, Jähne 1989) and will not be reproduced here.

   The theory concludes that the filter function in frequency domain is simply given by the absolute value of the spatial frequency $|s|$ if infinitely many projections (directions of irradiation) are known. This is, of course, a hypothetical case. In the presence of a finite number of projections, this filter must be limited by an additional low-pass filter, i.e. the resolution is thereby limited. The fact that only a few directions of irradiation are practicable in conformation therapy means that the filter function must be limited even at very low frequencies. The following discrete filter function is used:

$$H(k) = \begin{cases} |k| \exp\left(-k^4/k_0^4\right) & \text{for } k \neq 0 \\ \quad 1 & \text{for } k = 0, \end{cases}$$

where k is the discrete frequency variable related to the spatial frequency s and to the linear expansion in the spatial domain w via $s = k/w$. The value of k_0 determines the cut-off frequency. It depends on the number N of directions of irradiation:

$$k_0 \approx N\frac{2}{\pi}$$

(Brooks and Di Chiro 1976). It has been shown that better results can be obtained by lowering the filter function to zero with the low-pass $\exp\left(-k^4/k_0^4\right)$ "soft" than by simply "truncating" it at the value given by k_0 by a rectangular low-pass. Similar results are also known from CT, where *Hanning windows* are used for this purpose (Chesler and Riederer 1975).

   The value 1 for $H(k = 0)$ takes into account some peculiarities of conformation therapy. The mean value of the projections is thus obtained. In spatial space, this corresponds to the addition of a constant to the projections, i.e. fringes of constant intensity are superimposed from each direction. This takes into

account the fact that no negative intensities can be realized. Furthermore, the relative homogeneity of the dose in the target volume is improved in this way, although this is naturally at the expense of the dose in the surrounding normal tissue. The value 1 was empirically determined as the most favorable value.
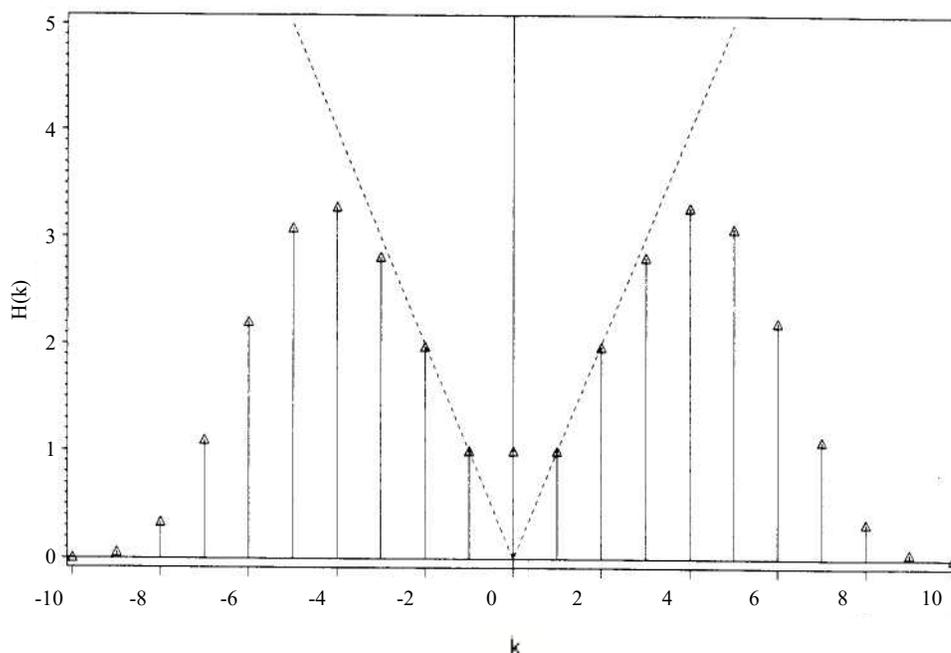
Fig. 2.3: *The filter function in frequency domain. The dashed curve is the |k| function. The cutoff frequency is $k_0 = 6$.*

Figure 2.3 shows the filter function $H(k)$ for the cut-off frequency $k_0 = 6$. This function is used with 9 fields uniformly distributed in the angular range 0-2π. If the directions of irradiation are not evenly distributed, the cut-off frequency must be determined in each case as a function of the local "field density". It should also be mentioned that filtering makes no sense with less than 5 fields, because k_0 becomes too small.

2.2.3   Influence of non-negativity

After filtering, the modulation profiles are obtained by truncating - as in the Brahme approach - negative values of the filtered projections that are still present despite the addition of the stripes (see above). The question arises as to whether the advantage of filtering is not nullified in this way. Figure 2.4 will be used to answer this question.

In the upper part of this plot, the modulation profiles were determined by simple projection of the horseshoe-shaped target dose distribution. The resulting dose distribution, shown in the form of isodose lines, does not show good agreement with the target dose distribution, i.e. with the target volume. In the lower part, the modulation profiles were obtained by filtering the projections with the filter function described above (Fig. 2.3). Negative values are already truncated in the display. However, it can be seen that most profiles have positive values in areas where the projections (see upper part) are not equal to zero. Only 3 of the 9 profiles indicate small areas of (truncated) negative values (arrows). These have a minor influence on the overall dose distribution. The dose distribution follows the shape of the target volume in terms of conformation therapy much better than that resulting from simple projection. The same is true for other target volumes studied so far.

Negative values of the filtered projections occur only where the projections have extended areas with large gradients. If the projections have a relatively flat course, this also applies to the filtered projections. These properties of the filtered profiles are caused by the filter function having both low-pass and band-pass behavior.

Larger areas of negative values of the filtered projections occur in the area not shown to the side of the field edges. However, these have *no influence on the dose distribution within* the target volume. On the contrary, they have the effect that the dose in healthy tissue in the vicinity of the target volume cannot be reduced to zero. This would only be possible if dose could be subtracted at these points, i.e. if negative intensities could be realized. For this reason, percutaneous radiotherapy always exerts a burden on healthy tissue; the aim can only be to reduce this burden to a tolerable level.

Here lies an essential difference between CT and conformation therapy: In CT, body regions can be reconstructed with zero density; in contrast, conformation therapy with modulated fields always results in positive dose values.
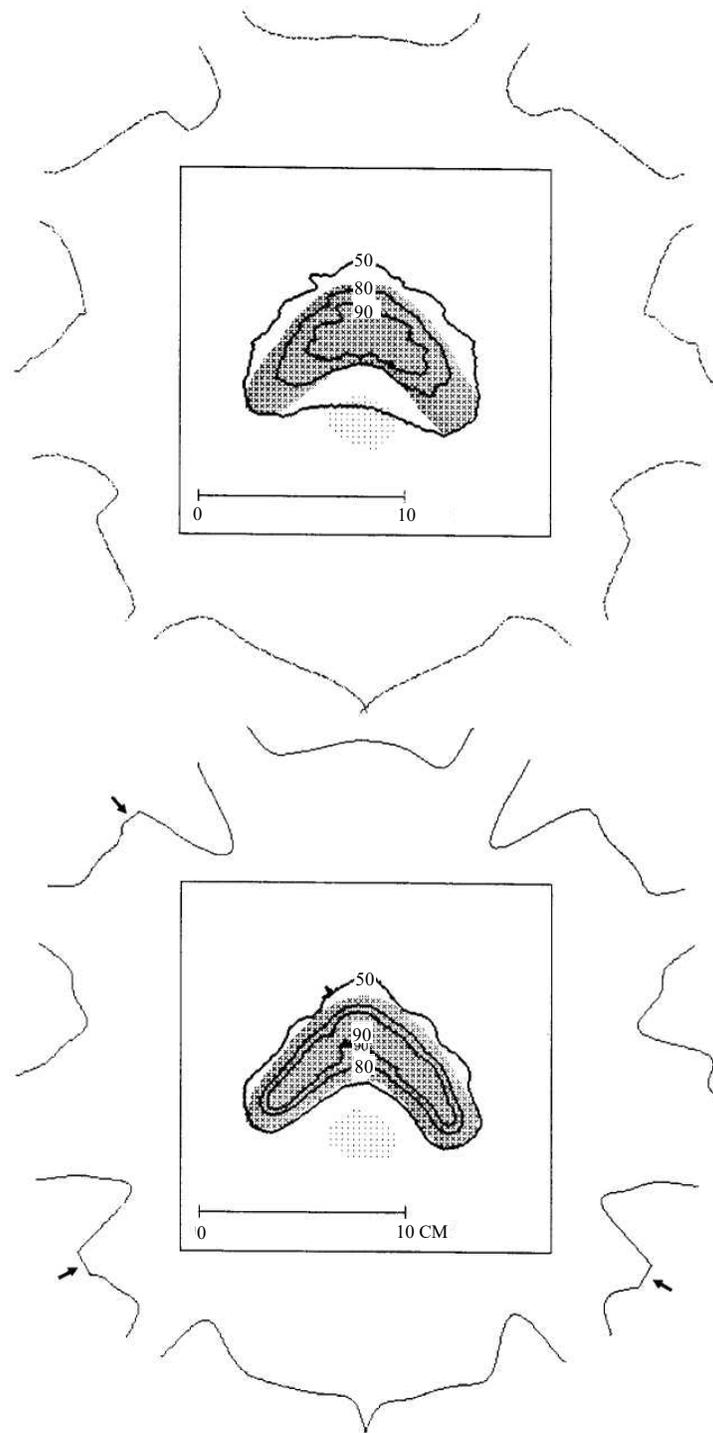
Fig. 2.4: *Dose distribution and modulation profiles for an irradiation with 9 fields (2-D slice). The target volume is represented by crosses, and the dots represent an organ at risk. Isodose data as a percentage of the maximum dose. Modulation profiles were determined by simple projection (top) and by filtered projection (bottom).*

2.3   Comparison of the methods

It was shown that the filtered projection method can be usefully applied in conformation therapy, although no negative values of the modulation profiles can be realized. However, both Brahme's approach and the filtered projection have two major shortcomings: First, both methods are based on the assumption of a beam unattenuated in the tissue (the Brahme method implicitly, the filtered projection explicitly). Without suitable corrections, the resulting error is too large for the accuracies required in radiotherapy (see II/3.).

Equally serious is the fact that no optimization criteria are included in the calculation, with the result that the dose distributions do not meet all requirements. Thus, although the shape of the dose distribution shown in Figure 2.4 (lower part) is in good agreement with the shape of the target volume: large areas are irradiated with less than 80% of the maximum dose, which cannot be tolerated from a medical point of view. Furthermore, radiation-sensitive at-risk organs are not given special consideration.

The considerations made so far apply equally to the two methods presented. The advantage of the filtered projection over the Brahme approach is that only 1-D filtering needs to be performed. This allows the modulation profiles to be determined much more quickly.

Because of the shortcomings described above, the filtered projection method is used in this paper only to determine a first approximation for the modulation profiles. These profiles are used as initial values for an iterative optimization procedure, which is described in chapter II/4.

3. 3-D dose calculation for modulated radiation fields

In this chapter, the physical principles of the *interaction between photons and matter* are first discussed. In the range of photon energies used for therapeutic purposes, the Compton effect is predominant. Although this effect is exactly described by the Klein-Nishina formula, it is not yet possible to determine the absorbed dose in the tissue with the help of this formula for practical reasons. However, for the *accuracies* required in radiotherapy, other simplified *calculation methods* are known, each of which is briefly described and their specific advantages and disadvantages are mentioned. Finally, a *new algorithm* for dose calculation for high-energy photons is described. This allows dose calculations for the irregular fields used in conformation therapy. The modulation of the fields is taken into account in the calculation.

The algorithm is based on splitting the dose into a *primary component* and two *scattering components.* The scattering components can be approximately identified as single scattering and multiple scattering. It is shown how each of these components can be determined using, respectively, a *2-D convolution operation* and simple *ray-tracing* procedures. These methods allow dose calculations to be performed very quickly, since no time-consuming 3-D convolutions or 3-D superpositions are required. The convolution cores can be easily determined from measured tissue-to-air or tissue-to-maximum ratios.

Although the algorithm presented here is specifically designed for modulated fields, it can also be used to compute any other fields. In this respect, this chapter is independent of the others.

3.1 Physical fundamentals

The physical effect responsible for the destruction of malignant cells in radiotherapy is the ionization of matter. A measure of ionization is the radiation energy E_{abs}, absorbed by this matter when ionizing radiation passes through it. The absorbed dose, or dose D for short, is the quotient of E_{abs} and the mass of the matter irradiated (ICRU 1980). The mass dm considered should be small so that the dose at a point can be defined; on the other hand, it should be large enough so that statistical fluctuations do not play a role. The definition is:

$$D = \frac{dE_{abs}}{dm}.$$

The unit of dose is the *gray* (Gy), $1Gy = 1J/kg$.

The basis of the dose calculation for irradiations with high-energy photons are the physical principles of the interaction between photons and matter, i.e. essentially the photoelectric effect, the Compton effect and pair formation. In the range of photon energies between 1 MeV and about 20 MeV used for therapeutic purposes, the Compton effect, i.e. the inelastic scattering of photons by electrons of the atomic shells, is predominant. An incident photon gives off part of its energy $h\nu$ to an electron. The scattered photon then has the residual energy

$$h\nu' = \frac{m_0 c^2}{1 - \cos\vartheta + m_0 c^2/h\nu}.$$

Where ϑ is the scattering angle and m_0 is the rest mass of the electron. Kinetic energy is transferred to the

$$T = h\nu - h\nu' = h\nu \frac{1 - \cos\vartheta}{1 - \cos\vartheta + m_0 c^2/h\nu}$$

electron. Importantly, the ionization effects that high-energy photons cause in matter are caused virtually exclusively by secondary electrons. This is shown in the following.

A photon produces a primary ionization by striking an electron of the atomic shell in the Compton effect (for smaller energies also in the photoelectric effect). The energy of this excited secondary electron is of the same order of magnitude as the energy of the incident photon. This becomes clear from the above equation for the kinetic energy T. The maximum energy that results at the scattering angle $\vartheta = \pi$ is

$$T_{max} = \frac{h\nu}{1 + m_0 c^2/2h\nu}.$$

The secondary electron emits its energy mainly by ionization and excitation of the atoms and molecules of the absorbing medium. For electron energies in the range of 1 MeV, only about 1% of the energy is emitted in the form of bremsstrahlung (Johns and Cunningham 1983). Assuming that the electron loses

about 32 eV per ionization, a 1 MeV electron produces about 30000 ion pairs before it comes to rest in the absorbing medium. The one primary ionization is thus completely negligible compared to the large number of secondary ionizations.

The range of the secondary electrons depends on the energy of the primary photons. For 1-2 MeV photons, the range of secondary electrons is only a few mm and is therefore negligible in the field of radiotherapy. For these energies, the absorbed energy approximately coincides with the so-called *kerma*. The concept of kerma is very important in medical physics and will be briefly explained here. Kerma stands for kinetic energy released in the matter. This quantity was introduced to describe the primary interaction between photons and matter (ICRU 1980). It is to be strictly distinguished from the *absorbed dose* defined above. Figure 3.1 illustrates this situation.

The kerma has the advantage that it is easy to calculate. It is given by

$$K = \phi \frac{\mu_{en}}{\varrho} h\nu$$

where ϕ is the *photon flux* (see below) and $\frac{\mu_{en}}{\varrho}$ is the *mass absorption coefficient,* which results from the *Klein-Nishina effective cross section* (Johns and Cunningham 1983). If the dose is approximated by the kerma, the complicated consideration of electron propagation in matter is omitted and the calculation is limited to the determination of the flux of primary and scattered photons. For photon energies greater than 2 MeV, however, this approximation is no longer valid, since here the range of the electrons can be up to a few cm. In this case kerma and absorbed dose at a point in space are equal only under the condition (bremsstrahlung is disregarded) that a so-called *electron equilibrium* prevails. This means that in a small volume around the given point, the same number of electrons enter and leave by collisions.

A fundamental quantity for dose determination is the photon flux. For the *primary* photon flux the *attenuation coefficient μ* is determining.
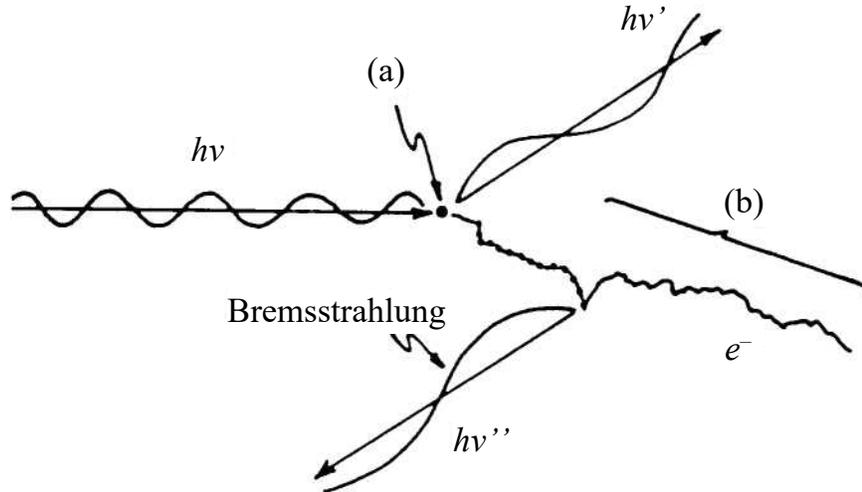
Fig. 3.1: *Schematic representation of energy transfer from photons to matter. The primary interaction takes place at point (a), with part of the primary energy hv being given to the electron as kinetic energy. The electron loses this energy along its path mainly through collisions with the atoms and molecules of absorbing matter. The energy transferred at point (a) is called kerma, along (b) is called absorbed dose. The photon with energy hv' is scattered by (a), the one with hv" is produced by bremsstrahlung. The kerma is equal in magnitude to the absorbed dose integrated via (b) plus the energy of the bremsstrahlung photons.*

This is given by the *total Klein-Nishina effective cross section σ* for the therapeutically used energies at which the Compton effect predominates:

$$\mu = \varrho_e \sigma$$

The quantity ϱ_e is the electron density of the absorbing matter, i.e. the number of electrons per unit volume. The total effective cross section σ can be calculated as follows (Evans 1955):

$$\sigma = 2\pi r_0^2 \left\{ \frac{1+\alpha}{\alpha^2} \left[\frac{2(1+\alpha)}{1+2\alpha} - \frac{1}{\alpha} \ln(1+2\alpha) \right] + \frac{1}{2\alpha} \ln(1+2\alpha) - \frac{1+3\alpha}{(1+2\alpha)^2} \right\}$$

Where r_0 is the classical electron radius and α stands for $hv/m_0 c^2$.

The primary photon flux ϕ is exponentially attenuated for a *parallel* beam as a function of depth d according to $\phi(d) = \phi_0 e^{-\mu d}$. In general, the tissue penetrated by the beam is not homogeneous. As a consequence of the electron density varying from point to point, also μ, and ϕ must be determined as follows:

3. Three-dimensional dose calculation

$$\phi(d) = \phi_0 e^{-\sigma \int_0^d \varrho_e(d')dd'}$$

The values of $\varrho_e(d')$ can be determined, for example, by CT measurements. Often these values are given relative to the electron density ϱ_{ew} of water: $\varrho_{rel} := \varrho_e/\varrho_{ew}$ (ICRU 1987). An *equivalent path length* or *radiological depth* d_{rad} is defined by

$$d_{rad}(d) = \int_0^d \varrho_{rel}(d')dd'$$

The flux ϕ is thus simply calculated to be

$$\phi(d) = \phi_0 e^{-\mu_w d_{rad}}$$

Since the beams used in practice are always divergent, an additional attenuation of the flux according to the square of the distance from the source has to be considered (Johns and Cunningham 1983).

In addition to the primary photon flux, the flux of scattered photons must be taken into account when calculating the dose. The scattering behavior of the matter is determined by the *differential Klein-Nishina effective cross section* and can thus in principle be calculated exactly for any given radiation field. However, since the scattered photons come from all spatial directions and since multiple scattering processes also occur, the calculation is extremely difficult. Complicated volume integrations have to be performed, and only in the very simplest cases can solutions be found in closed form. For this reason, only simplified methods for calculating dispersion are used in practice today. In the determination of the total dose, such simplifications do not play too great a role, because the dose fraction caused by scattering is generally much smaller than the primary fraction at the energies considered.

Fig. 3.2 shows measured depth dose curves for different photon energies. It should be borne in mind that these are all *energy spectra*. For the two bremsstrahlung spectra, the mean photon energy is well below the reported electron energy. It can be seen that the higher the energy, the flatter the curves. This is due to the energy dependence of the mean attenuation coefficients. The curves of the higher energies reach their maximum only at a certain depth below the entry point *(d = 0)*. The reason for this is that there is no electron equilibrium behind the entry point.
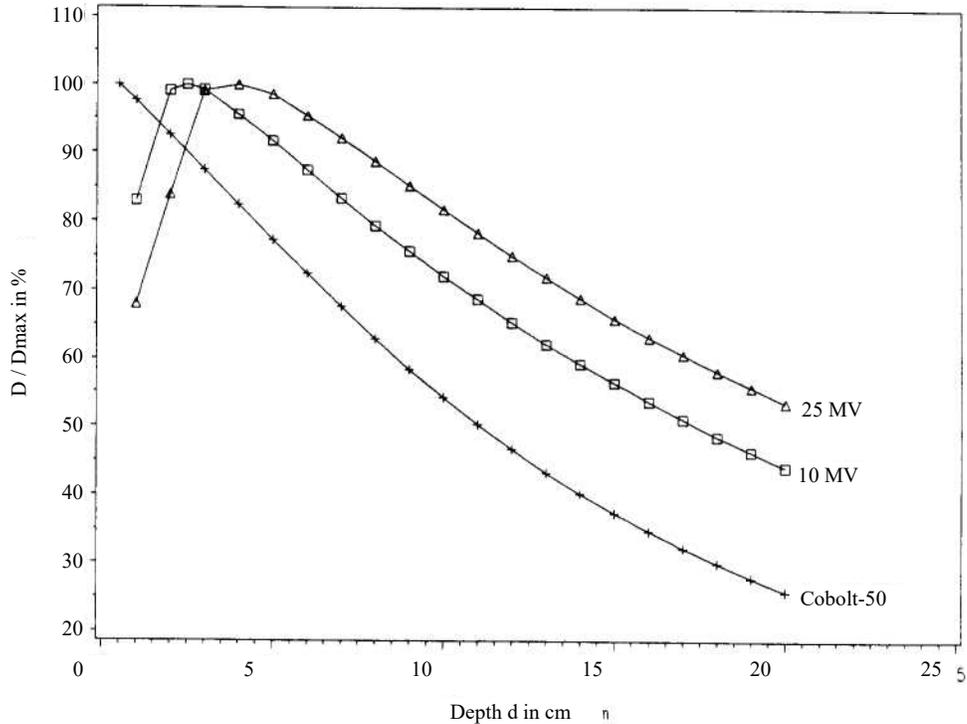
Fig. 3.2: *Relative depth dose profiles (with respect to the maximum dose) for different photon energies measured in a water phantom. The distance source-entry point is 1m each, the field size is $6 \cdot 6$ cm^2. "10 MV" or "25 MV" stands for bremsstrahlung spectra generated from braked electron beams with 10 MeV or 25 MeV energy, respectively, in medical linear accelerators. Cobalt-60 (^{60}Co) is a radioactive compound that, when decaying to ^{60}Ni, emits two lines with energies of 1.17 MeV and 1.33 MeV. This preparation is still used today in many places for radiotherapy. Data are taken from (Johns and Cunningham 1983).*

This equilibrium only builds up with increasing depth. It's called a *build-up effect.* The build-up effect is of great therapeutic benefit, as it avoids high doses in the area of the patient's skin and consequently no skin burns occur during the therapy of deep-seated tumors. In the case of ^{60}Co radiation, this effect is not yet visibly pronounced because the range of the secondary electrons is smaller (see above).

3.2   Accuracy requirements in radiotherapy

The accuracy requirements for dose determination in radiotherapy are based on the degree of dependence of the clinical/biological radiation effect on the dose. The effect is divided into the probability of tumor destruction (tumor control probability) and the probability of complications in healthy tissues and organs (see also Chapter II/1.). Confirmed results regarding the dose change that can just be clinically perceived

are hardly to be found in the literature. However, most radiation therapists have subjective views on this point based on experience.

A summary of the few results can be found in ICRU (International Commission on Radiation Units and Measurements) Report 24 (1976). It mentions some extreme cases where already a reduction of the tumor dose by only 10 % causes a reduction of the tumor control probability from 70 % to 10 %. In most cases, however, dependence appears to be less and changes in dose of less than 5% are usually not clinically relevant. The dependence of the effect on normal tissues on the dose is generally even less pronounced.

Based on the investigations performed up to 1976, an accuracy of ± 5 % for the dose determination is required in (ICRU 1976). However, due to the very small number of cases considered, this value cannot be considered as certain. According to more recent studies, even greater accuracy seems to be required.

3.3 Conventional methods for dose calculation

When calculating the dose, a compromise must always be made between the requirements of high accuracy and short calculation time. The three most important methods known today are briefly described here. They are ordered by increasing accuracy and therefore also by increasing calculation time. So far, only the first method is used in daily clinical practice. The accuracy requirements of radiotherapy are already met by this method in many simple cases. In more complicated cases, however, the accuracy is not sufficient. Here, the other, much more time-consuming procedures are promising.

3.3.1 Empirical methods

Most of the dose calculation algorithms used in radiotherapy planning today are based on a set of measured depth dose profiles and dose transverse distributions for different field shapes and sizes. In some cases these data are approximated by simple functions (Schoknecht 1968), so that the storage of the large amounts of data can be omitted. The computation essentially involves proper access to these data and interpolations (Schlegel et al. 1984), as well as some correction procedures.

Measurements of dose levels are generally performed in a water phantom with the beam incident vertically. In order to adequately transfer these values to the tissue, a number of corrections are necessary. This includes inhomogeneity corrections, corrections with respect to unmeasured, irregularly shaped or

modulated fields, consideration of obliquely incident rays, etc.. Consideration of tissue inhomogeneities is most often approached through the concept of radiographic depth. This concept, as stated above, is strictly valid only for the primary photon flux. When extended to the dose, this provides a source of error. Modulations of the fields are calculated by simply multiplying the measured cross profiles by the corresponding value of the modulation profiles. However, the scattering behavior changed by the modulation is not taken into account. The relative position of the skin entry points, which varies depending on the direction of irradiation and the course of the skin surface, is taken into account by a corresponding shift in the depth dose curves.

There are plenty of more elaborate correction methods that are not subject to such large errors (ICRU 1987). However, these are again so time-consuming that they have no advantage in this respect over the more exact methods described below.

3.3.2   Physical computation models

These methods do not require any measurements. The calculation is based solely on the physical principles of the interactions between ionizing radiation and matter (see 3.1). However, due to the complexity of the problem, this requires a number of approximations. The best-known methods of this type are the *convolution* (Mackie et al. 1985, Boyer and Mok 1985). The dose is then calculated by the following convolution integral

$$D(\mathbf{r}) = \iiint_{V'} \phi(\mathbf{r}')k(\mathbf{r} - \mathbf{r}')d\mathbf{V}'$$

Here, $k(\mathbf{r}) = k_e(\mathbf{r})+k_s(\mathbf{r})+k_{ms}(\mathbf{r})$ is a convolution kernel that accounts for electron propagation k_e, scattering photon propagation k_s and multiple scattering k_{ms}. These kernels can be determined e.g. with the yet to be described *Monte Carlo methods*. In this way, very accurate dose calculations are possible for arbitrarily shaped and modulated fields: Only the primary photon flux has to be determined (see 3.1), and the dose is then obtained after performing the integration. The very time-consuming calculation of the convolution integral can be accelerated according to the *convolution theorem* (Brigham 1987) via the fast Fourier transform.

Problems arise, however, when inhomogeneities have to be taken into account. Indeed, it is implicitly assumed that the kernels k are locationally invariant. However, this is only the case with homogeneous matter. There are approaches to account for inhomogeneities by scaling the kernels (Mackie et al 1985); however, then the integral can no longer be solved via the Fourier transform, and the execution times become prohibitive on the computational facilities available today.

3.3.3 Physically exact methods (Monte Carlo)

The only method that can be described as physically exact is based on the *Monte Carlo method* (see e.g. Raeside 1976). The tracks of a large number of photons are followed in the computer and the interactions with matter are simulated. At each interaction point, the type of interaction, i.e. Compton effect, photo effect or pair formation, is determined by random number generator (hence the name Monte Carlo). The random numbers are "weighted" with the known cross sections for these effects, so that at the energies considered the Compton effect strongly predominates. The direction of the secondary electrons is also determined by random number generator, weighted by the differential cross section, and the energy of the electrons is uniformly distributed up to their range. Then the scattering photons are followed in their further course.

The accuracy of this method is only limited by the number of photons considered and the density of possible interaction points. It is the only method with which inhomogeneities can be adequately treated, because the density of the tissue is exactly included in the calculations via the effective cross sections and the ranges of the secondary electrons. Naturally, this procedure requires extremely high calculation times if the statistical errors are to be kept small. Routine use in radiotherapy planning is not possible for this reason. The method is now mainly used as an alternative to measurements in the verification of simplified dose calculation procedures (Webb and Fox 1980).

3.4   3-D dose calculation by 2-D convolution and ray tracing

A new method for dose calculation is described here. Compared to the methods presented in section 3.3, it can be classified between 3.3.1 and 3.3.2 in terms of both speed and accuracy. In particular, this method is suitable to calculate the modulated fields considered in the present work with sufficient accuracy.

3.4.1   Coordinate systems

A coordinate system widely used in radiotherapy is the so-called *gantry system* (Siddon 1981). This is a right-handed rectangular coordinate system whose origin coincides with the *isocenter*. The isocenter is the point at which all the central rays intersect in the case of multi-field techniques or pendulum techniques (see Chapter II/1.). The z_g-axis points in the direction of the beam source and the y_g-axis is the axis of rotation of the gantry (Fig. 3.3).
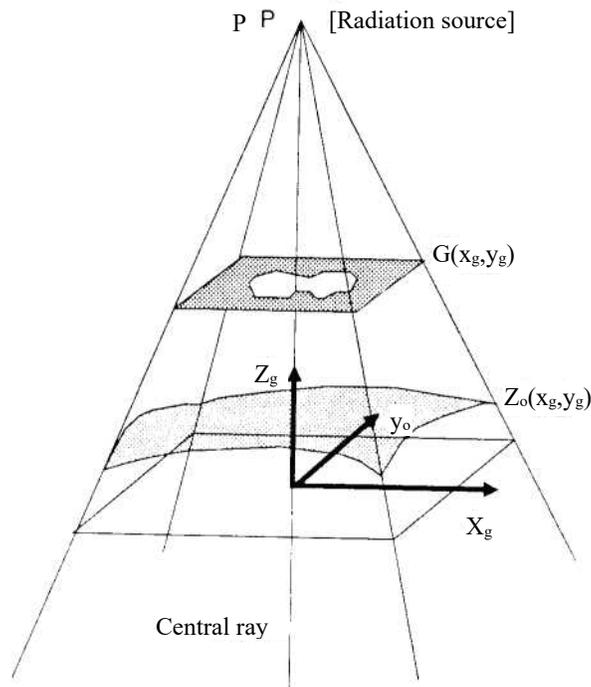
Fig. 3.3: Illustration of the gantry system

For the sake of simplicity, however, the following considerations will be based on a modified gantry system. The *z* coordinate axis of this *fan system* coincides with that of the gantry system, in

particular the central beam transforms into itself. The transformation of the coordinates is defined by the equations:

$$x = x_g \frac{P}{\sqrt{x_g^2 + y_g^2}} \arctan\left(\frac{\sqrt{x_g^2 + y_g^2}}{P - z_g}\right)$$

$$y = y_g \frac{P}{\sqrt{x_g^2 + y_g^2}} \arctan\left(\frac{\sqrt{x_g^2 + y_g^2}}{P - z_g}\right)$$

$$z = P - \sqrt{(z_g - P)^2 + x_g^2 + y_g^2}$$
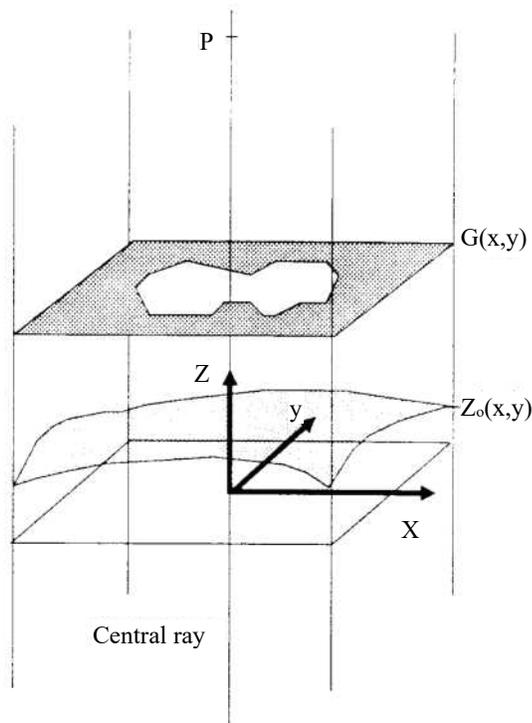
Fig. 3.4: *Illustration of the fan system*

Fig. 3.4 serves to illustrate this fan system. The transformation transforms beams directed at the beam source into parallel beams. It should also be noted that for the large distances between source and isocenter common in radiotherapy, the following simplified relationships are valid to a good approximation:

$$x = x_g \frac{P}{P - z_g}$$

$$y = y_g \frac{P}{P - z_g}$$

$$z = z_g$$

3.4.2 The variables GLV, SLV, GMV and SMV

To simplify dose determinations, the *Tissue Air Ratio* GLV ("Tissue Air Ratio", TAR) and the *Scatter Air Ratio* SLV ("Scatter Air Ratio", SAR) were introduced in radiotherapy. Since these variables are referred to in several places in this paper, they will be briefly explained here.

The GLV is defined by the quotient of the dose in a phantom at a point *(x,y,z)* with depth *d* below the surface and a reference dose at the same point without phantom, i.e. in air:

$$GLV(d.W) = \frac{D(x, y, z)}{D_{air}(x, y, z)}$$

W is the size of the field in depth *d*. The dependence *W(d)* is disregarded in the following because of the large values of *P*. A major advantage of the GLV is its independence from the source-isocenter distance *P*. The relationship between the GLV and the relative depth dose D/D_{max} is obtained by including the squared source distance and the tissue backscatter *B* to:

$$\frac{D}{D_{max}}(d, W) = GLV(d, W) \left(\frac{P - z_{max}}{P - z}\right)^2 \frac{1}{B(W)}$$

(Johns and Cunningham 1983). The quantity z_{max} determines the depth at which the dose reaches its maximum.

The scatter-air ratio determines the scattering fraction of the GLV (Cunningham 1972). It is defined by

$$SLV(d, W) = GLV(d,W) - GLV(d, 0).$$

The GLV for field size 0 is of course not directly measurable; it must be extrapolated from measured values for small fields.

For high-energy photons with energies > 2 MeV, the measurement of the air dose is difficult because of the electron build-up effect. Here, instead of GLV and SLV, the quantities *Tissue Maximum Ratio* GMV ("Tissue Maximum Ratio", TMR) and *Scatter Maximum Ratio* SMV ("Scatter Maximum Ratio", SMR) are used. They differ from the GLV and SLV only in that the reference dose is not measured in air, but also in the phantom, with the respective reference point being superimposed with just enough phantom material to achieve electron equilibrium. The GMV and SMV are also independent

of P.

3.4.3 Determination of the primary component

In order to determine the primary component of the dose, the primary photon flux must first be determined. As already shown, the flux of a monoenergetic photon beam passing through a homogeneous medium is exponentially attenuated. For the multienergy bremsstrahlung of a linear accelerator, which is frequently used in practice, an average attenuation coefficient μ can be applied (Mackie et al. 1985). The consideration of inhomogeneities is described in one of the following sections.

In addition to the exponential attenuation, the attenuation according to the distance squared from the source must also be taken into account. In the *(x, y, z)*-system, the primary flux ϕ can then be written simply as

$$\phi(x,y,z) = \begin{cases} \phi^{(xy)}\dfrac{1}{(P-z)^2}\,e^{-\mu(z_0-z)} & \text{for } z < z_0 \\ 0 & \text{otherwise} \end{cases}$$

The value of $z_0 = z_0(x,y)$ sets the source-skin distance $P - z_0$ (see Figs. 3.3 and 3.4). The value 0 for the flux above the skin surface is not correct from a physical point of view. This value is legitimized by the fact that in radiotherapy one is not interested in the photon flux but in the dose applied to the patient. For the calculation of the dose from the photon flux, however, the flux according to the above equation is to be applied. This will be further clarified in the following sections.

Now the function $\phi^{(xy)}$ which depends only on x and y has to be determined. This function has a number of parameters which are listed below:

$I^{(x\,y)} = I(x, y)$	The device-specific intensity distribution of the beam, which often leads to "horns" in the cross-dose profile of linear accelerators, for example.
$G^{(x\,y)} = G(x, y)$	The relative transmittance of the collimators used, i.e. $G(x,y) = 100\%$ inside the collimator aperture and $G(x,y) \approx 0\%$ outside the collimator aperture (see Figs. 3.3 and 3.4).

$K^{(x\,y)} = K(x, y)$ This function determines the relative transmission value of any compensators or wedge filters used.

$H^{(x\,y)} = H(x, y)$ The "source density function" responsible for penumbra (Treuer et al. 1987).

Knowing these functions, $\emptyset^{(x\,y)}$ can be determined by a 2-D convolution (Treuer et al. 1987):

$$\emptyset^{(xy)}(x,y) = \int\limits_{-\infty}^{\infty} \int\limits_{-\infty}^{\infty} I(x',y')G(x',y')K(x',y')H(x-x',y-y')dx'dy'$$

or in short:

$$\emptyset^{(xy)} = \left(I^{(xy)}G^{(xy)}K^{(xy)}\right) ** H^{(xy)}$$

It should also be mentioned that the size of the penumbra depends on the distance of the collimators from the source. This must be taken into account when determining H. In the following, as in the above equation, the number of asterisks (*) stands for the dimension of the space in which the convolution is performed.

Based on the primary flux, the primary component of the dose can be calculated. As already shown (section 3.1), practically all energy deposition in matter takes place via electrons, which are excited in the Compton effect. For photon energies up to about 1.5 Mev, it can be assumed that the electrons deposit their energy locally, i.e. in the immediate vicinity of the point of interaction between photons and matter. At higher energies, this assumption is no longer justified, and the finite range of the electrons must be included in the calculations. For this purpose, so-called *dose spread arrays* have been calculated by various authors using Monte Carlo methods. These matrices indicate the spatial distribution of energy deposited by such electrons and positrons propagating from the point of interaction of primary photons.

Since the superposition principle applies to the dose and since the matrices mentioned above are spatially invariant, at least for homogeneous media, the primary dose can be described by a three-dimensional convolution of the primary fluence with such a matrix $k_e(x, y, z)$, which in this case thus represents a convolution kernel (Boyer 1985):

$$D_p = \emptyset *** k_e \tag{3.1}$$

In Fig. 3.5, such a convolution kernel is shown in discrete form for the case of a 15 MV bremsstrahlung spectrum. This core is adapted from (Mackie et al. 1985). It is rotationally symmetrical around the z axis. The discrete variables i and k determine the distance from the interaction point $(0,0,0)$ in x- and $(-)z$-

direction.

i

k	0	1	2	3	4	5	6
-1	.0001						
0	1120	0051	.0001				
1	0908	0101	0006	0001			
2	0439	0104	0013	0003			
3	0249	0087	0018	0004	0001		
4	0143	0063	0015	0004	0001		
5	0080	0043	0012	0004	0002	0001	
6	0048	0031	0011	0004	0002	0001	
7	0031	0023	0010	0005	0002	0001	
8	.0020	0016	0009	0005	0002	0001	.0001
9	.0014	0012	0007	0005	0002	.0001	0001
10	.0010	.0009	.0006	0004	.0002	.0002	0001
11	.0007	.0007	.0005	0003	.0002	.0001	.0001
12	.0005	.0005	.0004	0002	.0002	0001	.0001
13	.0003	.0003	.0003	.0002	.0001	0001	
14	.0002	0002	0002	0002	.0001	.0001	
15	.0001	0001	.0001	.0001	.0001		
16	0001	0001	.0001	.0001	.0001		
17	.0001	0001					

0.2 cm

0.2 cm

Fig. 3.5: Convolution kernel to determine the primary dose from the primary fluence for 15 MV photons. The numbers go to the energy deposited in the corresponding voxel and thus the dose. The interaction between photons and matter is assumed to have occurred in the voxel with coordinates (0,0,0).

In the following, it is shown how the primary dose can be calculated on the basis of the "dose spread arrays" without having to perform the time-consuming three-dimensional convolution operation. The main effects resulting from the finite range of electrons in high-energy radiation are:

1. The dose maximum shifts from the skin entry point z_0 to greater depths, e.g. at a depth of 3 cm with 15 MV photons.
2. The penumbra is widening.

It is therefore necessary to investigate how these two effects can be derived from the shape of the

convolution kernel k_e. Because of the small z-dependence of the "distance term" $\frac{1}{(P-z)^2}$ at the usual large amounts of P can be written for the primary dose in a very good approximation:

$$D_p(x,y,z) = \frac{1}{(P-z)^2}\left(\left(\phi^{(xy)}\phi^{(z)}\right) *** k_\epsilon\right) \tag{3.2}$$

where $\phi^{(z)}$ is defined by:

$$\phi^{(z)}(x,y,z) = \begin{cases} e^{-\mu(z_0 \sim z)} & for\, z < z_0 \\ 0 & otherwise \end{cases}$$

To account for the two effects mentioned above, it is assumed that k_e can be approximated by a proportion $k_e^{(xy)}$ that depends only on x and y and a proportion $k_e^{(z)}$ that depends only on z: $k_e \approx k_e^{(xy)}k_e^{(z)}$, and that further $D_p(x, y, z)$ can be represented thereby as:

$$D_p(x,y,z) \approx \frac{1}{(P-z)^2}\left(\phi^{(xy)} ** k_e^{(xy)}\right)\left(\phi^{(z)} * k_e^{(z)}\right) \tag{3.3}$$

The function $k_e^{(xy)}$ causes the broadening of the penumbra and $k_e^{(z)}$ causes the shift of the dose maximum.

First, the calculation of $k_e^{(z)}$ shall be described. For this purpose, consider points (x, y, z) in whose x-y environment $\phi^{(xy)}$ is constant: $\phi^{(xy)} = c$. This is the case, for example, in the middle of a radiation field that is not too small. It is further assumed that z_0 does not change in this environment, i.e. that the skin surface is flat. The function $\phi^{(z)}$ then depends only on z.

For such points, the dose value determined according to equation (3.2) should now agree with the approximate value determined according to (3.3), i.e.:

$$c\left(\phi^{(z)} *** k_\epsilon\right) \stackrel{!}{=} \left(c ** k_e^{(xy)}\right)\left(\phi^{(z)} * k_\epsilon^{(z)}\right).$$

The two-dimensional convolution of the constant c with $k_e^{(xy)}$ again yields a constant which shall be called c_1: $c_1 := c ** k_e^{(xy)}$. If the convolution integral is written out, we then obtain:

$$c\int_{-\infty}^{\infty}\int_{-\infty}^{\infty}\int_{-\infty}^{\infty} \phi^{(z)}(z')k_e(x-x',y-y',z-z')dx'dy'dz' = c_1\int_{-\infty}^{\infty} \phi^{(z)}(z')k_e^{(z)}(z-z')dz'$$

The integral on the left side can be partially separated:

$$c \int_{-\infty}^{\infty} \phi^{(z)}(z') \int_{-\infty}^{\infty} \int_{-\infty}^{\infty} k_e(x - x', y - y', z - z') dx' dy' dz' = c_1 \int_{-\infty}^{\infty} \phi^{(z)}(z') k_e^{(z)}(z - z') dz'.$$

This equation can be satisfied for arbitrary only if the following holds:

$$k_e^{(z)}(z) = \frac{c}{c_1} \int_{-\infty}^{\infty} \int_{-\infty}^{\infty} k_e(x, y, z) dx dy.$$

Thus the equation of determination for $k_e^{(z)}$ is known.

The calculation of $k_e^{(xy)}$ can be performed accordingly. For this purpose, we now consider points (x,y,z) in whose z-environment $\phi^{(z)}$ is constant: $\phi^{(z)} = c$. Such points lie, for example, at greater depths in the case of high-energy photon radiation with correspondingly small attenuation coefficients.

For such points, again the dose value determined by equation (3.2) should agree with the approximate value determined by (3.3), i.e.:

$$c\left(\phi^{(xy)} *** k_e\right) \stackrel{!}{=} \left(\phi^{(xy)} ** k_e^{(xy)}\right)\left(c * k_e^{(z)}\right)$$

The convolution of the constants c with $k_e^{(z)}$ now results in a constant $c_2 := c * k_e^{(z)}$. If the convolution integral is written out, this gives:

$$c \int_{-\infty}^{\infty} \int_{-\infty}^{\infty} \int_{-\infty}^{\infty} \phi^{(xy)}(x', y') k_e(x - x', y - y', z - z') dx' dy' dz'$$

$$= c_2 \int_{-\infty}^{\infty} \int_{-\infty}^{\infty} \phi^{(xy)}(x', y') k_e^{(xy)}(x - x', y - y') dx' dy'$$

The integral on the left side can be separated into:

$$c \int_{-\infty}^{\infty} \int_{-\infty}^{\infty} \phi^{(xy)}(x', y') \int_{-\infty}^{\infty} k_\epsilon'(x - x', y - y', z - z') dz' dx' dy'$$

$$= c_2 \int_{-\infty}^{\infty} \int_{-\infty}^{\infty} \phi^{(xy)}(x', y') k_e^{(xy)}(x - x', y - y') dx' dy'$$

This equation can only be satisfied for any $\phi^{(x,y)}$ if the following holds:

$$k_e^{(xy)}(x, y) = \frac{c}{c_2} \int_{-\infty}^{\infty} k_e(x, y, z) dz$$

This result for $k_e^{(xy)}$ can be interpreted as the projection of k_e onto the x-y plane.

The curves for $k_e^{(xy)}$ and $k_e^{(z)}$ are shown in Fig. 3.6, where the constants c, c_1 and c_2 have been assigned the value 1. The course of $k_e^{(xy)}$ is very narrow. The full width at half maximum of this curve is in agreement with results from (Treuer et al. 1987). In contrast, $k_e^{(z)}$ is much wider. The reason for this is, of course, a corresponding behavior of the matrix shown in Fig. 3.5. From a physical point of view, this behavior can be explained by the fact that the electrons produced by the photons in the Compton effect are mainly pushed in the direction of the photon beam.
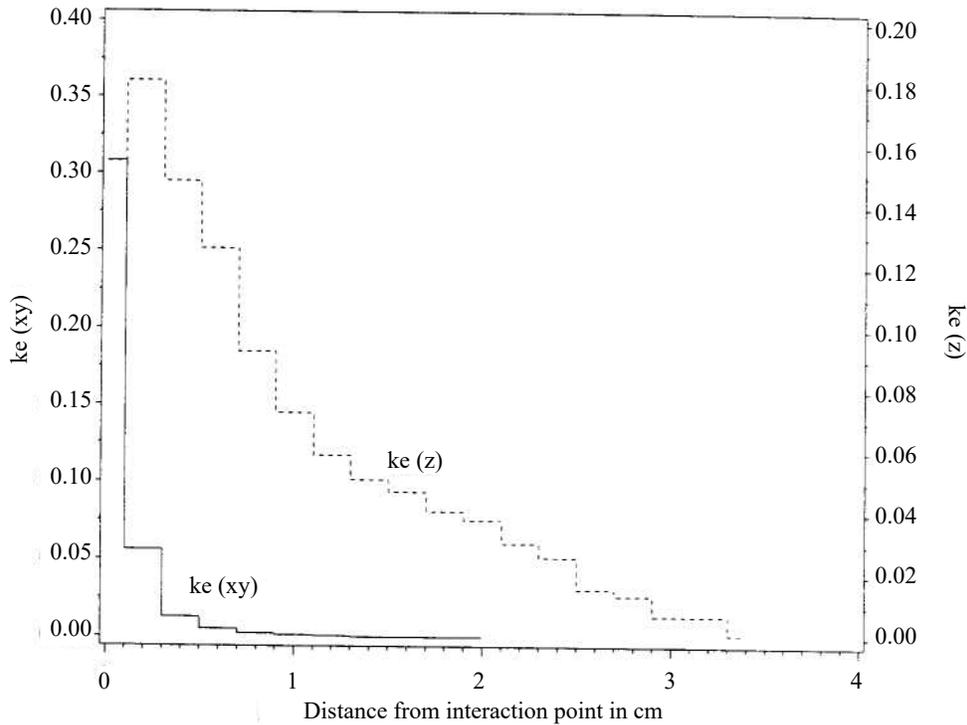
Fig. 3.6: *Graph of the functions* $k_e^{(xy)}$ *and* $k_e^{(z)}$.

The primary component of the dose $D_p(x, y, z)$ can be written simply according to equation (3.3) as:

$$D_p(x, y, z) = \frac{c_N}{(P - z)^2} D_p^{(xy)}(x, y) D_p^{(z)}(x, y, z)$$

c_N represents a normalization constant. The value of these constants is irrelevant, since initially only

relative dose values are of interest. The function $D_p^{(xy)}$ determines a 2-D transverse profile, which is calculated by

$$D_p^{(xy)} = \left(I^{(xy)}G^{(xy)}K^{(xy)}\right) ** H^{(xy)} ** k_e^{(xy)}$$

If one defines a new wider penumbra function $H_p^{(x,y)}$ by

$$H_p^{(xy)}(x,y) = H^{(x,y)} ** k_e^{(xy)}$$

it follows for $D_p^{(xy)}$:

$$D_p^{(xy)} = \left(I^{(xy)}G^{(xy)}K^{(xy)}\right) ** H_p^{(xy)}$$

Accordingly, the transverse profile can be determined by only one 2 D convolution.

The depth dose profile $D_p^{(z)}$ is obtained by numerical convolution of $\phi^{(z)}$ with $k_e^{(z)}$. This convolution is to be performed only once for a given value of z_0. The course for other z_0 values is then calculated simply by shifting the $D_p^{(z)}$ thus obtained Figure 3.7 shows this function as a function of depth $d = z_0 - z$ for 15 MV photons. The normalization was chosen so that the maximum value is 1. For comparison, the tissue maximum ratio GMV(d, 0) extrapolated from measured dose values to field size 0 is plotted in this figure (source of data: Paul et al. 1983). Since there are no scattering components at the field size 0 and since the dependence on the source distance is eliminated by the ratio formation, this ratio should agree with $D_p^{(z)}$. In fact, the figure demonstrates an excellent match.

This shows how the primary component of the dose can be practically determined: First, a 2-D matrix given essentially by the transmittance values of the collimators must be convolved with a penumbra function that takes the lateral electron propagation into account. The function obtained in this way serves as a weighting function for the depth dose curves $D_p^{(z)}$. These must then be traced along the rays within the field, and the respective dose value must be entered into a 3-D dose matrix at the corresponding position ("ray tracing"). The square distance from the source must also be taken into account. In this way, a 3-D dose distribution is finally obtained. Notable deviations from the much more complex 3-D convolution methods only occur at field edges in the area of the build-up effect.

In the following sections it will be shown that also the scatter components of the dose can be calculated with appropriate methods.

2. Three-dimensional dose calculation
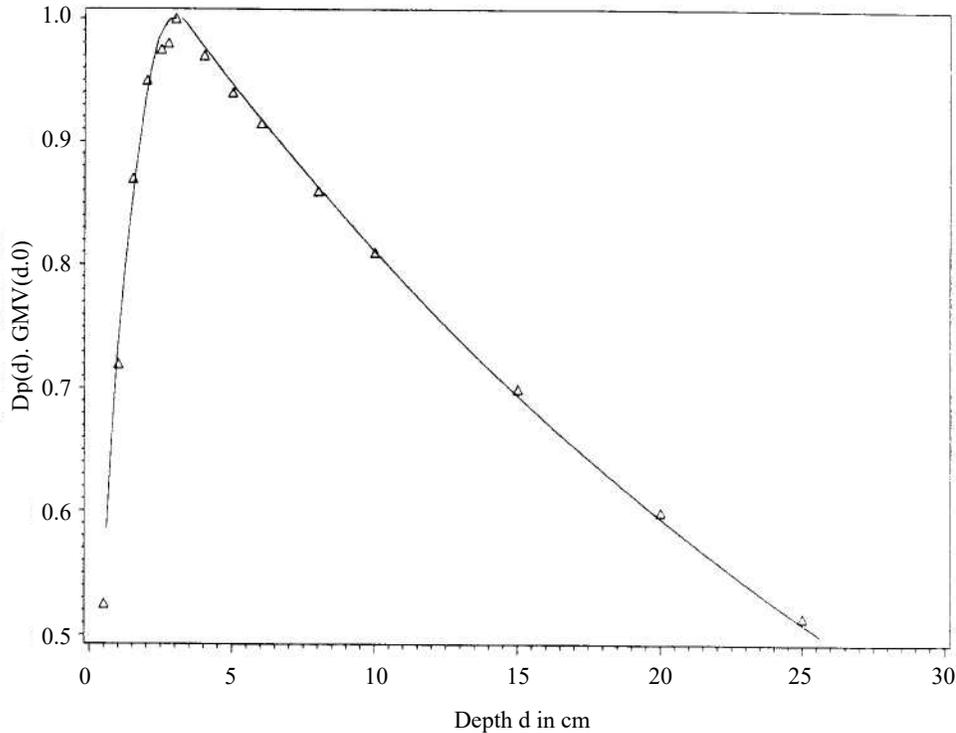
Fig. 3.7: *The depth dose profile of the primary component $D_p^{(z)}$ (d) for 15 MV photons (solid line). The triangles represent values of tissue maximum ratio GMV (d,0) extrapolated from measurements.*

3.4.4 Determination of scattering components

3.4.4.1. Is the consideration of scattering effects necessary?

In order to roughly estimate the influence of scattering effects, first the fraction E_s of the total energy E deposited in the tissue caused by scattering photons is to be determined. Since the ratio of the primary fraction E_p of energy to the total energy is simply given by the ratio of the absorption coefficient μ_{en} to the attenuation coefficient μ (Boyer 1985), it follows for the scattering fraction:

$$\frac{E_s}{E} = 1 - \frac{E_p}{E}$$
$$= 1 - \frac{\mu_{en}}{\mu}$$

Assuming water-equivalent tissue with density 1, this ratio is 56% for 1 MeV photons. At an energy of 15 MeV, the value decreases to 26%. This means that, for example, in the case of ^{60}Co radiation, more than half of the energy applied to the tissue is due to scattering effects. It is therefore essential to take these effects into account. If we consider a 15 MV bremsstrahlung spectrum with an average energy of 5 MeV, the value is still 37%.

II Methodology   - 48 -

It must be emphasized once again that the previous considerations only provide rough estimates, since only globally the total energy was considered. In practice, one is more interested in the corresponding local dose ratios in the radiation field. Here, the ratios naturally depend strongly on the field size and the depth *d*. From measured tissue-air ratios or scatter-air ratios (Johns and Cunningham 1983) it can be seen that for ^{60}Co radiation the scattering component of the dose at a depth of 10 cm at a field radius of only 2 cm is 7.5% of the maximum dose. With a radius of 6 cm, the proportion is already 18%. For 15 MV bremsstrahlung, the corresponding values are 3.5% and 6.5%. These values also make it clear that the scattering effects are smaller for higher-energy radiation. In order to be able to meet an accuracy requirement of the dose calculation of better than ± 5%, however, the scatter must be taken into account in any case.

3.4.4.2. Approximation of a formula of Schoknecht

In 1968, Schoknecht gave a formula for determining the tissue-to-air ratio (GLV) or tissue-to-maximum ratio (GMV) *g* (Schoknecht 1968). Taking into account the distance-squared law, the dose in the central beam can easily be determined from this. The formula is still used in many places today. It is valid for round and rectangular fields with sizes from $4 \cdot 4$ cm^2 to $15 \cdot 15$ cm^2. The formula is:

$$g\left(d, \frac{F}{u}\right) = a_e(d)T_0 e^{-\left(\mu - G_1\frac{E}{u}\right)d}(1 - S_0 e^{-S_1 d}) \qquad (3.4)$$

The quantity $a_e(d)$ is defined by $a_e(d) = 1 - A_0 e^{-A_1 d}$ and describes the dose build-up effect, T_0, G_1, S_0, S_1, A_0 and A_1 are constants and $\frac{F}{u}$ is the quantity characteristic of the field extent given by the ratio of field area to field perimeter. Based on this formula, a new formula will be developed in the following sections, which has a much wider range of validity. This should then make 3-D dose calculations possible, and it should also be possible to take irregular fields and compensators into account.

Since the calculation of the primary component of the dose has already been described in the previous section, the above formula shall first be modified so that primary and scatter components can be separated. Only the scattering components are then considered. For this purpose, the term $e^{G_1\frac{F}{u}d}$ is first developed according to:

$$e^{G_1\frac{F}{u}d} \approx 1 + G_1\frac{F}{u}d.$$

Thus, equation (3.4) reads as follows:

$$g\left(d, \frac{F}{u}\right) \approx a_e(d)T_0 e^{-\mu d}\left(1 + G_1\frac{F}{u}d\right)(1 - S_0 e^{-S_1 d}). \qquad (3.5)$$

If furthermore the term $G_1\frac{F}{u}dS_0 e^{-S_1 d}$ is disregarded (this is allowed because of $S_0 G_1 \ll 1\,\text{cm}^{-2}$) it follows from (3.5):

$$g\left(d,\frac{F}{u}\right) \approx a_e(d)T_0\left(e^{-\mu d} + G_1\frac{F}{u}de^{-\mu d} - S_0 e^{-(\mu+S_1)d}\right). \tag{3.6}$$

Finally, after another simple transformation, we get:

$$g\left(d\cdot\frac{F}{u}\right) \approx a_e(d)T_0\left((1-S_0)e^{-\mu d} + S_0\left(e^{-\mu d}-e^{-(\mu+S_1)d}\right) + G_1\frac{F}{u}de^{-\mu d}\right). \tag{3.7}$$

The quality of the approximation obtained in this way is shown in Tables 3 and 4 in the Appendix. Notable deviations are only seen in larger fields at great depths.

3.4.4.3. Identification of the individual terms

For the further considerations, the build-up effect described by $a_e(d)$ is initially disregarded. The three terms $(1-S_0)e^{-\mu d}$, $S_0\left(e^{-\mu d} - e^{-(\mu+S_1)d}\right)$ and $G_1\frac{F}{u}de^{-\mu d}$ of equation (3.7) are considered. The first term can be identified as the primary component of dose, which is not further examined in this section. The second term is interpreted as the single scattering component. This is justified in more detail below. The transformation step from (3.6) to (3.7) in the previous section, which at first seems rather arbitrary, was carried out to allow this interpretation. For the high-energy photon radiation investigated here, the backscattering is very small and negligible within the required accuracy (Paul et al. 1983). This means that scattering components at depth d = 0 must assume the value zero. The transformation step from (3.6) to (3.7) has exactly this effect, since in (3.7), in contrast to (3.6), only the first term, i.e. the primary component, is different from zero at $d = 0$.

To justify the interpretation of $S_0\left(e^{-\mu d} - e^{-(\mu+S_1)d}\right)$ as a single - scattering component, the primary flux is written as a function of depth d:

$$\phi^{(z)}(d) = \begin{cases} e^{-\mu d} & for\ d > 0 \\ 0 & otherwise \end{cases}$$

and a new function $k_s^{(z)}(d)$ is introduced, defined by

$$k_s^{(z)}(d) = \begin{cases} e^{-(\mu+S_1)d} & for\ d > 0 \\ 0 & otherwise \end{cases}$$

The function $e^{-S_1 d}$ describes the propagation of scatter photons (Schoknecht 1968), and because of $\mu \ll S_1$ this is also true for $k_s^{(z)}$. The d-dependent part in the second term of (3.7) can be represented by a convolution of $\phi^{(z)}$ with $k_s^{(z)}$. To show this, the size [quantity]

$$D_s^{(z)}(d):= \phi^{(Z)} * k_s^{(z)}$$

is introduced. Writing out the convolution integral gives

$$D_s^{(z)}(d) = \int_{-\infty}^{\infty} \phi^{(z)}(d') k_s^{(z)}(d-d') dd' = \int_0^d e^{-\mu d'} e^{-(\mu+S_1)(d-d')} dd'$$

and provide some simple transformations:

$$D_s^{(z)}(d) = e^{-(\mu+S_1)d} \int_0^d e^{S_1 d'} dd'$$

$$= \frac{1}{S_1} e^{-(\mu+S_1)d} \left(e^{S_1 d} - 1\right)$$

$$= \frac{1}{S_1} \left(e^{-\mu d} - e^{-(\mu+S_1)d}\right), d > 0.$$

A comparison of this result with the second term of (3.7) gives an indication that the d-dependent part of this term can be interpreted as the "scattering depth dose curve" $D_s^{(z)}$ for simply scattered photons.

An interpretation of the third term $G_1 \frac{F}{u} d e^{-\mu d}$ as a scattering component for multiple scattered photons is obvious. This conjecture is supported by the fact that the d-dependent part $d e^{-\mu d}$ of this term is obtained by a convolution of the primary flux with a long-range kernel

$$k_{ms}^{(z)}(d) = \begin{cases} e^{-\mu d} & \text{for } d > 0 \\ 0 & \text{otherwise}, \end{cases}$$

which is identical to the primary flux, can be represented. The proof proceeds along the lines of the one above:

$$\phi^{(z)} * k_{ms}^{(z)} = \int_{-\infty}^{\infty} \phi^{(z)}(d') k_{ms}^{(z)}(d-d') dd'$$

$$= \int_0^d e^{-\mu d'} e^{-\mu(d-d')} dd'$$

$$= e^{-\mu d} \int_0^d dd'$$

$$= d e^{-\mu d}, d > 0.$$

A new quantity $D_{ms}^{(z)}(d)$ is introduced, which in this case describes the depth dose curve for multiple scattered photons:

$$D_{ms}^{(z)}(d) := \phi^{(z)} * k_{ms}^{(z)}$$

In the previous considerations for the determination of the scattering components, the build-up effect represented by the term $a_e(d)$ in the Schoknecht formula was not taken into account. This is acceptable as long as the energy of the photons is below about 1.5 MeV. As already shown in the considerations on the determination of the primary dose, the build-up effect at higher energies must, however, be taken into account.

It can be assumed that the build-up effect causes a shift of the dose distribution from the amount of the build-up depth. This assertion is supported by the fact that there are no scattering components in the build-up depth region at the highest energy radiation (Paul et al. 1983). It is therefore obvious to shift the scattering depth dose curves for these high-energy photons by the amount of the build-up depth. This procedure is also justified by the good agreement of the results thus obtained with measurements (see III/4.). Accordingly, new depth dose histories for the single scattering are defined by

$$D_s^{(z)}(d) = \begin{cases} \dfrac{1}{S_1}\left(e^{-\mu(d-d_{max})} - e^{-(\mu+S_1)(d-d_{max})}\right) & \text{for } d > d_{max} \\ 0 & \text{otherweise} \end{cases}$$

and for multiple scattering by

$$D_{m_0}^{(z)}(d) = \begin{cases} (d - d_{max})e^{-\mu(d-d_{max})} & \text{for } d > d_{max} \\ 0 & \text{otherweise .} \end{cases}$$

In Fig. 3.8 these curves are plotted for ^{60}Co radiation without taking the build-up effect into account, i.e. with $d_{max} = 0$. Fig. 3.9 shows the corresponding curves for 15 MV bremsstrahlung, taking into account a build-up depth of $d_{max} = 3$cm.

Finally, it should be noted that effects caused by scattered electrons directly below the skin surface cannot, of course, be taken into account with the methods described here. In practice, however, this is irrelevant, since the aforementioned high accuracy requirements for dose determination are not normally imposed on areas directly below the skin surface.
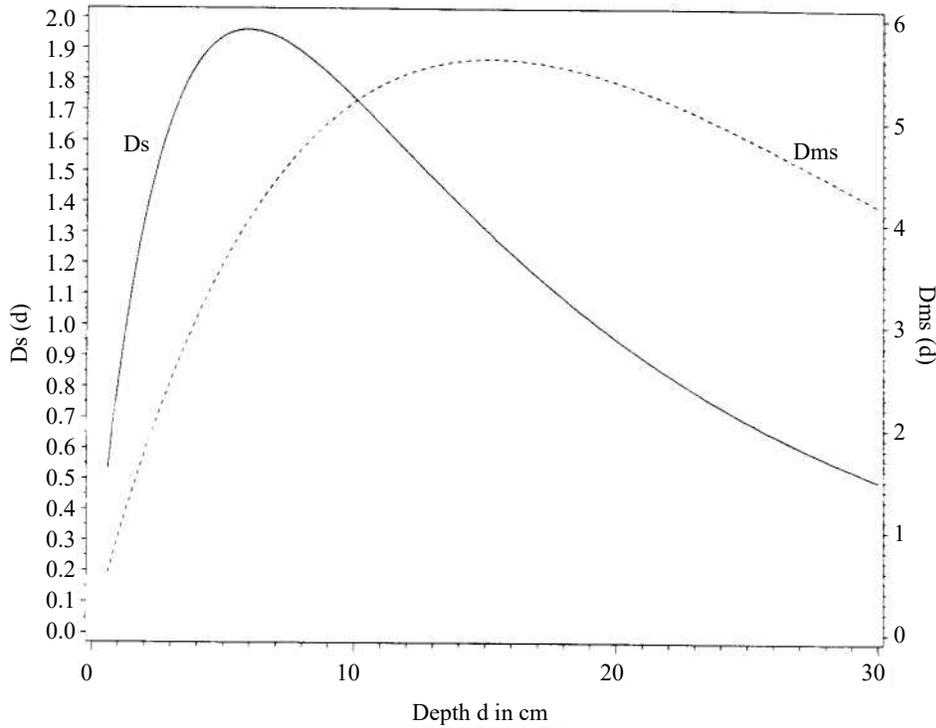
Fig. 3.8: *The "scattering depth dose curves" for single scattered photons $D_s^{(z)}(d)$ and for multiple scattered photons $D_{ms}^{(z)}(d)$ for ^{60}Co radiation.*
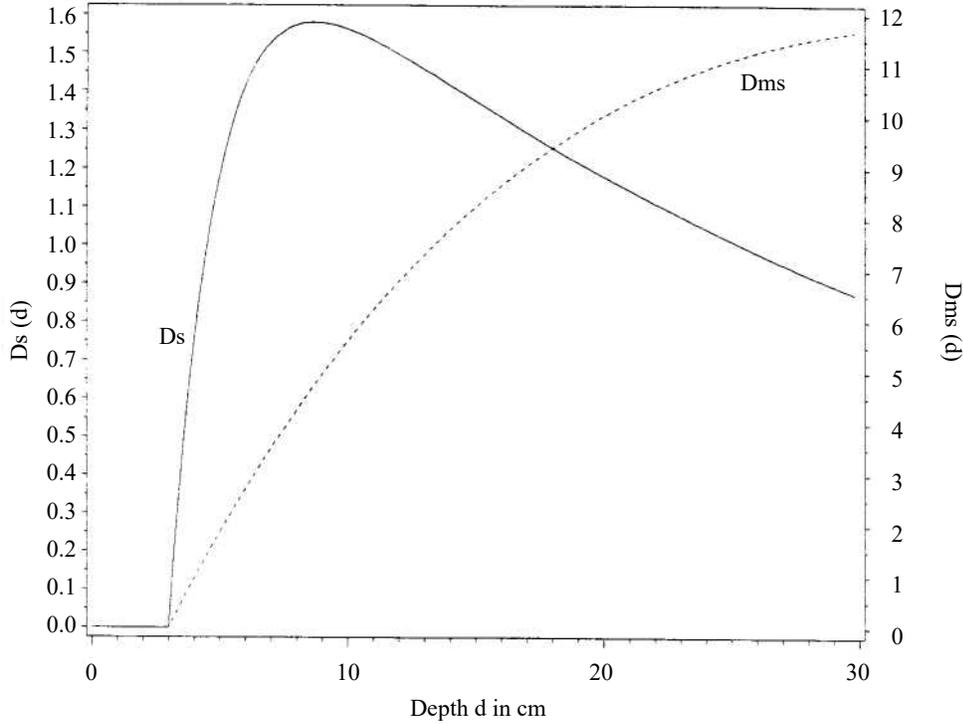
Fig. 3.9: *The curves according to Fig. 3.8 for 15 MV bremsstrahlung*

3.4.4.4. Adjustment to measurements

In the last two sections, Schoknecht's formula (3.4) served as a motivation for the introduction of the functions $D_s^{(z)}$ and $D_{ms}^{(z)}$. In this section, these functions are directly adapted to measurement results for different field sizes. In this way, some shortcomings of the Schoknecht formula can be circumvented. These inadequacies become apparent when the approximation formula (3.7) is examined in detail.

Looking at the second term of this formula, which has been identified as being responsible for the single scattering, we see that it does not depend on the field size F/u. For very small fields, however, the influence of scattering effects is known to decrease. The missing dependence of the term on the field size F/u thus causes the Schoknecht formula to lose its validity for very small fields. Similarly, the linear dependence of the third term, representing multiple scattering, on F/u appears to be highly questionable from a physical point of view. This is because this linear dependence causes the third term to grow indefinitely as the fields increase, which is physically incorrect. Rather, the multiple dispersion component tends toward an upper bound. This discrepancy explains the restriction of the validity of the formula to fields up to a maximum of $15 \cdot 15 \text{ cm}^2$.

In the following, the Schoknecht formula will not be considered further. The only quantity from this that still occurs in the further considerations is S_1. In (Schoknecht 1968) this quantity is tabulated

for different beam qualities. The following considerations show how S_1 can be easily determined for other beam qualities as well.

To do this, first calculate the depth $d_{max,}$ where $D_S^{(z)}$ assumes its maximum. By zeroing the derivative of $D_S^{(z)}$ to d this depth becomes

$$d_{\text{micx}_s} = -\frac{1}{S_1} \ln \left(\frac{\mu}{\mu + S_1} \right) + d_{max}$$

Thus, knowing d_{max}, d_{max_s} and μ, S_1 can be determined by numerically solving this equation. The build-up depth d_{max} and the attenuation coefficient μ are assumed to be known. Furthermore, since single scattering predominates for small fields (Cunningham 1978), d_{maxs} can be read from measured values s_{mess} of the scatter-to-air ratios SLV or scatter-maximum ratios SMV for small fields.

For ^{60}Co, according to Table 1 (Appendix A1), the value is $d_{maxs} = 6$ cm and thus $S_1 = 0.27$ (Schoknecht: $S_1 = 0.28$). At 15 MV bremsstrahlung of the linear accelerator Siemens Mevatron 77 used at our institute one determines from table 2: $d_{maxs} = 8$ cm and thus $S_1 = 0.5$. The function $D_S^{(z)}$ shown in Fig. 3.9 has been determined with this value.

Now the field size dependence of the scattering components is determined. As mentioned above, the approach via linear dependencies realized in the Schoknecht formula is not adequate. Instead, for s, i.e. for the total scattering fraction of the GLV or GMV, the more general expression

$$s_{ans}(d,r) = \alpha(r)D_S^{(z)}(d) + \beta(r)D_{ms}^{(z)}(d) \tag{3.8}$$

is applied for round fields with radius r at first. ($\alpha(r)$ and $\beta(r)$ are arbitrary functions, which must be determined in the following in such a way that the expression above reflects the measured SLV or SMV s_{meas} as well as possible. For this purpose, a "*least squares fit*" is performed, i.e. the expression

$$\|s_{\text{mess}}(d,r) - s_{\text{ans}}(d.r)\|^2 \overset{!}{=} \text{Min}$$

is minimized.

For a fixed value of the radius $r = r_o$ the conditional equations for α and β are obtained using the minimum conditions:

$$\frac{\partial}{\partial \alpha} \left(\|s(d,r_0) - \alpha(r_0)D_S^{(z)}(d) + \beta(r_0)D_{ms}^{(z)}(d)\|^2 \right) = 0$$

and

$$\frac{\partial}{\partial \beta} \left(\|s(d,r_0) - \alpha(r_0)D_S^{(z)}(d) + \beta(r_0)D_{ms}^{(z)}(d)\|^2 \right) = 0.$$

Performing the differentiation and explicitly writing out the terms leads to the system of equations:

$$\alpha(r_0) \sum_d (D_s^{(z)}(d))^2 + \beta(r_0) \sum_d D_s^{(z)}(d) D_{ms}^{(z)}(d) + \sum_d D_s^{(z)}(d) s(d, r_0) = 0$$

$$\alpha(r_0) \sum_d D_s^{(z)}(d) D_{ms}^{(z)}(d) + \beta(r_0) \sum_d \left(D_{ms}^{(z)}(d) \right)^2 + \sum_d D_{ms}^{(z)}(d) s(d, r_0) = 0.$$

This system of equations can be simply solved for $\alpha(r_0)$ and $\beta(r_0)$ after calculating the individual sums. This should not be done here, as the expressions become quite long and confusing.

The resulting values for α and β are plotted in Figure 3.10 for ^{60}Co versus radius. Figure 3.11 shows the corresponding curves for 15 MV photons. Since measured values for this energy were only available for square fields, the side length of the fields is plotted on the abscissa.
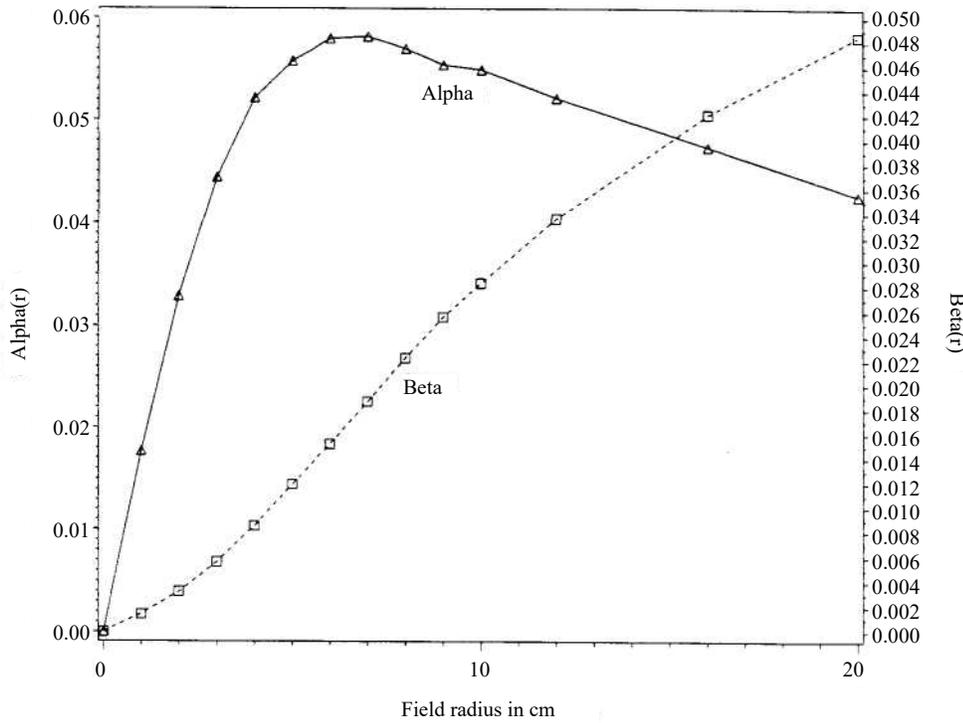
Fig. 3.10:   *The values of α and ß for determining s_{ans} according to (3.5) for ^{60}Co*
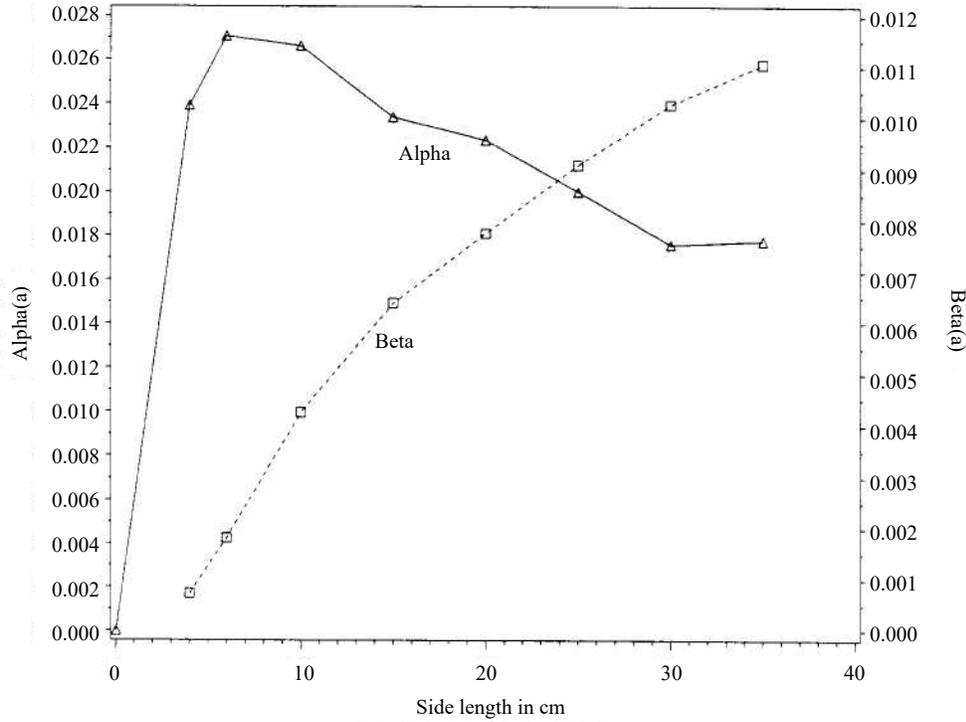
Fig. 3.11:   *The values of α and ß for 15 MV bremsstrahlung*

Two things stand out when looking at these curves. First, the curve of $\alpha(a)$ for the energy 15 MV is not very smooth. This is probably due to the small number of measurements (see Table 2 in the Appendix) included in the calculation. In the case of ^{60}Co, where more measured values are known (see Table 1), the curve is much smoother.

Secondly, it is noticeable that the values of α decrease again with larger radii. If $\alpha(r)D_s^{(z)}(d)$ alone represented the single scatter, then α would have to increase strictly monotonically with radius. So the previous interpretation of $D_s^{(z)}$ is not quite correct. However, the following considerations will provide further evidence that this interpretation is at least approximately valid. Fig. 3.12 will be used for this purpose.

The figure first shows the excellent agreement of the measured values (triangles) with the values calculated according to (3.5) (solid line).

More interesting for the above considerations, however, is a comparison of the curve calculated with the Klein-Nishina formula (fine dashed line) with the curve resulting from $\alpha(r) D_s^{(z)}(d)$ (rough dashed line). The Klein-Nishina curve was obtained by numerical integration of the Klein-Nishina scattering coefficients (Cunningham 1978). Therefore, only the first-order scattering is included in this function. Comparison shows that for radii up to about 4 cm this function agrees quite well with the function given by $\alpha(r) D_s^{(z)} (d)$. This provides further justification for identifying this function as a first-

order scattering component. The decrease of this function at larger radii is possibly due to the fact that $\beta(r)D_{ms}^{(z)}$ does not only represent the higher order scattering, but also contains first order components.
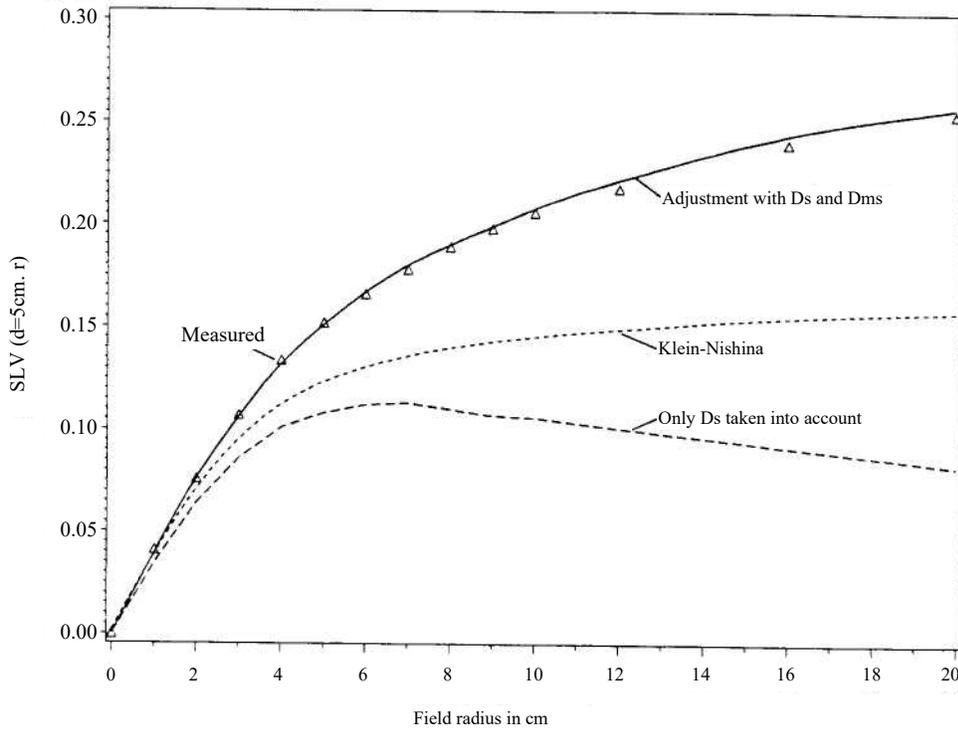
Fig. 3.12: *Scatter-air ratios for ^{60}Co at 5 cm depth as a function of field radius. Comparison of measured values and values calculated by different methods.*

3.4.4.5. Consideration of arbitrary field shapes

As early as 1941, J. R. Clarkson described a method with which depth dose curves for irregular fields can be calculated from the corresponding curves for round fields. The method, known as the *"sector integration method"*, is based on the fact that an arbitrarily shaped field can be thought of as being composed of segments of circles with different radii. The following figure illustrates this for a rectangular field.

Now the superposition principle applies to scattered dose fractions. The scattering fraction *s* for one of the considered points O, P or Q is therefore linearly composed of the scattering fractions of the individual circle segments around the corresponding point. Since for the scattering part s_{seg} of a circle segment with radius *r* the following applies:
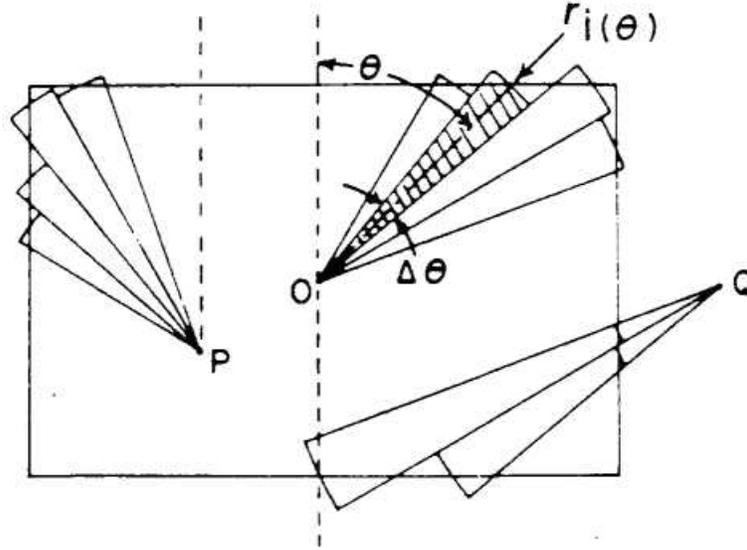
Fig. 3.13: *Composition of a rectangular field of circle segments with radii r_i and angles $\Delta\theta$ for points O, P, and Q.*

$$s_{seg}(d) = s(d,r)\frac{\Delta\theta}{2\pi},$$

the total scattering fraction for any irregular field is given by

$$s_{\text{irreg}}(d) = \sum_i s(d,r_i)\frac{\Delta\theta_i}{2\pi}.$$

Points such as point Q shown, where circle segments intersect the field edge several times, must be given special treatment. Suffice it to say that various algorithms for performing the sector integration described above are known (see, e.g., Cunningham et al. 1972a).

Up to now it was implicitly assumed that the whole irregular field is irradiated uniformly. Wedge filters or compensators can therefore not be taken into account in the method described above. If the method is to be extended to such more complicated cases, each segment of the circle must be further subdivided (Cunningham 1972). Such methods are referred to in the literature as *differential scatter air ratio (dSAR)* -methods. A - segments are considered, which cause the scattering part in the

$$s_{\Delta seg}(d) = \frac{\Delta\theta}{2\pi}(s(d,r+\Delta r) - s(d,r)) = \frac{\Delta\theta}{2\pi}\Delta s(d,r)$$

central beam. The total scattering fraction is again obtained by summation over such Δ-segments, but

now a weighting is performed with the primary flux $\phi^{(xy)}$ so that compensators and wedge filters are taken into account:

$$s_{irreg}(d) = \sum_i \frac{\Delta\theta_i}{2\pi} \sum_j \Delta s(d, r_j)\phi^{(xy)}(r_j, \theta_i)$$

The summations over the angle elements i and the radius elements j can be replaced by integrations:

$$s_{irreg}(d) = \int_0^{2\pi} \int_0^\infty \phi^{(xy)}(r, \theta)\frac{1}{2\pi}\frac{\Delta s}{\Delta r}(d, r)dr d\theta$$

If now for $s(d,r)$ the approach according to equation (3.5) is used, the above equation can be transformed to:

$$s_{irreg}(d) = D_s^{(z)}(d)\int_0^{2\pi}\int_0^\infty \phi^{(xy)}(r, \theta)\frac{1}{2\pi}\frac{\Delta\alpha}{\Delta r}(r)dr d\theta +$$

$$D_{ms}^{(z)}(d)\int_0^{2\pi}\int_0^\infty \phi^{(xy)}(r, \theta)\frac{1}{2\pi}\frac{\Delta\beta}{\Delta r}(r)dr d\theta$$

The quantities over which integration is performed now no longer depend on the depth d. With the definitions

$$k_s^{(xy)}(r) = \frac{1}{2\pi r}\frac{\Delta\alpha}{\Delta r}(r)$$

and

$$k_{ms}^{(xy)}(r) = \frac{1}{2\pi r}\frac{\Delta\beta}{\Delta r}(r)$$

follows further:

$$s_{irreg}(d) = D_s^{(z)}(d)\int_0^{2\pi}\int_0^\infty \phi^{(xy)}(r, \theta)k_s^{(xy)}(r)r dr d\theta +$$

$$D_{ms}^{(z)}(d)\int_0^{2\pi}\int_0^\infty \phi^{(xy)}(r, \theta)k_{ms}^{(xy)}(r)r dr d\theta$$

Finally, a transformation to Cartesian coordinates yields:

$$s_{irreg}(d) = D_s^{(z)}(d)\int_{-\infty}^\infty\int_{-\infty}^\infty \phi^{(xy)}(x', y')k_s^{(xy)}(x' \cdot y')dx' dy' +$$

$$D_{ms}^{(z)}(d)\int_{-\infty}^\infty\int_{-\infty}^\infty \phi^{(xy)}(x', y')k_{ms}^{(xy)}(x', y')dx' dy'.$$

The above function initially describes only the scattering component for the central beam, i.e. for $x = y = 0$. However, since the central ray is in no way distinguished from other rays in the equation, the scattering fraction for arbitrary points can simply be calculated by a corresponding shift of the *(x,y,d)* - coordinate system in *x* - *y* direction. So one obtains

$$S_{irreg}(x, y, d) = D_s^{(z)}(d) \int_{-\infty}^{\infty} \int_{-\infty}^{\infty} \phi^{(xy)}(x' + x, y' + y) k_s^{(xy)}(x', y') dx' dy' +$$

$$D_{ms}^{(z)}(d) \int_{-\infty}^{\infty} \int_{-\infty}^{\infty} \phi^{(xy)}(x' + x, y' + y) k_{ms}^{(xy)}(x', y') dx' dy',$$

or, because of the symmetry of $k_s^{(xy)}$ or $k_{ms}^{(xy)}$:

$$S_{irreg}(x, y, d) = D_s^{(z)}(d) \int_{-\infty}^{\infty} \int_{-\infty}^{\infty} \phi^{(xy)}(x', y') k_s^{(xy)}(x - x', y - y') dx' dy' +$$

$$D_{ms}^{(z)}(d) \int_{-\infty}^{\infty} \int_{-\infty}^{\infty} \phi^{(xy)}(x', y') k_{ms}^{(xy)}(x - x', y - y') dx' dy'$$

Since these are convolution integrals, they can be written abbreviately:

$$S_{irreg}(x, y, d) = D_s^{(z)}(d) \left(\phi^{(xy)} ** k_s^{(xy)} \right) + D_{ms}^{(z)}(d) \left(\phi^{(xy)} ** k_{ms}^{(xy)} \right).$$

The functions $k_s^{(xy)}$ and $k_{ms}^{(xy)}$ could therefore be called *"scatter - convolution kernels"*. Figures 3.14 and 3.15 show contour plots of the product of these functions with radius $r = \sqrt{x^2 + y^2}$. The clearly visible staircase structure, especially for 15 MV photons, which becomes even more prominent when multiplied by *r* is due to the discrete presence of the values of $\alpha(r)$ and $\beta(r)$. Since the values of α and ß in the case of 15 MV photons were determined only as a function of the side length *a* of square fields, the method of equivalent fields (Johns and Cunningham 1983) was used here in accordance with

$$r = 2.235a$$

the radii of the round fields equivalent with respect to the scattering behavior are calculated.
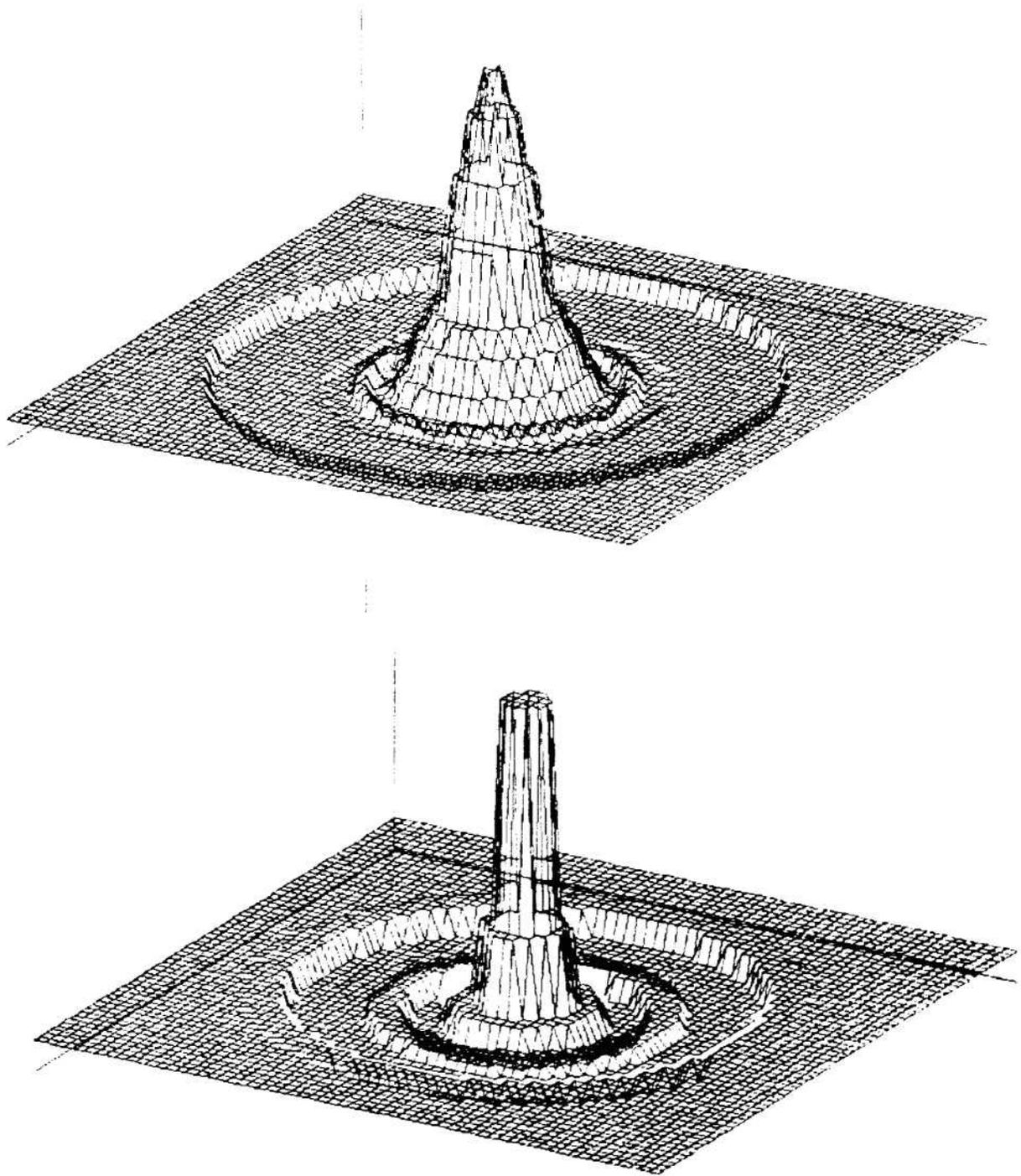
Fig. 3.14: *Contour plot of functions* $rk_s^{(xy)}(x,y)$ *for* ^{60}Co *(top) and 15 MV (bottom). The distance between the contour lines corresponds to 8 mm.*
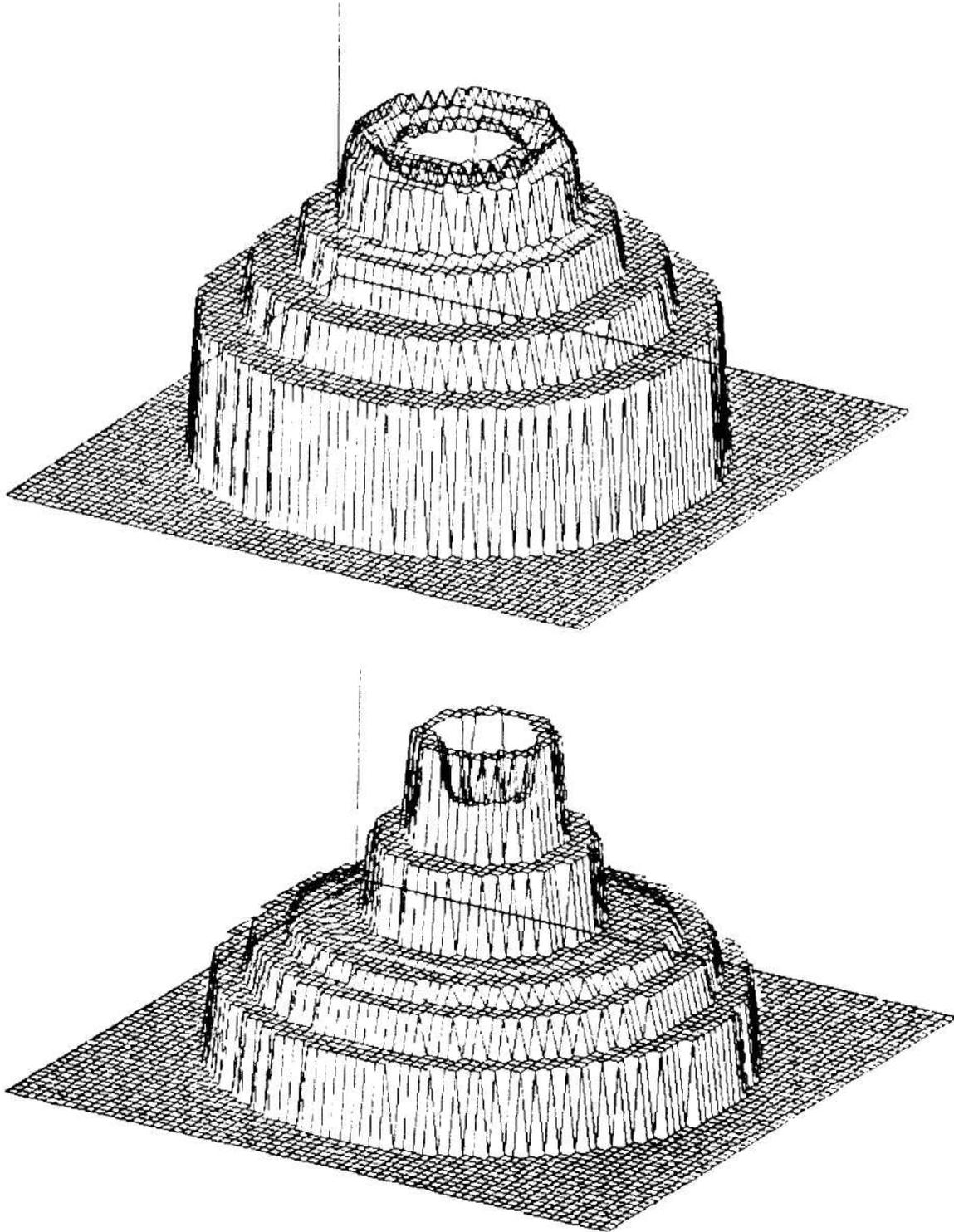
Fig. 3.15: *Contour plot of functions* $rk_{ms}^{(xy)}$ *(x, y) for* [60] *Co (top) and 15 MV (bottom). The distance between the contour lines corresponds to 8 mm.*

Finally, the part of the dose due to scattering effects $D_s + D_{ms}$ can be written in a form corresponding to the primary component, namely:

$$D_s(x,y,z) + D_{ms}(x,y,z) = \frac{c_N}{(P-z)^2}\left(D_s^{(xy)}(x,y)D_s^{(z)}(x,y,z) + D_{ms}^{(xy)}(x,y)D_{ms}^{(z)}(x,y,z)\right)$$

with the definitions

$$D_s^{(xy)}(x,y) = \phi^{(xy)} ** k_s^{(xy)}$$

and

$$D_{ms}^{(xy)}(x,y) = \phi^{(xy)} ** k_{ms}^{(xy)}.$$

3.4.5   Determination of the total dose

The total dose applied to the tissue is obtained by adding the primary portion and the scatter portions to

$$\begin{aligned}
D(x,y,z) &= D_p(x,y,z) + D_s(x,y,z) + D_{ms}(x,y,z) \\
&= \frac{CN}{(P-z)^2}\left(D_p^{(xy)}D_p^{(z)} + D_s^{(xy)}D_s^{(z)} + D_{ms}^{(xy)}D_{ms}^{(z)}\right).
\end{aligned} \tag{3.9}$$

The mathematical structure of the fractions is identical. The quantities $D_p^{(z)}, D_s^{(z)}$ and $D_{ms}^{(z)}$ are the depth dose profiles of the respective fractions. These quantities depend on the coordinates x, y and z only via the depth $d = z_0(x,y) - z$. They can therefore be stored before the calculation as a function of d and then only have to be shifted by the amount of z_0 during the calculation. The actual calculation consists - as already explained in the determination of the primary component - of a simple ray tracing with these depth dose curves, weighted with $D_p^{(xy)}, D_s^{(xy)}$ and $D_{ms}^{(xy)}$.

The quantities $D_p^{(xy)}, D_s^{(xy)}$ und $D_{ms}^{(xy)}$ which depend only on x and y are obtained by two-dimensional convolutions, as described in the previous sections. As for the primary component (see section 3.4.3), new ''penumbra'' functions can also be defined for the scattering components and saved in advance according to the specifications:

$$\begin{aligned}
H_s^{(xy)}(x,y) &= H^{(x,y)} ** k_s^{(xy)}, \\
H_{ms}^{(xy)}(x,y) &= H^{(x,y)} ** k_{ms}^{(xy)}.
\end{aligned}$$

This again allows the scatter components $D_s^{(xy)}$ and $D_{ms}^{(xy)}$ and the primary component $D_p^{(xy)}$ to be written in a unified form:

$$D_p^{(xy)} = \left(I^{(xy)}G^{(xy)}K^{(xy)}\right) ** H_p^{(xy)}.$$
$$D_s^{(xy)} = \left(I^{(xy)}G^{(xy)}K^{(xy)}\right) ** H_s^{(xy)},$$
$$D_{ms}^{(xy)} = \left(I^{(xy)}G^{(xy)}K^{(xy)}\right) ** H_{ms}^{(xy)}.$$

Consequently, each component can be calculated by only one 2-D convolution.

According to the convolution theorem, convolutions can be replaced by multiplications in frequency domain (Brigham 1987). This saves a lot of time, especially when using Fast Fourier Transform (FFT) routines (Boyer 1985).

3.4.6   Influence of the surface curvature

Until now, the patient's body surface area $z_0(x, y)$ was included in the calculation by shifting the depth dose curves for the primary component and the scattering components by a corresponding amount. This leads to correct results for the primary component, since the curvature is certainly negligible in the lateral range of the electrons.

On the scattering part of the dose at a certain point, however, laterally more distant areas also have an influence. This is evident, for example, from the relatively large radial extent of the convolution kernels shown in Figs. 3.14 and 3.15. Therefore, $z_0(x, y)$ is generally not constant in the lateral range where the scattering effects play a role. The scattering behavior under curved surfaces is therefore different from that under flat surfaces perpendicular to the beam.

It is possible to extend the algorithm described here to account for scattering behavior modified by surface curvature. However, research has shown that the resulting effect is small (Cunningham 1972a). It generally leads to an error of less than 1 - 2 % for ^{60}Co and is even smaller for higher energy radiation.

3.4.7   Consideration of inhomogeneities

In the dose calculation described above, it was assumed that the tissue irradiated is homogeneous. Of course, this is generally not the case. There are several ways to account for inhomogeneities. The simplest is again to scale the calculated depth dose curves according to the concept of radiological depth (see Section 3.1). This is associated with the sources of error already mentioned. By splitting the dose into primary and scatter components, however, the errors can be kept smaller. In fact, the scaling according to the radiological depth can be limited to the primary depth dose curve $D_p^{(z)}$. For the scattering components that cannot be precisely localized, an attenuation coefficient μ averaged over the entire tissue irradiated should be applied when calculating the depth dose curves.

More accurate results are obtained if the scaling is not applied to the depth dose histories, but directly to the photon flux ϕ (where the concept of radiological depth leads to accurate results) and to the nucleus $k_e^{(z)}$. This method was also proposed in (Mackie et al. 1985) for the 3-D convolution methods. In the present work, the convolution integral $D_p^{(z)} = \phi^{(z)} * k_e^{(z)}$ must be replaced by the following *superposition integral* for this purpose:

$$D_p^{(z)}(z) = \int_{-\infty}^{\infty} \phi^{(z)}(z')k_\epsilon\big(\bar{\varrho}'(z,z') \cdot (z - z')\big)dz',$$

where $\bar{\varrho}'$ represents the average relative density between z and z'. Since this density generally varies from point to point in the tissue, the kernel k_e is no longer spatially invariant. As a result, fast methods for calculating the integral via the Fourier transform are not applicable. However, since this is only a 1-D superposition, a calculation should still be possible in a realistic amount of time.

The described inhomogeneity corrections have not yet been implemented. The data presented in Results-Part III are also based on homogeneous tissues. This means that the presented algorithm cannot yet be reasonably applied to body regions with large density fluctuations, such as those occurring in the lungs.

4.   An iterative procedure for solving the inverse problem

In this chapter, the inverse problem is treated as an optimization problem. Criteria are set up according to which the optimization is to take place. This is a critical issue as radiotherapists do not agree on these *optimization criteria* and the results of this study will be used as a basis for further research. However, the optimization algorithm described in the following is so flexible that the criteria can be changed at any time without great effort and new criteria can also be included.

Based on the established criteria, the optimization problem is first *mathematically defined.* To solve the problem, an iterative algorithm is used that takes into account arbitrary constraints in the form of *penalty functions.* The derivation of the algorithm is described. The resulting algorithm is structurally identical to a technique known from CT image reconstruction called the *algebraic reconstruction technique (ART)*. The initial value for the iterative optimization are modulation functions obtained by the filtered projection method described in chapter 11/2. The result of the optimization are modulation functions whose associated dose distributions can be described as optimal. Thus, an algorithm has been found that replaces the often extremely time-consuming optimization work of the radiotherapist "by hand" and solves the inverse problem.

The optimization algorithm can be based on any dose calculation method. The procedure described in II/3.4 is particularly suitable for this purpose. At present, a simplified calculation according to the formula of Schoknecht (1968) is still installed. The accuracy that can be achieved with this method is considerably lower than with the new method from II/3.4, but considerably better than with the [coarse] methods from II/2. The error is in the order of 10%. Finally, a computer program is described with which the optimization is realized. Special problems related to the discrete presence of the data are addressed. Furthermore, an approach to parallelize the problem is described.

4.1   The inverse problem as an optimization problem

In II/1. it was shown that the inverse problem must be regarded as an optimization problem, since a given dose distribution can generally not be realized exactly for physical reasons (see also Goitein 1990). To define the inverse problem as an optimization problem, first *optimization criteria* must be established, which a "good" irradiation plan must satisfy. This is a central problem in radiotherapy planning, and there is still no unanimous opinion among radiotherapists regarding the criteria and their ranking. Building on a number of publications establishing such criteria (see e.g. Hope et al. 1967, Redpath et al. 1976), the following criteria are considered in the present paper:

1. In the target volume, the dose must reach the value prescribed for tumor destruction.
2. The dose should be distributed as homogeneously as possible over the target volume, i.e. fluctuations in the dose should be kept small there.
3. The dose in particularly radiation-sensitive at-risk organs must remain below a maximum permissible value.
4. In the surrounding healthy tissue, the dose should be low.

Today, these criteria are sometimes defined more quantitatively using *dose-volume histograms* (see III). It should be stressed that these are provisional criteria. They are used to show that the optimization algorithm described below can adequately account for a wide variety of constraints. Important criteria not previously considered are provided by the concept of tumor control probabilities and complication probabilities recently introduced by Lyman (1989).

To obtain a mathematical formulation of the optimization problem, an *objective function* to be minimized must be defined. In the following, an objective function is defined in which the first two criteria are included. The third criterion is taken into account by an appropriately defined constraint. The somewhat imprecise formulation of the fourth criterion must first be clarified.

A low dose exposure in healthy tissue is equivalent to a concentration of the high dose area on the target volume in terms of conformation therapy. This means that the dose gradient at the edge of the target volume should be as large as possible. To achieve this, the requirement is that the 60% isodose should lie within a small margin of given width around the target volume. This causes the dose drop to 60% to occur close to the target volume, so that the required large dose gradient occurs at the edge of the target volume. Figure 4.1 serves to illustrate this point.
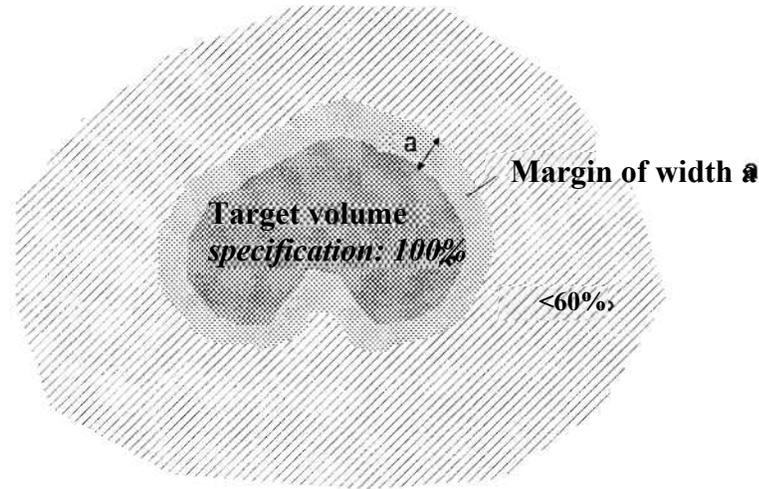
Fig. 4.1: *Illustration of the criterion for concentrating the area of high dose on the target volume to protect surrounding healthy tissue (criterion 4).*

4.2 Mathematical formulation

The mathematical definition of the objective function F_1 used here is given by

$$F_1 = \sum_{i \in Z} (d_i - p)^2 \overset{!}{=} \text{Min.} \tag{4.1}$$

where d_i represents the calculated dose in the tissue and p represents the prescribed dose value. The summation is performed over all volume elements (voxels) of the target volume, i.e. a discrete spatial representation of the target volume is assumed here. Thus, F_1 is the squared deviation of the calculated dose from the prescribed dose in the target volume. A minimization of this function takes into account the first two of the criteria established above. This quadratic objective function has also been used by a number of other authors (Starkshall 1984, Redpath et al. 1976, McDonald et al. 1977, Legras et al. 1986, Webb 1989).

Now F_1 should be written as a function of the modulation profiles, which finally have to be determined. For this purpose, a vector x_k is introduced, the components of which indicate the intensity values within the radiation field for the field k. This is a one-dimensional column vector in which the values of the 2-D modulation profiles are entered one below the other. The components of $\mathbf{x}_k$ can also be thought of as the intensity of individual *needle beams* from which the beam fields can be thought of as being composed. From the $\mathbf{x}_k$ for the different fields a new vector $\mathbf{x}$ is composed:

$$X = (x_1, x_2, ..., x_N)',$$

where N is the number of fields, i.e. the directions of irradiation (typically 7 or 9). Due to the superposition principle, the dose at each voxel in the tissue can be represented by a linear combination of the components x_i :

$$d = \mathbf{D}x.$$

$\mathbf{D}$ is a "dose calculation matrix" whose component D_{ij} gives the contribution of the needle beam j to the volume element i.

$\mathbf{D}$ is introduced here for the purpose of simplifying notation, but it should be noted that in most practical cases it will hardly be possible to handle this matrix in the computer. To demonstrate this, we will assume as an example that an irradiation is to be optimized with 9 fields, each consisting of 1000 needle beams. The size of the modulation matrix is therefore about 32. 32. If the sampling is such that the relevant tissue (i.e. target volume and organs at risk) is composed of 10000 volume elements, then $\mathbf{D}$ has dimension $10000 \cdot 9000$. This is a very large amount of data even for the most powerful computers (360 Mbytes for REAL*4), even if the matrix is sparse in practice. In the current realization, the elements of D are therefore repeatedly recomputed during the execution of the optimization (similar problems arise in image reconstruction when computing the *weighting matrix* (Brooks and Di Chiro 1976)).

Equation (4.1) can thus be written as

$$F_1(\mathbf{x}) =\| \mathbf{Z}(\mathbf{Dx} - \mathbf{p}) \|^2, \tag{4.2}$$

where $\mathbf{Z}$ is a "target volume operator" that extracts only the target volume voxels from all tissue volume elements. $\mathbf{Z}$ is a diagonal matrix with $Z_{ii} = 1$ if $i \in Z$ and $Z_{ii} = 0$ otherwise.

As mentioned above, some constraints have to be taken into account. An important condition is the limitation of the dose in radiation-sensitive at-risk organs to a tolerable maximum value:

$$d_i \leq g_i, i \in R. \tag{4.3}$$

R is an index set extracting the at-risk organ voxels and g_i is the upper dose limit for these voxels. The g_i will generally have the same value within an at-risk organ and will only differ between at-risk organs. But this is not a necessary condition. Another constraint is the "conformational constraint", i.e. the protection of the surrounding tissue. As shown above, this condition can be formulated similarly:

$$d_i \leq 60\%, i \in U.$$

Here, U is an index set that specifies the vicinity of the target volume outside the specified margin; "60%" represents 60% of the maximum dose.

In the further considerations, only the criterion of the upper dose limit in organs at risk is taken into account. Other criteria are implemented in the same way. For this purpose, corresponding *penalty functions* (penalty functions) rP are defined, which are added to the objective function F_1. They are defined such that minimization of the resulting objective function $F = F_1 + rP$ leads to modulation profiles x that converge to a solution of the constrained optimization problem for a sequence of r-values tending towards ∞ (Künzi and Oettli 1969). In this way, the present constrained optimization problem is transformed into a sequence of free optimization problems. For the constraint formulated in equation (4.3), the following penalty function is defined:

$$rP(\mathbf{x}) = r \parallel \mathbf{R}(\mathbf{Dx} - \mathbf{g}) \parallel^2.$$

The parameter r can be interpreted as a weighting factor of the constraint. $\mathbf{R}$ is like $\mathbf{Z}$ a diagonal matrix whose elements are given by

$$R_{ii} = \begin{cases} 1 & \text{falls } i \in R \text{ and } d_i > g_i \\ 0 & \text{otherwise} \end{cases}.$$

Consequently, $P(\mathbf{x})$ is positive exactly when the constraint is not satisfied.

In addition to the medically justified constraints, there are also physical restrictions that require the modulation profiles to be non-negative everywhere. Thus the optimization problem can be defined by

$$F(\mathbf{x}) = \parallel \mathbf{Z}(\mathbf{Dx} - \mathbf{p}) \parallel^2 + r \parallel \mathbf{R}(\mathbf{Dx} - \mathbf{g}) \parallel^2 \overset{!}{=} \text{Min}$$

with the restrictions

$$x_i \geq 0, i = 1, 2, \dots, n$$

where n is the total number of needle beams.

4.3 Solution of the optimization problem

To solve such minimization problems, a variety of iterative algorithms are known, all of which are more or less similar to the *Newton iteration*:

$$\mathbf{x}(t+1) = \mathbf{x} \mid (t) - \gamma (\nabla^2 F(\mathbf{x}(t)))^{-1} \nabla F(\mathbf{x}(t)).$$

The gradient $\nabla F(\mathbf{x})$ in the present application, ignoring the factor 2, is given by:

$$\nabla F(\mathbf{x}) = \mathbf{D}'\mathbf{Z}(\mathbf{Dx} - \mathbf{p}) + r\mathbf{D}'\mathbf{R}(\mathbf{Dx} - \mathbf{g}).$$

The inverse of the *Hesse Matrix* $\nabla^2 F(\mathbf{x}) = \mathbf{D}'\mathbf{ZD} + r\mathbf{D}'\mathbf{RD}$ cannot be determined in an acceptable time due to the large dimension of $\mathbf{D}$. For this reason, the Hessian matrix is approximated by a diagonal matrix $\mathbf{S}$ whose diagonal elements coincide with those of the Hessian matrix:

$$S_{jj} = \sum_{i \in Z} D_{ij}^2 + r \sum_{i \in R, d_2 > g_1} D_{ij}^2$$

This matrix can easily be inverted by forming the reciprocal of the diagonal elements. $\mathbf{S}^{-1}$ can then be taken as the scaling matrix of the gradient. This gives the iteration equation:

$$\mathbf{x}(t+1) = \mathbf{x}(t) - \frac{1}{N}\mathbf{S}^{-1}\big(\mathbf{D}'\mathbf{Z}(\mathbf{Dx}(t) - \mathbf{p}) + r\mathbf{D}'\mathbf{R}(\mathbf{Dx}(t) - \mathbf{g})\big). \qquad (4.4)$$

If components of x(t + 1) become negative by subtracting the expression in parentheses, they are set to zero, i.e. x(t + 1) is projected onto the set of allowed non-negative values of x_i. The optimization algorithm defined by equation (4.4) is called the *scaled gradient projection algorithm* (Bertsekas and Tsitsiklis 1989). The normalization constant γ is assigned the value $\frac{1}{N}$.

A few comments should be added regarding convergence. The optimization problem defined above is a *convex problem,* since the objective function F is quadratic and thus, in particular, convex, and since the set of non-negative numbers projected to after each iteration step is a convex set. For such problems, it can be proved that the iteration algorithm (equation 4.4) converges to a minimal solution of the optimization problem (Bertsekas and Tsitsiklis 1989), at least for a constant value of r. However, the solution cannot be guaranteed to be unique; in fact, in general it will be non-unique because the problem is underdetermined. It can then be shown that in this case the iteration algorithm converges to a solution closest to the initial value of the iteration x(0) (Youla and Webb 1982). For this reason, it is important to start the iteration with a suitable starting value for the modulation profiles. In the context of this work, the result of the filtered projection is always used as the initial value.

To account for the medical constraints, the optimization problem must be solved according to the theory of penalty functions for a sequence of increasing values of r. The solutions then converge towards

a solution of the restricted problem (Künzi and Oettli 1969). It has been shown that this process is not critical. The constraints are already approximately fulfilled for relatively small values of *r* and this is quite sufficient for radiotherapy. Good results can also be obtained by setting *r* to a constant value of, for example, 30.

4.4   Comparison with ART

The iterative optimization algorithm defined by equation (4.4) has much resemblance to iterative algorithms known from image reconstruction (Rosenfeld and Kak 1982, Brooks and Di Chiro 1976, Jähne 1989). There the corresponding algorithm is called *algebraic reconstruction technique* (ART) and is used to reconstruct images from projections, e.g. in CT. In these applications, the vector of gray values or density values represents the left side of the iteration equation and the difference between measured projections and calculated (pseudo) projections represents the right side. The structure of the equation including scaling and normalization is identical to equation (4.4). Therefore, the experience made in image processing with such iterative algorithms can be directly adopted. The advantage of introducing penalty functions to account for constraints is the similarity of the terms with **Z** and with **R** on the right-hand side of equation (4.4). Restricted optimization can therefore be performed in the same way as free optimization.

The question of when to stop iteration is not easy to answer in image reconstruction (Brooks and Di Chiro 1976), and the same is true for conformation therapy. Based on studies in image reconstruction, according to which 5 to 10 iteration steps are required, at least 7 iterations are performed in the present work. If the dose at any point in the target volume is less than 80% of the maximum dose, further iterations are performed. If a satisfactory dose distribution in the target volume cannot be achieved, the constraints must be attenuated or more fields must be used.

4.5 Practical realization

The current realization of the optimization algorithm is based on the *contours* of the patient, the target volume and the organs at risk. The contour of the patient surface is automatically found in the corresponding CT data sets (Hyrum 1989). The contours of the target volume and the organs at risk are drawn in each CT slice by the radiotherapist. This set of contours defines the corresponding volumes. For this purpose, a three-dimensional data cube is created in the computer. Within this cube, the maximum permissible dose value is entered for each voxel if it is an at-risk organ voxel. If it is a target volume voxel, the prescribed dose value is entered. Points outside the "60% margin" (see section 4.1, criterion 4) are assigned - 1.

The target dose or maximum dose values are given as relative values. Later on, a normalization has to be carried out so that the desired absolute dose values are achieved. In principle, any target dose distributions can be specified. At present, in accordance with common practice, a *constant value* of 100% is applied to the total target volume. It has been shown that in this case the best results in terms of dose homogeneity in the target volume can be achieved if the maximum value of the dose d_{max} is normalized to this 100% after each iteration step. The objective function F_1 (Equation 4.2) is thus modified as follows:

$$F_1(\mathbf{x}) = \|\mathbf{Z}(\mathbf{Dx} - \mathbf{d_{max}})\|^2.$$

The results presented in III have all been calculated in this way.

The flow of the iteration is now as follows: Based on modulation profiles x(0) obtained by the filtered projection method, a dose calculation is performed: $\mathbf{Dx}(0)$. The Schoknecht formula described in II/3.4 is currently used for this purpose: Starting with the skin entry point given by the patient contour, the dose value determined by this formula is entered into a 3-D dose cube along each needle beam. The divergence of the radiation field is taken into account. Each needle beam is weighted with the corresponding value of the modulation profiles. The needle beams are assumed to be independent of each other; this means that scattering is not adequately accounted for. The resulting error can be up to 10% in unfavorable cases (see III/4.). The extent and voxel size of the dose cube is identical to the cube described above. Thus, the size of the voxels is determined by pixel and slice spacing of the CT image data. As in image reconstruction, the width of the needle beams must be greater than the edge length of the voxels (Jähne 1989).

After dose calculation, differences between the calculated and the prescribed (or maximum) dose in the target volume are determined according to equation (4.4): $\mathbf{Z}(\mathbf{Dx}(0) - \mathbf{p})$. Similarly, differences according to $\mathbf{R}(\mathbf{Dx}(0) - \mathbf{g})$ are formed in those areas of the organs at risk where the calculated dose is greater than the permitted value. These differences are multiplied by r. If a "conformation criterion" (see 4.1, criterion 4) is given, then the same procedure is followed in the areas outside the margin around the

target volume. The determined difference values are entered into another 3-D cube.

This "difference cube" is now projected along the needle beams, weighted by the respective depth dose value, onto the modulation profiles (this corresponds to the application of **D'**) and scaled by $\frac{1}{N}$ **S**$^{-1}$. The beam divergence is also taken into account here, i.e. a *fan projection* is performed. The profiles thus obtained are correction profiles which have to be subtracted from the original profiles x(0) according to equation (4.4). Negative values are truncated. This gives new profiles x(l). In the next iteration step, these are treated in the same way as x(0). The value of *r* is increased by 5 at each iteration step, starting with *r* = 5.

The described algorithm is currently implemented in FORTRAN on a VAXstation 3200 (Digital Equipment). The execution time for one iteration step is in the order of 3 minutes. For the 2-D optimizations shown in III/2. this time is only about 10 seconds.

4.6   An Approach to Parallelization

The entire optimization (7 iteration steps) requires about 20 minutes of computing time. As this procedure only has to be carried out once for each patient, this is still acceptable. Now, however, it is desirable to implement the more accurate dose calculation from II/3.4 instead of the Schoknecht formula. The associated greater computational effort would lead to an increase in execution times by more than a factor of 3 (triple execution of ray tracing, additional 2-D convolutions). Therefore, the calculation should be accelerated. One way to do this is to slightly modify the optimization algorithm.

The currently implemented version of the ART with the form

$$\mathbf{x}(t+1) = \mathbf{x}(t) - \mathbf{S}^{-1}\nabla F(\mathbf{x}(t))$$

(Equation 4.4) is called the *Jacobi algorithm* (Bertsekas and Tsitsiklis 1989) or *simultaneous iterative reconstruction technique* SIRT (Brooks and Di Chiro 1976). As described above, all modulation profiles are corrected simultaneously, which explains the name. However, another variant of ART is commonly used in image reconstruction. The following modified iteration rule is used:

$$x_i(t+1) = x_i(t) - \frac{\nabla_i F(\mathbf{z}(i,t))}{S_{ii}}$$

with

$$\mathbf{z}(i,t) = (x_1(t+1), \dots, x_{i-1}(t+1), x_i(t), \dots, x_n(t))'$$

In mathematics, such algorithms are called *Gauss-Seidel* algorithms (Bertsekas and Tsitsiklis 1989). In terms of conformation therapy, the difference with the Jacobi algorithm is that the modulation profiles are corrected after computing *each component* of the gradient at the appropriate point, rather than after

computing the entire gradient. This means that the latest information is always taken into account. As a result, Gauss-Seidel type algorithms generally converge faster than Jacobi algorithms.

In the present work, a Gauss-Seidel type optimization algorithm has been implemented experimentally. However, the expected improvement in convergence behavior was small. Sensitive dependencies on the correction order of the modulation profiles were found. Problems arose because the modulation profile values that were corrected first were given too much weight, which caused the intensities of the radiation fields to be unevenly distributed even in cases where this was not necessary. The small improvement in convergence is thus associated with a number of difficulties, and consequently work continues with the SIRT algorithm.

Another way to speed up the computation is to *parallelize* the algorithm. The special hardware required for this has become available at affordable prices in recent years, in particular through the development of *transputers*. Now, the Gauss-Seidel iteration is a sequential algorithm already by its approach, and the interdependence of the correction values of the modulation profiles leads to the fact that a parallelization is not possible.

[Radiation source]

CT. Cube Dose cube

Target vol.

Transputer 1

Radiation source

CT. Cube Dose cube

Target vol.

Transputer 2

CT. Cube Dose cube

Target vol.

Transputer 3

Radiation source
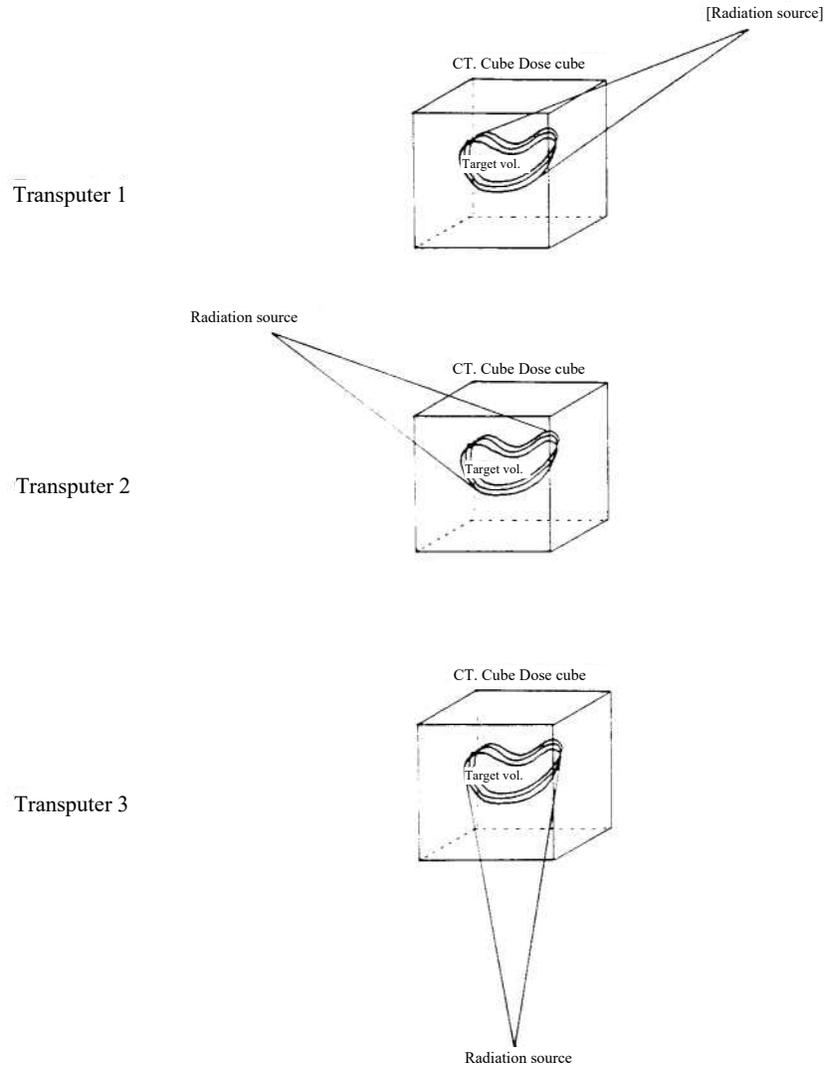
Fig. 4.2: *Schematic representation of the optimization of a three-field irradiation with 3 transputers.*

In contrast, the calculations in the SIRT algorithm are not coupled between the individual radiation fields, and it is therefore obvious to use a transputer for each field that performs the calculation steps described above independently. The only process that has to be performed by a central transputer is the superposition of the dose values resulting from the individual fields and the formation of the differences. Thus, the possibility of parallelization also speaks for the SIRT algorithm.

III   Results

In this part of the paper, the result of an investigation concerning the required *number of radiation fields* is first presented. It turns out that in most practical cases 7 or 9 fields are sufficient. When the number is increased further, the resulting dose distribution generally does not lead to clinically significant improvements.

The results of the methods presented in II/2 and II/4 are first demonstrated using a *two-dimensional study*. It is mainly those cases that can hardly be treated adequately even with the most modern methods available today that are presented. One such case is irradiation of the para-aortic lymph nodes, where the target volume is horseshoe-shaped. The filtered projection method described in II/2 is used to determine an initial value for the modulation profiles. The final solution to the inverse problem is found using the iterative procedure from II/4. Finally, a *3-D optimized dose distribution* based on a clinical case is shown.

It has been shown that with the new procedures described here satisfactory results can be obtained even in cases considered to be particularly difficult. The assessment of the calculated dose distributions is performed quantitatively using *dose-volume histograms*. In addition, visual assessments of the 2-D and 3-D representations of the dose distributions are made.

Finally, a comparison with measured data is performed to verify the new dose calculation method presented in II/3.

1. Number of radiation fields

Since field modulation is currently realized by individually cast compensators (Bürkelbach 1990, Lind and Källman 1990), it is desirable for practical reasons to get by with as few modulated beam fields as possible. Now it was shown in II/1.5 that the radiation fields can be compared with the projections of the CT. There, the number of projections is on the order of 100 or more (Rosenfeld and Kak 1982). To transfer such an order of magnitude to the number of radiation fields in conformation therapy is completely unrealistic. However, this is also not necessary, since the "resolution" of the dose distributions required in radiotherapy is significantly lower than the image resolution required in CT.

The few studies published so far in the literature concerning the number of fields come to very different results. A. Brahme uses about 5 fields. In contrast, a recent paper by S. Webb (1989) reports that at least 32 fields are required. This discrepancy can be partly explained by the fact that Webb always assumes an even number of fields. With uniformly distributed directions of irradiation in the angular range $0 - 2\pi$ this means that in each case two fields are incident in an opposing manner. In the range of the considered high energies and the associated low attenuation coefficients, however, no significantly better dose distribution can be achieved by two opposing fields than by one field. This fact has already been mentioned in (Brahme 1988). The consequence is that with 32 fields in the angular range $0 - 2\pi$ the same results are obtained as with 15 or 17 fields or even with 16 fields in $0 - \pi$. Similar is the case with the algorithm developed in the present work.

To show this, Figure 1.1 *dose-volume histograms* are shown for different numbers of fields. The ordinate of these histograms shows the number of volume elements (voxels) that are exposed to a relative dose greater than or equal to the value plotted on the abscissa. The underlying target volume is horseshoe-shaped, with a at-risk organ in the indentation (see Fig. III/2.1). The boundary condition is a maximum dose value of 40% in the organ at risk. The modulation of the fields was calculated using the procedures described here, i.e. first filtered projection and then iterative optimization. A 15 MV energy spectrum was assumed. The graph shows that the curves for 3 and 6 fields and 7 and 14 fields are practically identical. For this reason, the present work always uses an odd number of fields.
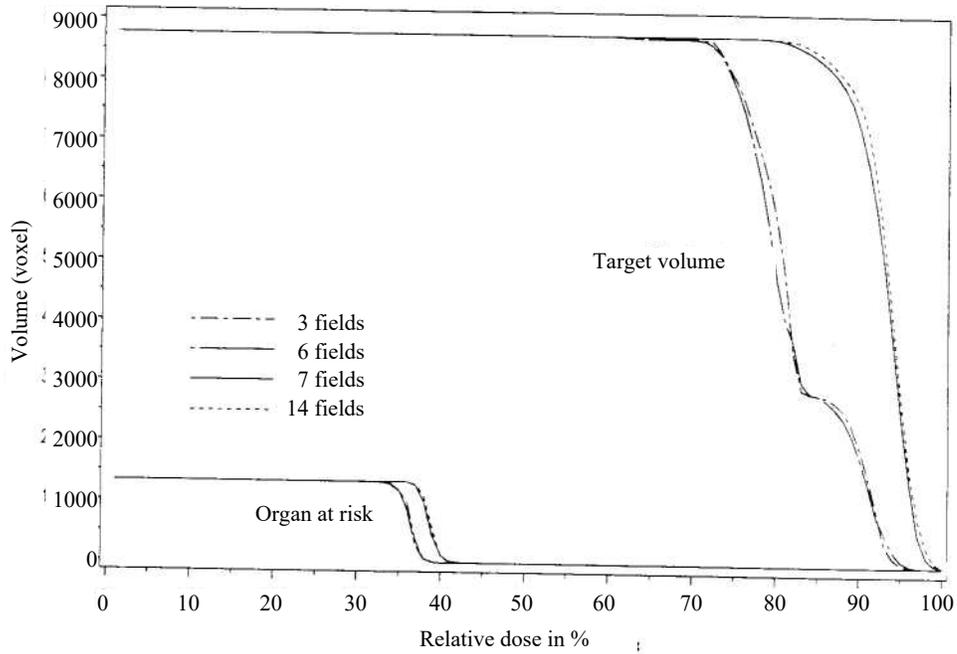
Fig. 1.1: *Dose volume histograms to compare even / odd number of fields. Virtually identical results can be obtained with 3 and 6 fields or 7 and 14 fields.*
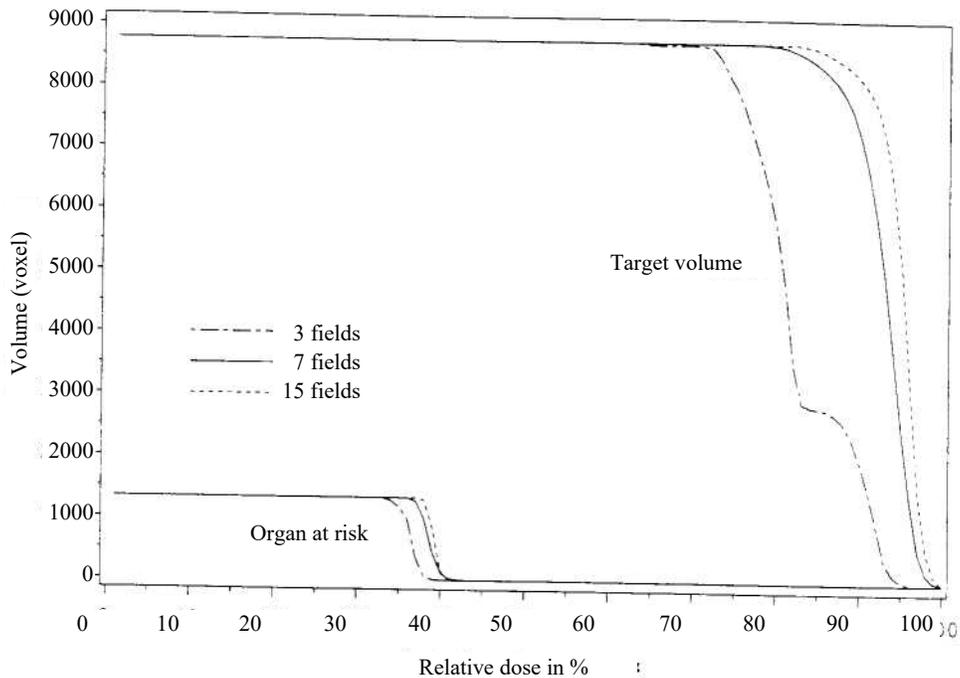
Fig. 1.2: *Dose-volume histograms for various odd field numbers. The improvement from 7 to 15 fields is not clinically relevant.*

In the same way, the dose distributions resulting from 3 to 15 radiation fields were compared for different target volumes. Figure 1.2 shows the corresponding dose-volume histograms for the horseshoe-shaped target volume with 3, 7 and 15 fields. In general it can be said that with increasing number of fields better and better dose distributions are obtained (assuming odd number). However, if the number of fields is increased from 7 to 15, the improvement is by far not as significant as from 3 to 7 fields, and the much greater effort required for 15 fields therefore does not appear to be justified. A clinical significance of the improvement from 7 to 15 fields cannot be expected, as the resulting dose differences are below 5%. Similar results are shown for other target volumes, so that in the present work we generally work with 7 or 9 fields.

Certainly, some extreme situations are conceivable in which no satisfactory dose distributions can be produced with 7 or 9 fields. In such cases, a larger number must be used. However, based on past experience, these appear to be few exceptions.

2.   Results of a 2-D study

Some complicated cases are considered which can hardly be treated adequately by conventional methods. All these cases are discussed in detail in the literature. The results obtainable with the new methods presented here are presented in the form of dose distributions and dose-volume histograms. All examples assume irradiation with 9 fields and 15 MV photons. The source-isocenter distance is 1 m in each case. A homogeneous cylindrical phantom is assumed, the diameter of which corresponds to the side length of the squares shown. The dose calculation is performed according to the Schoknecht formula described in II/3.4. The dose values presented are therefore still subject to errors of up to 10% (see III/4.2). For all cases, the filtered projection is applied first, and then *7* steps of iterative optimization are performed.

2.1   The horseshoe dose specification

In many clinical cases, two-dimensional sections through the target volume are horseshoe-shaped. Examples include irradiation of the *paraaortic lymph nodes* (Nemeth and Schlegel 1987), treatment of *esophageal carcinoma* and that of *collum carcinoma* (Morita 1974). Often, radiation-sensitive at-risk organs are located exactly in the concave indentation of the target volume. In the case of irradiation of the paraaortic lymph nodes, it is the spinal cord that should not be exposed to more than 30 Gy if possible (Becker 1989). With a required dose in the target volume of 60 Gy, which should be reached at 80% of the maximum dose, the tolerance limit in the spinal cord is consequently 40%.

 With these specifications and boundary conditions, the inverse problem was solved using the methods described. The results are shown in Figure 2.1. The good agreement of the 80% and 90% isodose with the edge of the target volume is clearly visible. The at-risk organ is left out. The dose-volume histogram shows that the boundary condition of a maximum dose of 40% in the organ at risk is fulfilled. The dose in the target volume after optimization is between 80% and 100%. A comparison of the dose-volume histograms for the results after the filtered projection (init.) and after the iterative optimization (opt.) is very clearly in favor of the iterative optimization because of the much greater homogeneity of the dose in the target volume. However, the load on the at-risk organ becomes somewhat greater and the 40%. Tolerance limit is completely exhausted.
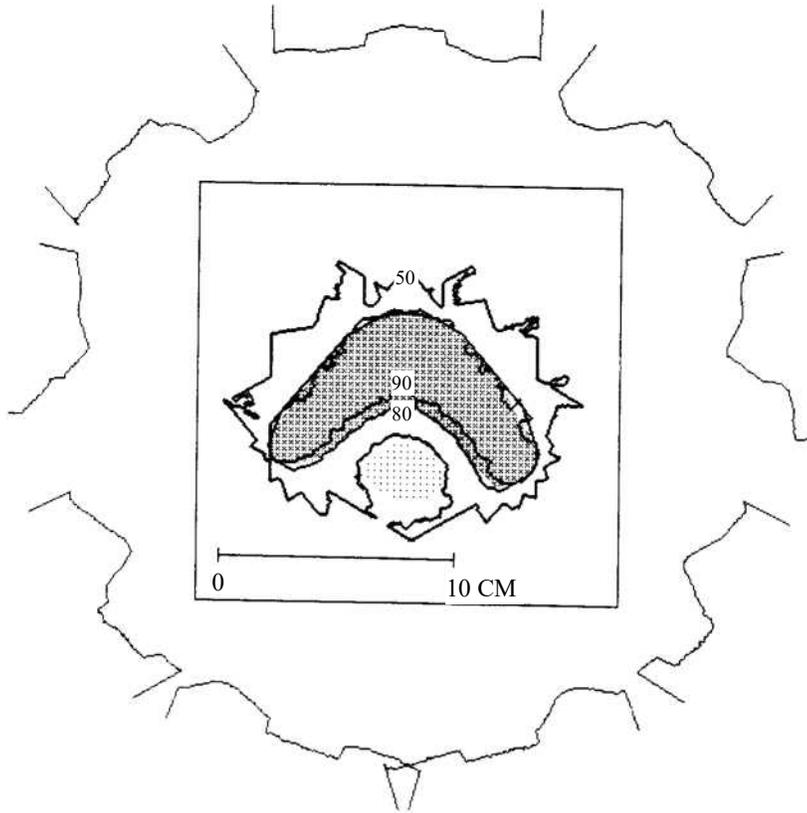
Dose Volume Histogram. Horseshoe Dose
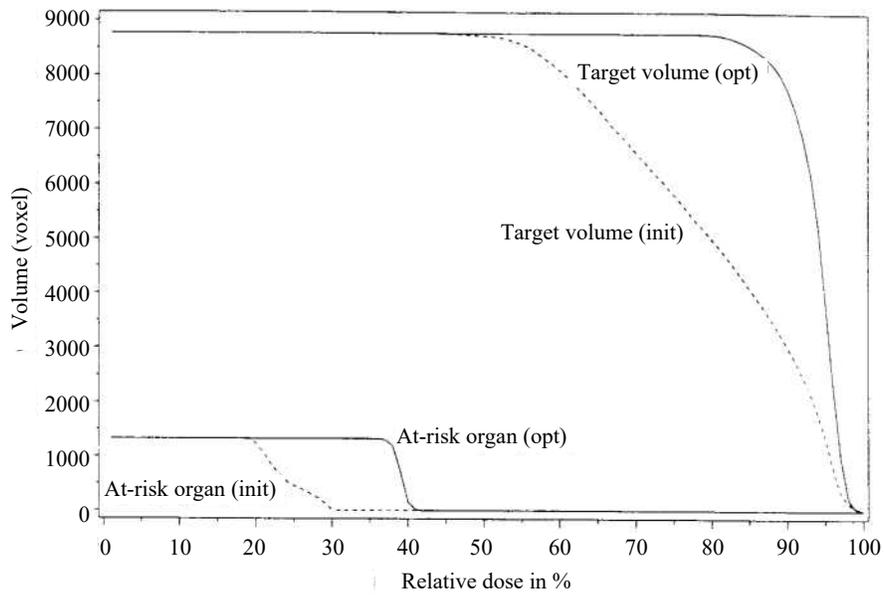
Fig. 2.1: *Irradiation of a horseshoe-shaped target volume (crosses) with consideration of a at-risk organ (points). Plot of dose distribution (50%. 80% and 90% isodose lines), modulation profiles and dose-volume histogram.*

2.2 The Brahme dose specification

A target volume with two concave regions occurs in the irradiation of *cervical stump carcinoma* with lymph node involvement. Similar forms are also seen in some slices of collum carcinoma. This target volume, much used in Brahme's (1988) studies, is shown in Figure 2.2. No at-risk organs to be given special consideration are indicated here. The goal is to realize a treatment limited to the target volume in the sense of conformation therapy and to achieve the greatest possible homogeneity of the dose distribution in the target volume. Therefore, a maximum distance of the 60% isodose line from the target volume of 2 cm is specified as a boundary condition.

Looking at the results in Figure 2.2, it is noticeable that with these criteria a very good fit of the dose distribution to the target volume is achieved. Only the 40% isodose no longer follows the shape of the target volume. The dose-volume histogram shows that the already quite good result of the filtered projection (init.) can be improved again considerably by the iterative optimization. The dose in the target volume then only varies between 85%> and 100%.
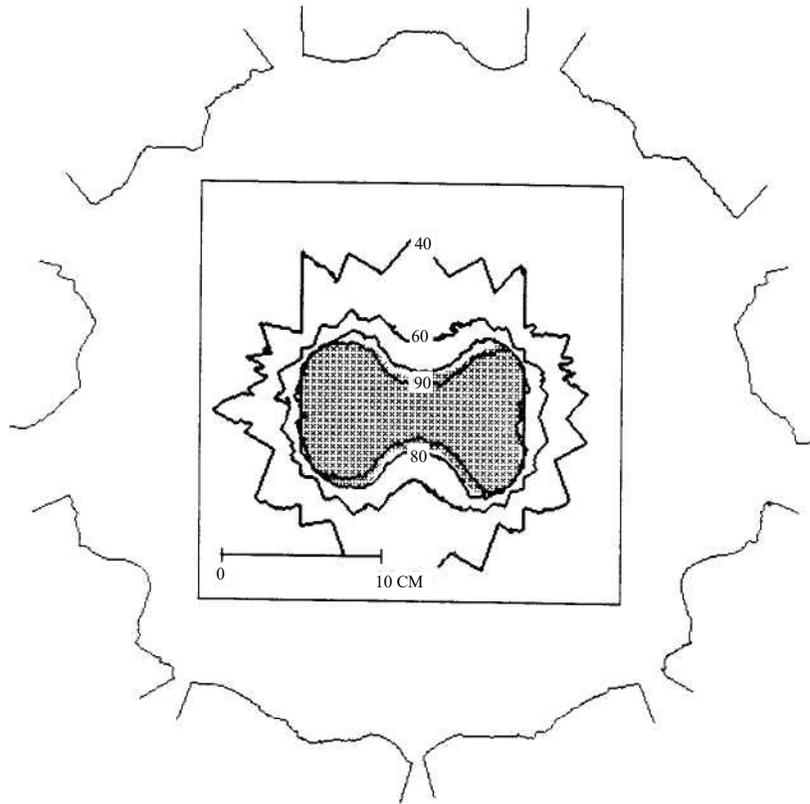
Dose Volume Histogram. Brahme dose
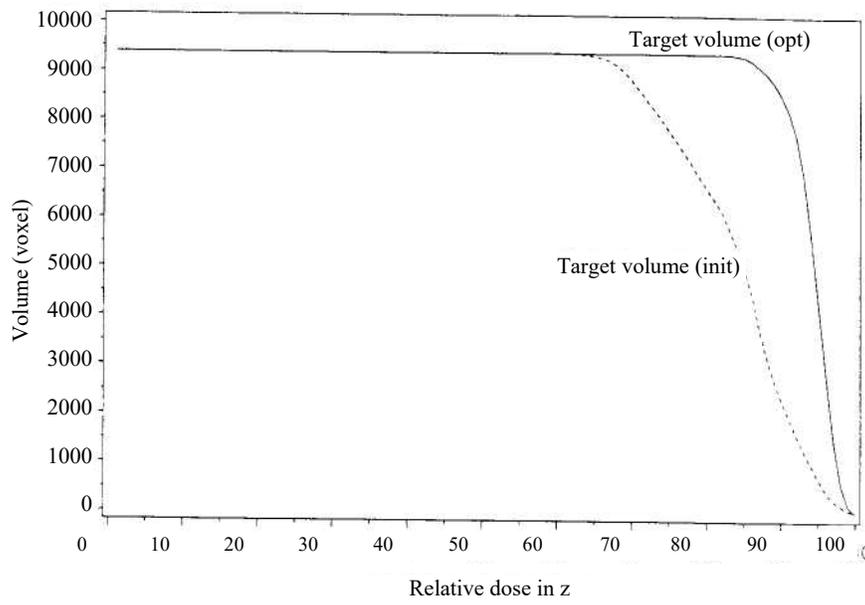
Fig. 2.2: Irradiation of the Brahme target volume as a model of cervical stump carcinoma or collum carcinoma. Shown are the dose distribution (40%, 60%, 80%. and 90% isodose lines), modulation profiles, and dose-volume histogram.

2.3   The Takai dose specification

In the following it will be shown that the use of the modulation technique is also useful for non-concave target volumes. For this purpose, a case discussed by Takai (1987) is used. It is the radiation of a bladder carcinoma. Because of the simple shape of the target volume, this alone is not a major problem. However, in order to spare the patient unpleasant side effects in the rectum, this must be protected to the maximum, which is difficult to achieve with conventional methods. In the present observation, a maximum value of 20% is specified for the rectum. Such a low value is not clinically essential; it is only intended to demonstrate the performance of the methods described here. A similar case, where the greatest possible protection of an organ at risk is absolutely necessary, occurs, for example, in the irradiation of brain tumors, where the lens of the eye may be irradiated with a maximum of 10 Gy in order to prevent clouding.

The representation of the result in Figure 2.3 shows that the given requirements can be fulfilled. After iterative optimization, the dose in the target volume varies only between 90 and 100%. Here, as the dose-volume histogram shows, the optimization results in both an improvement of the dose distribution in the target volume and a significant reduction of the exposure of the organ at risk to the permitted 20%.
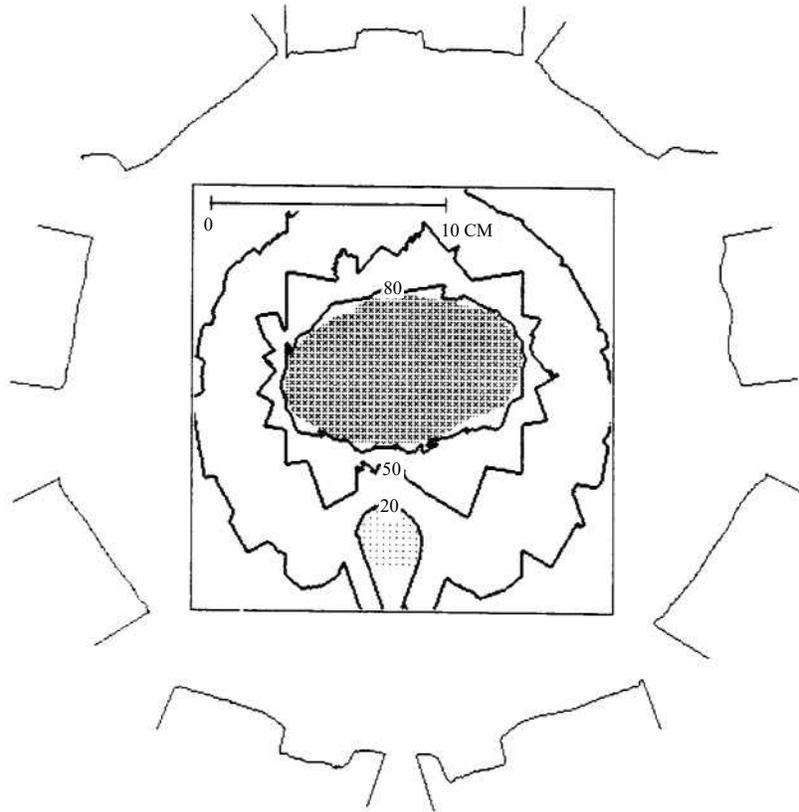
Dose Volume Histogram. Takai dosage
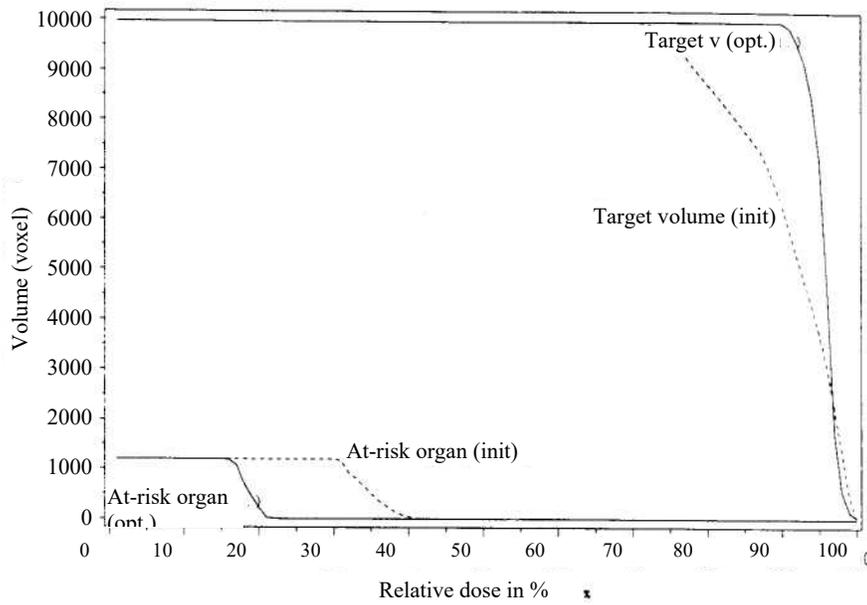
Fig. 2.3: *Irradiation of Takai target volume as a model of bladder carcinoma. The target volume is indicated by crosses and the dots represent the organ at risk (rectum). The dose distribution is shown here by the 20%, 50%, and 80%. isodose lines.*

3.   3-D optimization of a clinical case

The case of a 53-year-old female patient suffering from a small cell carcinoma of the nasopharynx (nasopharyngeal carcinoma) is considered. This is a tumor that grows extraordinarily fast. The patient has already been irradiated once. However, due to metastasis, follow-up radiation was required. For prophylactic reasons, a generously dimensioned target volume was chosen, which projects far into the frontal sinus. The target volume is convex in the lower slices and becomes horseshoe-shaped in the upper levels. Particularly critical are the middle slices, where the eye lenses are located as as-risk organs that require special protection. If the dose exceeds 10 Gy at these sites, lens opacities are unavoidable.

In applying the methods described here to this case, irradiation with 9 intensity-modulated fields and an energy of 15 MV was again assumed. The dose limit in the eyes was set at 20% of the maximum dose. The width of the "60% margin" was set at 3 cm. The result can be seen in Figure 3.1. The good agreement of the range of the therapeutic dose represented by the 80% isodoses with the target volume is clearly visible. The eye lenses shown in green are outside this range.
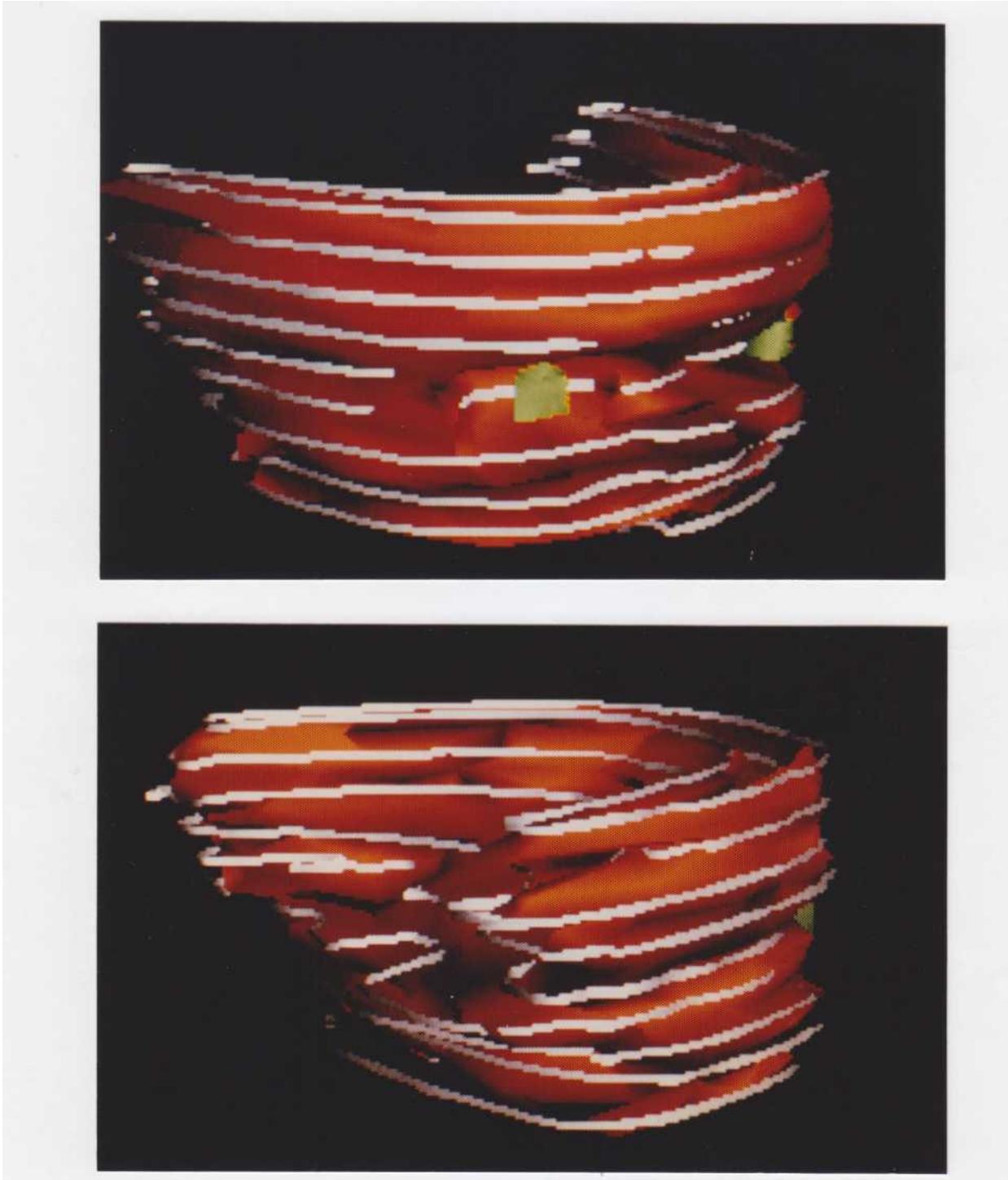
Fig. 3.1: Result of 3-D optimization: Representation of the target volume (red), the 80% isodoses (white bands) and the eye lenses (green) under different viewing angles. In the upper plot, it can be clearly seen that the lenses of the eye are outside the range of the therapeutic dose.

In order to be able to compare the new methods, these results are compared in the following with a complex radiation plan according to which the patient is currently being treated at the DKFZ. In doing so, the technologies available today are fully exploited. Irradiation takes place over four fields, which are irregularly blanked with the multi-leaf collimator. In the case of two fields, the irradiation direction is not in the plane of the CT slices *(non-coplanar technique),* thus approximating the complex shape of the target volume. To distinguish it from the plan optimized according to the new methods, this plan will be referred to in the following as the "conventional" plan for short. For the orientation of the radiation fields see. Figure 3.2.
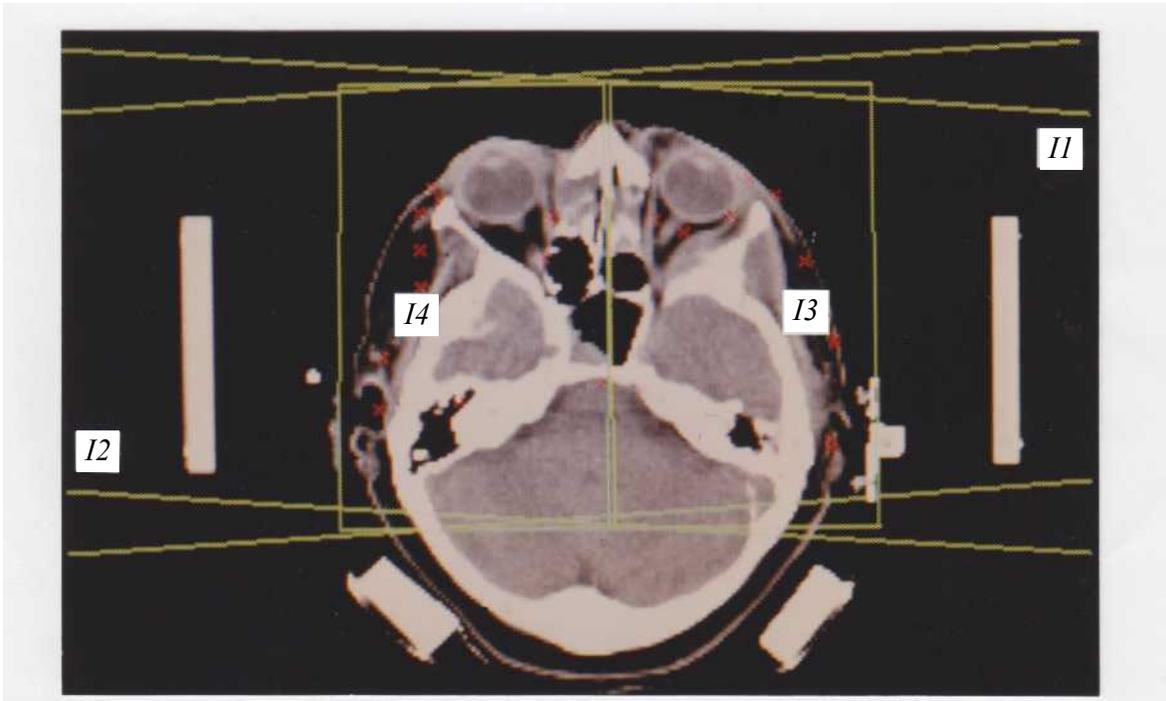
Fig. 3.2: Location of the radiation fields in the "conventional" plan. The field boundaries are represented by green lines. Fields I1 and I2 are oppositely incident from lateral directions. The directions of the fields I3 and I4 are perpendicular to the plane of representation. The drawn rectangles correspond to the borders of these fields. Their distance is about 2 mm. All fields are additionally blanked by the multi-leaf collimator according to the projection of the target volume onto the beam source.

On the following pages (Fig. 3.3a-d), the dose distributions of the "conventional" plan are compared with the optimized plan. The comparison is made in different sections of the CT dataset. The dose range 60-80% in dark blue and 80-100% in light blue is shown in the so-called "colorwash" representation. The CT images are overlaid with the corresponding dose color.
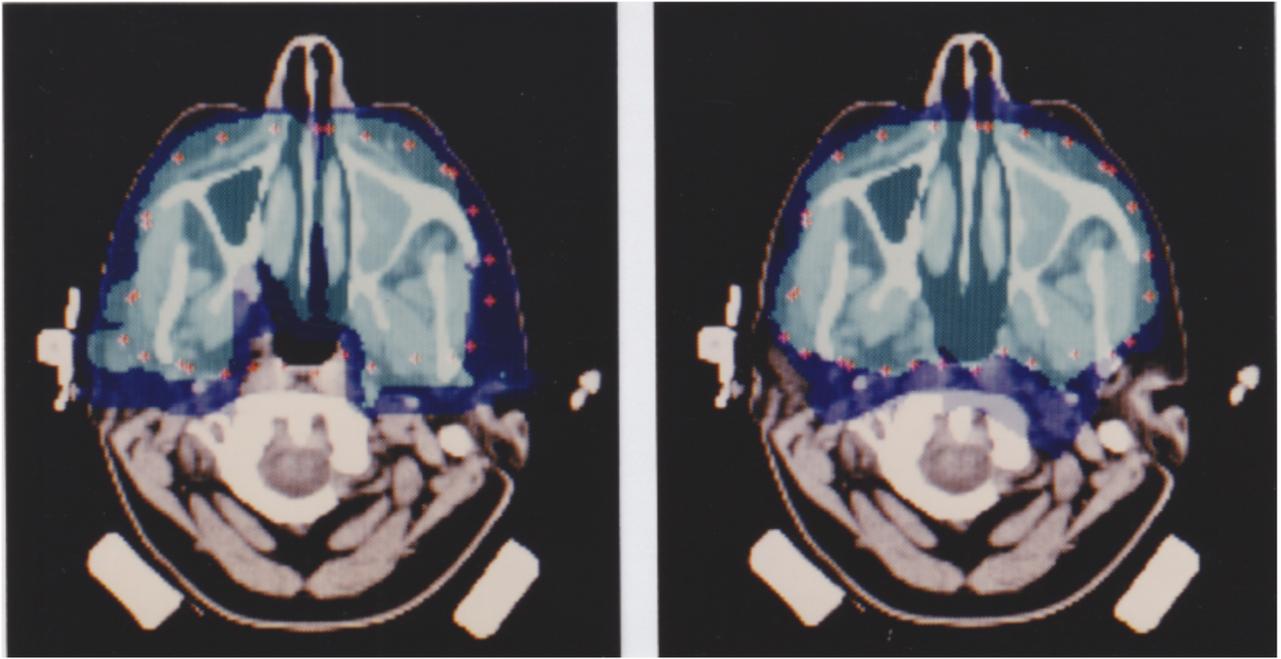
Fig. 3.3a: *Transverse section in CT slice 6*
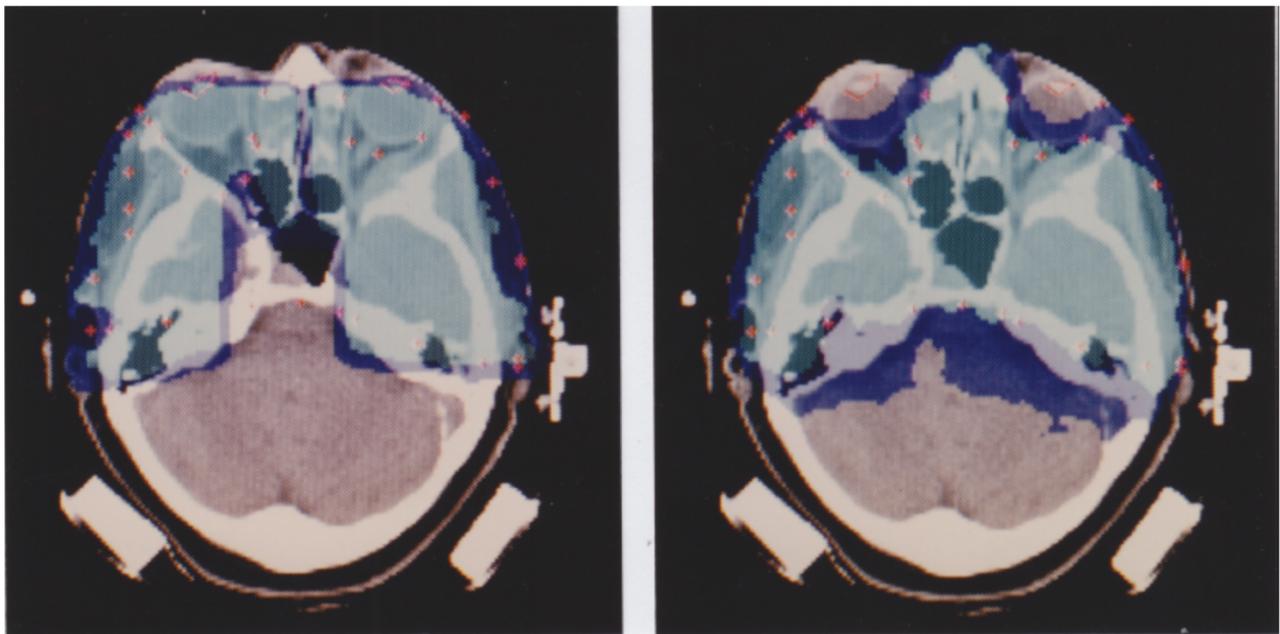
Fig. 3.3b: *Transverse section in CT slice 14*
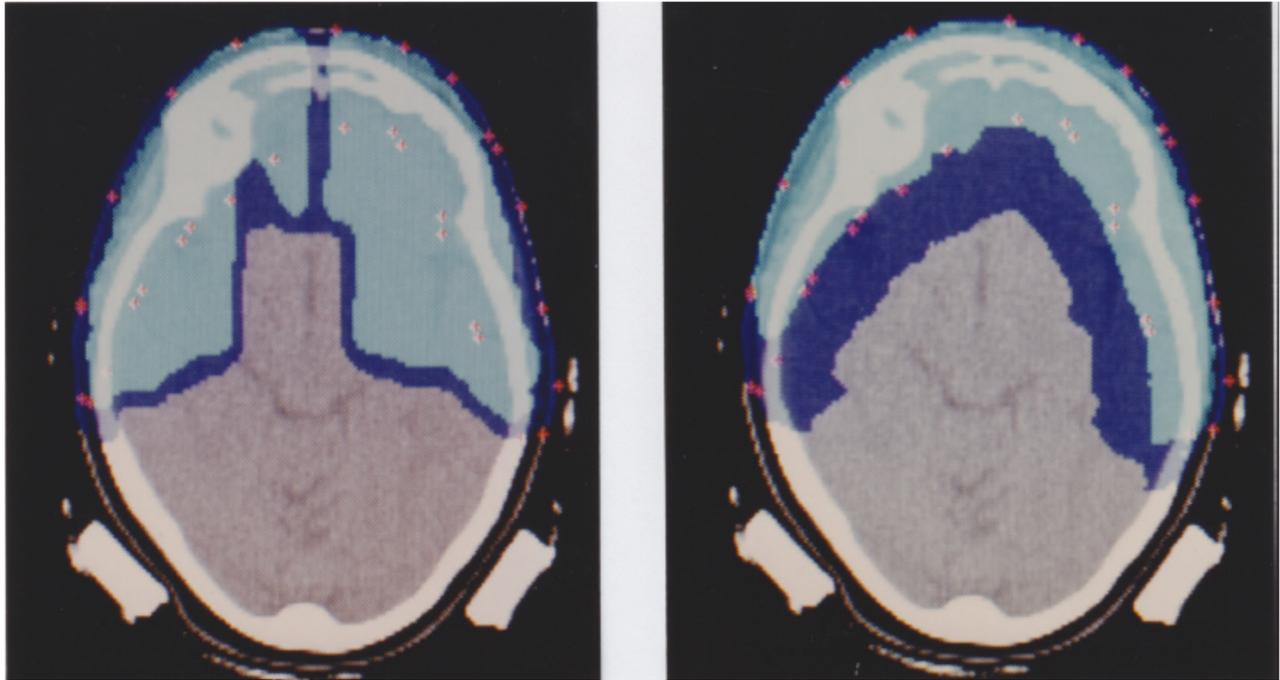
Fig. 3.3c: *Transverse section in CT slice 20*
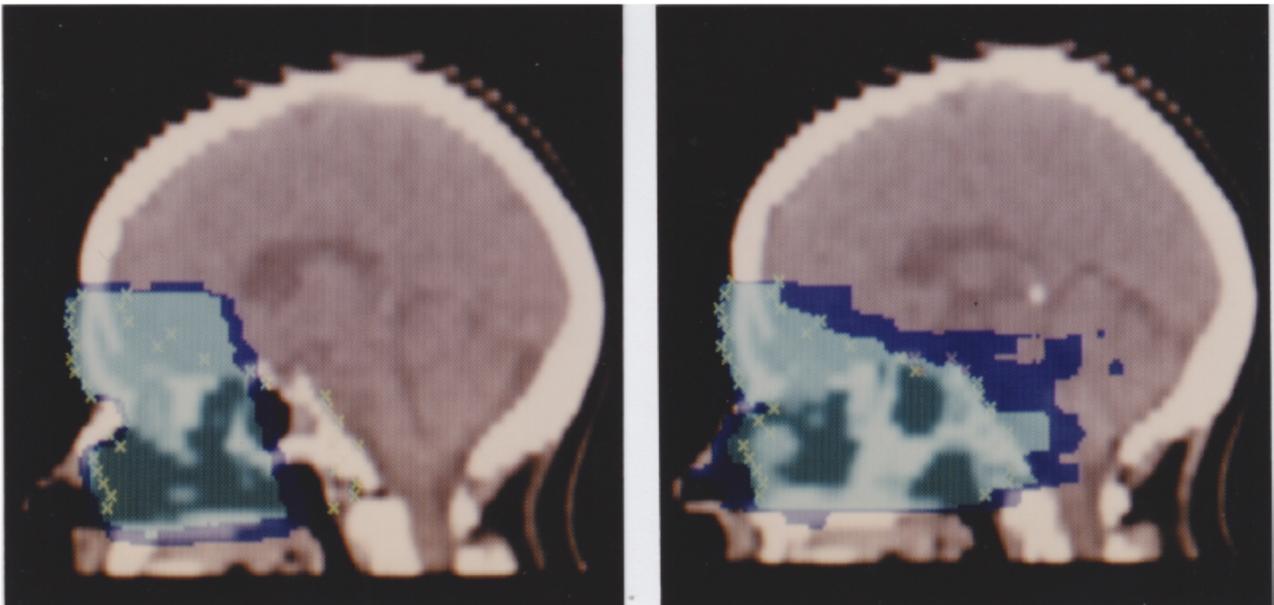
Fig. 3.3d: *Sagittal section*

The left side shows the "conventional" plan and the right side the optimized plan. When looking at these illustrations, the following stands out:

3.3a   The target volume is simply convex in shape in this region. The optimized plan shows a good fit of the dose areas to the target volume represented by red crosses. In the "conventional" plan, underdosing occurs in the middle range.

3.3b   A middle slice at the level of the eyes is shown. The target volume has a complicated shape. Again, the optimized plan shows a good match of the high dose area with the target volume. The eye lenses outlined in red are clearly outside this area. With the "conventional" plan, on the other hand, the lenses are not protected. Also, the underdosing in the middle shows up again.

3.3c   In this upper slice, both plans are acceptable.

3.3d   The sagittal section again shows clear advantages in favor of the optimized plan. The edge of the target volume is indicated here by green crosses. With the "conventional" plan, there are both under- and overdoses.

The comparison of the dose-volume histograms also clearly shows the difference between "conventional" planning and the new methods presented here (Fig. 3.4). In the "conventional" plan, the dose-volume histogram of the ocular lenses differs only slightly from that of the target volume, i.e. the lenses are loaded with practically the full therapeutic dose. The optimized plan, on the other hand, shows a much lower load on the lenses. However, the secondary condition according to which a maximum of 20% of the maximum dose is allowed in the organ at risk is not yet fulfilled after the performed 7 iteration steps due to the extreme proximity of the organs at risk to the target volume. To achieve this goal, the weighting factor of the penalty function r would have to be increased even further. However, this would worsen the dose homogeneity in the target volume. The solution found after 7 steps can therefore be considered a good compromise. This fact also speaks in favor of the introduction of the penalty functions: If the constraints cannot be fulfilled exactly, there is at least a useful compromise. To achieve even better results in this particularly difficult case, more radiation fields would have to be used.

Dose-volume histogram. conventional
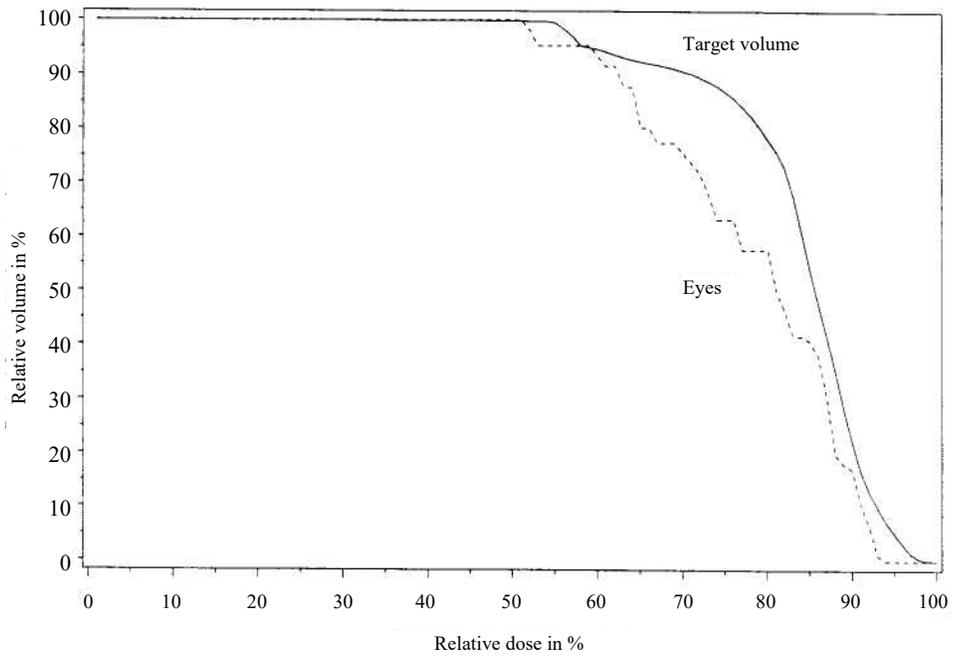
Dose-volume histogram. optimized
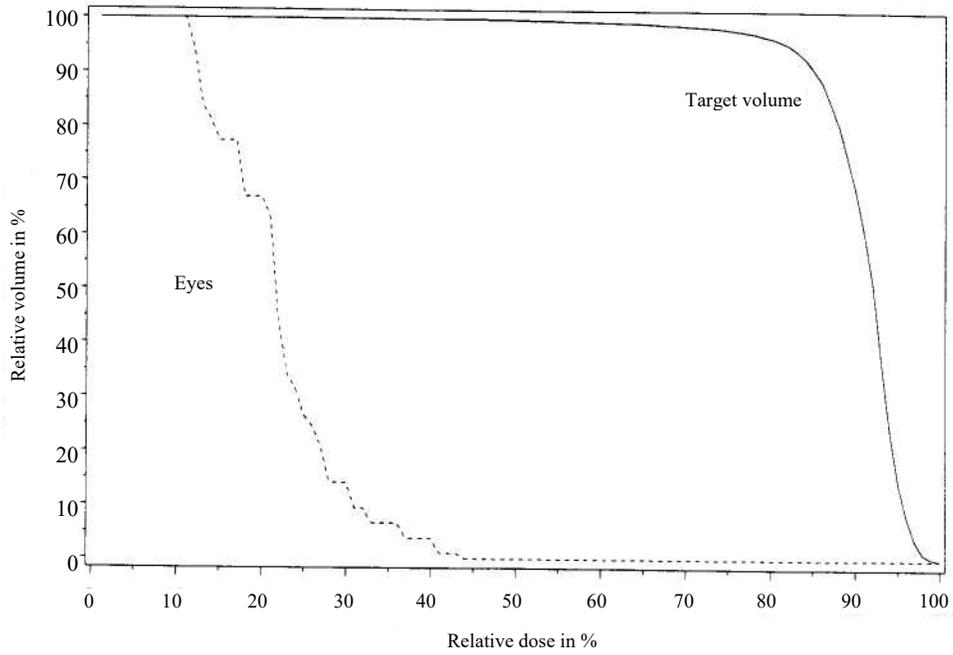
Fig. 3.4: Comparison of dose-volume histograms for the "conventional" plan (top diagram) and the optimized plan (bottom diagram). Both target volume and organs at risk (ocular lenses) were normalized to 100%.

4. Verification of dose calculation - comparison with measurements

4.1 Depth dose curves

Figures 4.1 and 4.2 show depth dose curves calculated according to the method described in II/3.4 (equation 3.9) for ^{60}Co and 15 MV photons at different field sizes (solid lines). The factor $1/(P\text{-}z)^2$ was not considered, i.e. an infinite source-isocenter distance was assumed. The curves should therefore correspond to measured GLV or GMV values (see II/3.4).

The comparison shows that the deviations are less than 1% for depths greater than the build-up depth. The lower attenuation in the larger fields, which is due to scattering, is well captured. Larger deviations can be seen in the area of the build-up effect. This is due, as described in II/3.4, to the electron contamination in this region, which is not considered in the model presented there.

4. Comparison with measurements
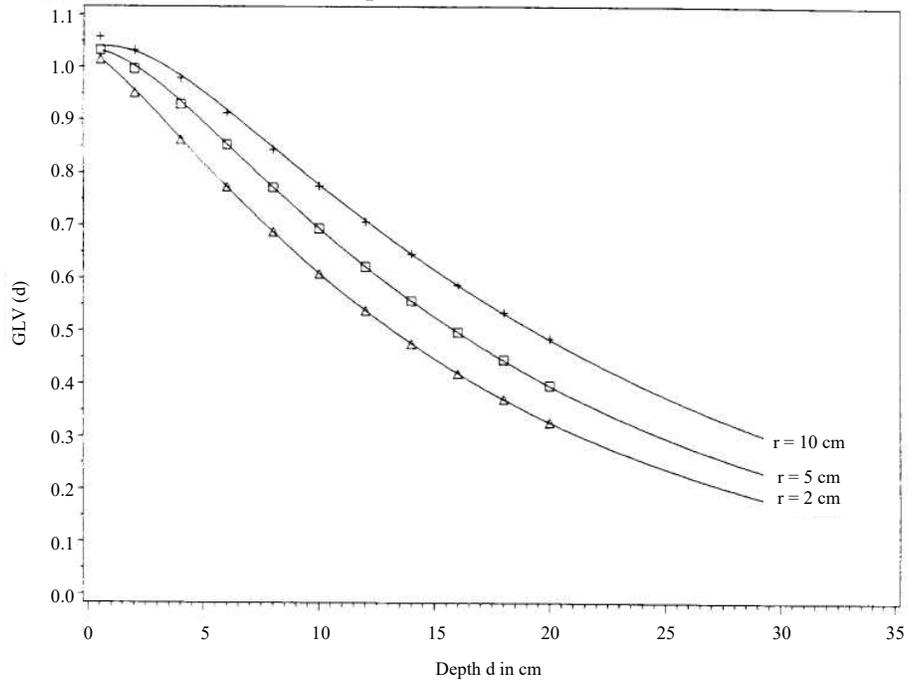
Fig. 4.1: *Comparison of measured GLV values for ^{60}Co at different field radii (+, □, Δ) and values calculated according to II/3.4 (solid lines). Source of measured data: (Johns and Cunningham 1983).*
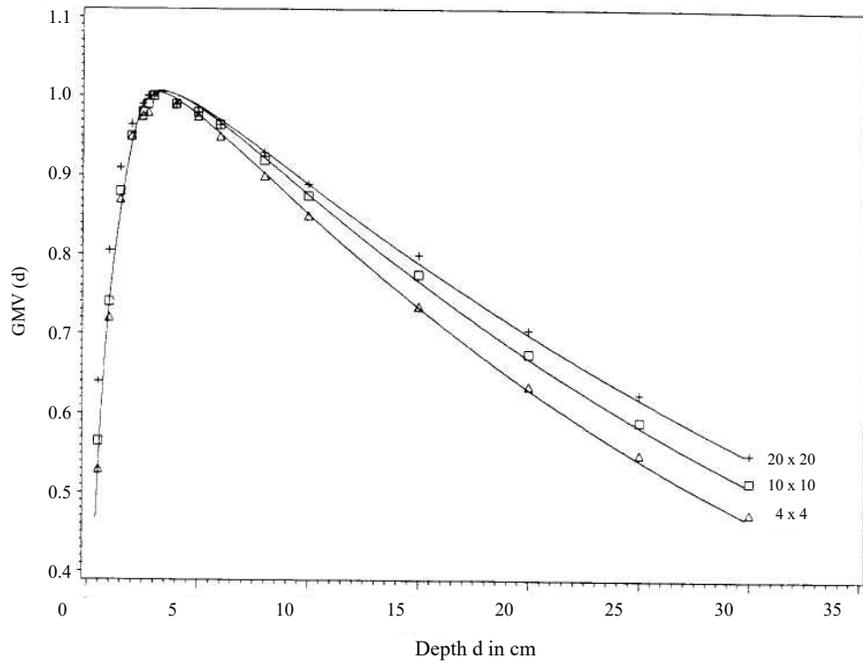
Fig. 4.2: *Comparison of measured GMV values for 15 MV bremsstrahlung at different field sizes (+, □, Δ) and values calculated according to II/3.4 (solid lines). These are square fields; the areas refer to the unit cm². Source of measured data: (Paul et al 1983).*

4.2 Transverse distributions

In order to investigate the accuracy of dose calculation for modulated fields, a $10 \cdot 10$ cm² field is considered, which is provided with a 1.5 cm wide block. The attenuation of the primary flux [by/through] this block is 97%. This can be considered an extreme form of modulation.

Figure 4.3 shows the tissue maximum ratios GMV along a lateral profile for this field. The dose values determined with the dose calculation from II/3.4 are in good agreement with measured values. The deviations are also smaller in the area of the penumbra under the block than *3%*: only in the area of the largest gradient the error is larger. The dose produced by scattered photons under the block is thus correctly detected by the calculation.

Also shown in Fig. 4.3 are GMV profiles obtained by neglecting the scattering effects (dashed lines). Deviations from the measured data and from the more exact calculation are in the order of 10%. This means that errors of up to this magnitude may occur in the results presented in III/2 and III/3, where the scatter has not yet been adequately taken into account.
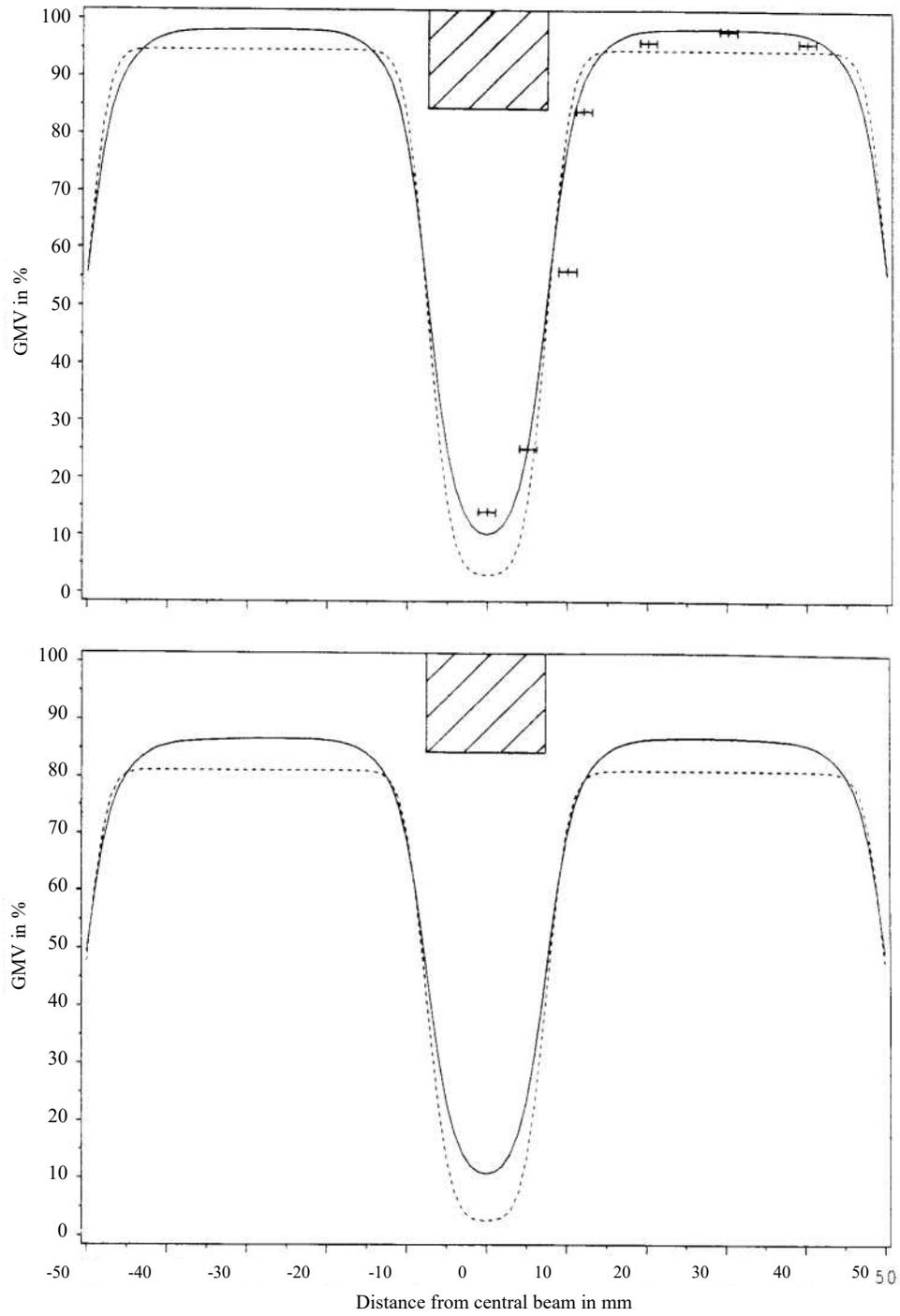
Fig. 4.3: *GMV profiles for 15 MV photons at a* $10 \cdot 10$ *cm²* *large field at 5 cm depth (top) and at 10 cm depth (bottom). The field is provided with a 1.5 cm wide block with 97% attenuation. The solid lines are based on calculated values according to II/3.4. The dashed lines result from disregarding the scattering effects. Additional measured values are entered in the upper plot (source: Mackie et al. 1985).*

IV Discussion and outlook

The determination of radiation parameters is one of the most important processes in radiotherapy planning. A dose distribution appropriate to the individual patient geometry, the respective tumor shape and the location of particularly endangered at-risk organs must be realized. With the introduction of modulation technology by Cormack (1987) and Brahme (1988), this has become possible, at least in principle. However, the determination of suitable modulation profiles is computationally very complex and can in no case be performed "by hand" by the radiotherapist.

The method of *filtered projection* adopted from image reconstruction and modified accordingly in the present work for this purpose allows very fast calculation of the modulation profiles. However, it is based on a number of approximations and simplifications. It is therefore only used to determine initial values for an iterative optimization. However, by further improvements of the filter function as well as by an implementation of correction methods to take into account physical conditions such as beam attenuation, it should be possible to find solutions that are closer to the optimum. Very few iteration steps would then be required. However, it cannot be expected that in the filtered projection such criteria as the specification of a maximum dose value in at-risk organs can also be integrated. The setting of a negative target dose value in the area of the organs at risk, as propagated by Brahme in the method he developed for this purpose, again amounts to "trial and error" procedures, which are precisely what should be avoided.

Iterative optimization also relies on methods that have long been used in image reconstruction. The introduction of *penalty functions* makes it possible for the first time to take various medical criteria into account. This is a significant advantage over another recently published method based on *simulated annealing* (Webb 1989). No radiation-sensitive areas can be particularly protected there. Another advantage of the method developed here is that it is a true 3-D optimization. Thus, unlike other methods, a parallel beam is not assumed and the 3-D optimization is replaced by slice-by-slice 2-D optimizations, but the beam divergence in all directions is taken into account. Furthermore, the low time expenditure is to be emphasized: The total execution time of the currently implemented optimization algorithm for a complete 3-D optimization is about 20 minutes on a VAXstation 3200 (Digital Equipment). Webb's method, on the other hand, takes about 12 hours for only one 2-D slice (!) on the VAX 750, which is, however, slower by a factor of 4-6.

The iterative optimization method can be based on any dose calculation algorithm. Particularly suitable for this purpose is an algorithm newly developed in the present work, which adequately takes into account the scattering behavior changed by the modulation of the fields. First comparisons with measured data prove that sufficient accuracies can be achieved even with extremely modulated (e.g.

blocked out) fields. However, one shortcoming of the algorithm at present is that inhomogeneities of the tissue are not adequately taken into account in the calculation. Further developments and measurements are needed in this respect.

In the current implementation of the optimization algorithm, the newly developed dose calculation algorithm is not yet used. Instead, a simplified calculation formula according to Schoknecht (1968) is used. The comparison with measured data shows that in extreme situations deviations of up to 10% of the maximum dose can occur. Therefore, an early implementation of the new algorithm is desirable. Major changes are not necessary, since the new algorithm is also essentially based on *ray-tracing* methods.

The application of the methods developed here to some target volume models taken from the literature and considered to be particularly difficult shows that very good results can be obtained in these cases. In general, 7 or 9 radiation fields are sufficient. When applied to a clinical case, a significantly better dose distribution can be achieved than with the most modern methods available today. It should be emphasized once again that this does not require any "trial and error" procedures, but that the optimal parameters are found automatically. Extensive clinical studies would have to be carried out in order to show that significantly better success in tumor treatment can be achieved with the new methods. Such investigations would then also have to take into account the large personnel and technical effort required for the individual production of the compensators. However, should scanning accelerators become available on a larger scale in the future, at least the personnel effort would be reduced.

In the algorithm realized so far for the determination of the irradiation parameters, the physical dose distribution is optimized. The physician must know the effect of the dose on the various organs and specify the dose required to destroy the tumor in the target volume and the maximum tolerated dose in the respective organs at risk. It would therefore be desirable to include criteria that directly take into account the radiobiological effect. Here, the concept of tumor control probability and complication probability in organs at risk, recently introduced by Lyman (1989), should be explored in particular. Finally, it should be explored whether a departure from the conventional target dose specification in radiotherapy (homogeneous dose in the target volume, if possible no dose outside) appears to be reasonable. This can be done, for example, on the basis of tumor growth models (Düchting 1989). Should other dose distributions subsequently prove to be more favorable, such distributions could also be obtained using the methods described here. In this way, conventional fractionation schemes could be reviewed and, if necessary, modified.

For the planning and execution of a precision radiation therapy, many other steps are important in addition to the computational determination of the radiation parameters. In the area of planning, the main point to be mentioned here is the definition of the target volume. While CT information is essential for dose calculation, determination of target volume and organs at risk can often be better performed using NMR images (Lohrum 1989), in which soft tissue structures are much better resolved. Recently, the inclusion of positron emission tomography (PET) in the process of determining the relevant volumes has also been sought. In order to exploit the specific advantages of these different imaging techniques, the corresponding images must be correlated with each other, i.e. it must be possible to find a marked area of one image data set in the other data sets (End 1990). Defining the target volume requires a great deal of expertise on the part of the physician, which goes far beyond the information content provided by imaging techniques. For this reason, it has not yet been possible to determine the volumes automatically, although initial approaches have been presented in this regard (Wolf et al. 1989, Iglesias et al. 1989).

Another important process for the implementation of precision radiotherapy is the exact transfer of the calculated irradiation parameters to the irradiation on the patient. In the case of therapy with modulated fields, particular attention must be paid to the exact positioning of the compensators. An error estimate is still pending in this regard. However, it has been pointed out that under unfavorable circumstances even the smallest positioning errors can cause a large error in the dose distribution (Goitein 1990). However, first measurements have shown that the deviations from the calculated dose in practical cases are in the order of magnitude of the errors given by the simplifications in the calculation (Bürkelbach 1990, Lind and Källman 1990). Another problem is the exact positioning and immobilization of the patient during irradiation. In the head and neck region, a positioning accuracy of ± 1 mm can be achieved today using suitable devices (stereotactic frame) (Pastyr 1989). However, in other parts of the body, not least due to breathing, much larger errors are to be expected. Here it is necessary to develop suitable systems for positioning and possibly tracking the irradiation device during irradiation.

Only the interaction of all these sub-disciplines will make it possible in the future to improve local tumor control and at the same time reduce harmful side effects through more precisely adapted dose distributions. There is no question that this will mean a gain for the patient; the only question is how big this gain will be and how big the necessary effort, i.e. the costs, will be in comparison.

V Summary
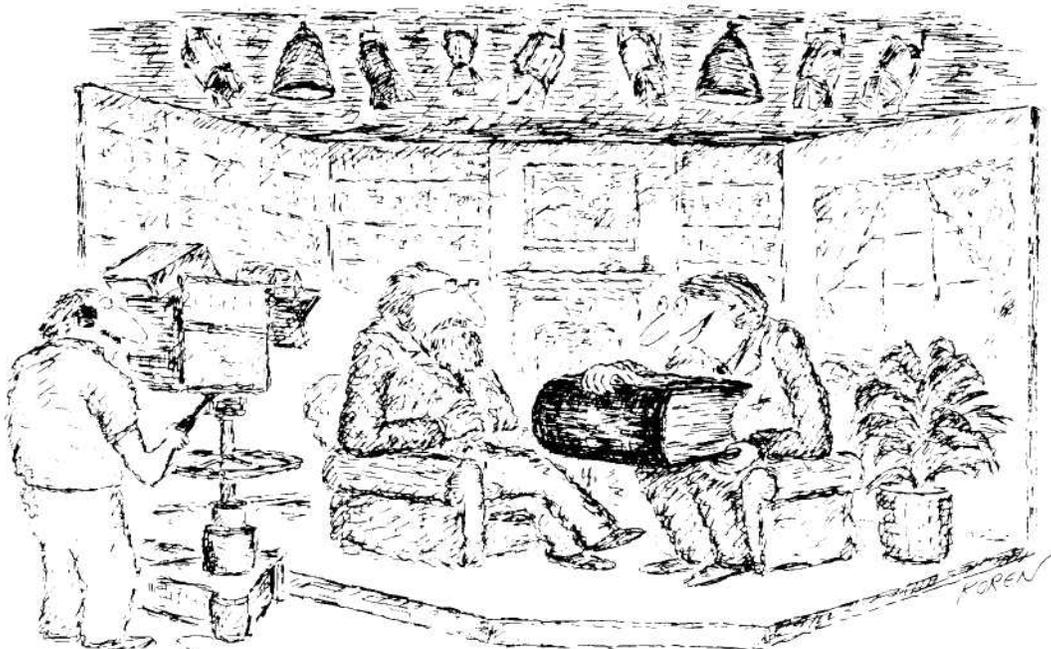
"If you were to boil your book down to a few words, what would be its message?"

New methods for the automatic determination and optimization of irradiation parameters for percutaneous radiotherapy with high energy photons are developed. The methods are based on an irradiation technique with intensity-modulated radiation fields. The essential problem is therefore to determine the shape of the modulation profiles for the individual fields, based on the specified target dose distribution. This problem is called the *inverse problem* of radiotherapy planning. It is shown that this is the mirrored version of the problem of reconstructing an image from its projections, such as occurs in computed tomography (CT).

Based on this fact, the methods for image reconstruction known from CT are consistently transferred to the optimization of radiotherapy. By appropriate modifications of the methods, special features characteristic for this new field of application are taken into account. This includes in particular the fact that no negative radiation intensities can be realized and that one is limited to a few fields for practical reasons. It is shown that in most cases seven or nine radiation fields are sufficient and that the use of more fields does not lead to clinically significant improvements.

The main methods of image reconstruction, namely filtered back projection and iterative reconstruction technique, are used alternatively in CT. In the present application, on the other hand, these

methods are used quasi "symbiotically". The filtered back projection, referred to here as *filtered projection* is used to quickly determine a starting value for the modulation profiles. These initial profiles are further optimized by an iterative procedure corresponding to the iterative reconstruction technique. The introduction of *penalty functions* makes it possible for the first time to adequately consider medically indicated constraints.

The iterative optimization procedure is based on an algorithm for three-dimensional dose calculation. Therefore, another focus of this work is the development of such an algorithm for intensity modulated radiation fields. Conventional dose calculation algorithms cannot adequately account for modulations. To verify the newly developed method, a first comparison of the dose calculated with it with measured data is carried out.

The methods presented here allow the direct determination of the irradiation parameters without the trial and error procedure that is common today. In addition, dose distributions can be generated that are hardly feasible even with the most complex conventional irradiation techniques. These are especially those with extended concave areas. Some examples of this type are presented.

VI Appendix

A1 Tables for dose calculation

Depth in cm	1	2	3	4	5	6	7	8	9	10	12	16	20
						Field radius in cm							
0.5	7	14	19	26	32	37	43	48	54	58	67	78	85
1.0	13	25	37	48	58	66	73	78	84	89	98	109	118
2.0	23	45	64	80	91	102	110	116	122	127	139	152	160
3.0	32	61	84	103	118	130	139	147	154	161	172	187	198
4.0	38	71	99	121	137	151	162	170	179	186	197	215	228
5.0	41	76	107	134	152	166	178	189	198	206	218	240	255
6.0	42	80	114	141	160	176	190	201	211	219	234	257	272
7.0	42	81	115	143	164	181	196	209	220	229	246	273	290
8.0	41	80	114	142	165	185	199	214	225	236	254	285	301
9.0	40	78	112	140	164	183	200	216	228	240	260	292	312
10.0	38	75	109	136	161	181	199	215	229	242	262	295	318
11.0	36	71	104	132	157	178	197	213	227	241	262	296	322
12.0	35	69	99	128	153	174	194	210	225	239	261	297	324
13.0	34	66	95	124	149	170	190	207	223	237	260	298	325
14.0	32	63	92	120	145	168	186	204	220	235	258	297	326
15.0	31	60	89	116	140	162	182	200	216	231	255	295	325
16.0	30	58	86	112	136	157	177	196	212	227	252	292	322
17.0	29	56	83	108	132	153	172	191	207	223	248	288	318
18.0	27	54	80	104	128	148	167	186	202	218	244	284	313
19.0	26	52	77	101	124	144	162	181	197	213	239	280	309
20.0	24	49	74	97	119	139	157	176	192	207	234	275	305
22.0	22	44	67	88	109	128	146	163	180	194	222	264	295
24.0	20	40	60	80	99	118	136	152	168	182	208	252	281
26.0	18	36	54	73	91	108	125	142	156	170	196	236	266
28.0	16	32	49	67	83	98	115	132	156	159	184	222	251
30.0	15	30	45	61	76	89	105	121	134	146	170	208	236

Tab. *1 Scatter–to-air ratios for ^{60}Co (values inflated by a factor of 1000).* Source: Johns and Cunningham 1983.

Depth in cm	4	6	10	15	20	25	30	35
				Side length of the field in cm				
3.0	0	0	0	0	0	0	0	0
4.0	20	20	20	20	20	20	20	20
5.0	35	40	40	40	40	40	40	40
6.0	35	45	50	50	50	50	50	50
8.0	40	50	60	65	70	70	70	75
10.0	40	50	65	70	80	85	85	90
15.0	35	50	75	90	100	110	120	130
20.0	35	50	75	95	105	115	125	135
25.0	35	50	75	95	110	120	130	140
30.0	30	45	70	90	105	120	130	135

Tab. *2 Scatter-maximum ratios for 15 MV bremsstrahlung (values inflated by a factor of 1000). Source: Paul et al. 1983.*

Depth in cm	Field radius in cm									
	1		2		4		7		10	
1	1.030	1.030	1.032	1.033	1.036	1.037	1.042	1.044	1.047	1.050
2	1.001	1.002	1.005	1.006	1.012	1.014	1.024	1.026	1.035	1.038
3	0.964	0.964	0.969	0.970	0.980	0.982	0.997	0.999	1.013	1.016
4	0.922	0.922	0.929	0.929	0.943	0.944	0.964	0.965	0.985	0.987
5	0.877	0.878	0.885	0.886	0.902	0.903	0.927	0.928	0.953	0.953
6	0.832	0.832	0.841	0.841	0.860	0.860	0.889	0.889	0.919	0.917
7	0.787	0.787	0.797	0.797	0.818	0.818	0.850	0.849	0.884	0.879
8	0.742	0.742	0.753	0.753	0.776	0.776	0.811	0.809	0.848	0.842
9	0.700	0.700	0.711	0.711	0.735	0.734	0.773	0.769	0.813	0.804
10	0.659	0.659	0.671	0.671	0.696	0.695	0.736	0.731	0.778	0.767
11	0.619	0.619	0.632	0.632	0.658	0.657	0.700	0.694	0.744	0.731
12	0.582	0.582	0.595	0.595	0.622	0.620	0.665	0.658	0.711	0.697
13	0.547	0.547	0.560	0.560	0.588	0.586	0.632	0.624	0.679	0.663
14	0.514	0.514	0.527	0.527	0.555	0.553	0.600	0.592	0.649	0.631
15	0.482	0.482	0.496	0.495	0.524	0.521	0.570	0.560	0.619	0.600
16	0.453	0.453	0.466	0.466	0.495	0.492	0.541	0.531	0.591	0.570
17	0.425	0.425	0.439	0.438	0.467	0.464	0.513	0.503	0.564	0.541
18	0.399	0.399	0.412	0.411	0.441	0.437	0.487	0.476	0.538	0.514
19	0.374	0.374	0.388	0.387	0.416	0.412	0.462	0.450	0.513	0.488
20	0.351	0.351	0.364	0.363	0.392	0.389	0.438	0.426	0.490	0.464
21	0.329	0.329	0.343	0.342	0.370	0.366	0.416	0.403	0.467	0.440
22	0.309	0.309	0.322	0.321	0.349	0.345	0.395	0.381	0.446	0.418
23	0.290	0.290	0.303	0.302	0.330	0.325	0.374	0.361	0.425	0.396
24	0.272	0.272	0.284	0.283	0.311	0.307	0.355	0.341	0.406	0.376
25	0.255	0.255	0.267	0.266	0.293	0.289	0.337	0.323	0.387	0.357

Tab. 3 *Comparison of g-values for ^{60} Co radiation according to the Schoknecht formula (II/3.4) (left column in each case) and the approximation formula (II/3.7) (right column).*

Depth in cm	Field radius in cm									
	1		2		4		7		10	
1	0.729	0.729	0.730	0.730	0.731	0.732	0.734	0.735	0.736	0.738
2	0.824	0.825	0.826	0.827	0.829	0.830	0.834	0.836	0.839	0.842
3	0.856	0.856	0.858	0.859	0.863	0.864	0.871	0.872	0.879	0.880
4	0.857	0.857	0.860	0.860	0.867	0.867	0.878	0.878	0.888	0.889
5	0.844	0.844	0.848	0.848	0.856	0.856	0.869	0.869	0.882	0.882
6	0.824	0.824	0.829	0.829	0.839	0.839	0.854	0.854	0.870	0.869
7	0.802	0.802	0.808	0.808	0.819	0.819	0.836	0.836	0.854	0.852
8	0.779	0.779	0.785	0.785	0.798	0.798	0.817	0.816	0.837	0.835
9	0.756	0.756	0.763	0.763	0.777	0.776	0.798	0.796	0.820	0.817
10	0.733	0.733	0.740	0.740	0.755	0.755	0.778	0.777	0.802	0.798
11	0.711	0.711	0.719	0.719	0.735	0.734	0.759	0.757	0.785	0.780
12	0.689	0.689	0.698	0.697	0.715	0.714	0.741	0.738	0.768	0.7 63
13	0.668	0.668	0.677	0.677	0.695	0.694	0.722	0.720	0.751	0.745
14	0.648	0.648	0.657	0.657	0.676	0.675	0.705	0.702	0.735	0.728
15	0.628	0.628	0.638	0.637	0.657	0.656	0.687	0.684	0.719	0.712
16	0.609	0.609	0.619	0.618	0.639	0.638	0.670	0.666	0.703	0.695
17	0.590	0.590	0.600	0.600	0.621	0.620	0.654	0.649	0.688	0.679
18	0.572	0.572	0.583	0.582	0.604	0.603	0.638	0.633	0.673	0.663
19	0.555	0.555	0.566	0.565	0.587	0.586	0.622	0.617	0.658	0.648
20	0.538	0.538	0.549	0.548	0.571	0.569	0.607	0.601	0.644	0.633
21	0.522	0.521	0.533	0.532	0.555	0.554	0.592	0.586	0.630	0.618
22	0.506	0.505	0.517	0.516	0.540	0.538	0.577	0.571	0.616	0.603
23	0.490	0.490	0.502	0.501	0.525	0.523	0.563	0.556	0.603	0.589
24	0.475	0.475	0.487	0.486	0.511	0.508	0.549	0.542	0.590	0.575
25	0.461	0.461	0.472	0.472	0.497	0.494	0.535	0.528	0.577	0.562

Tab. 4 *Corresponding values for 15 MV bremsstrahlung*

VII Literature

Airds, E.G.A. (1989):
Radiotherapy Today and Tomorrow – An Introduction to Optimisation of Conformai Radiotherapy,
Phys. Med. Biol., **34,** 1345-1348.

Bahr, G.K., Kereiakes, J.G., Horwitz, H., Finney, R., Galvin, J., Goode, K. (1968):
The Method of Linear Programming Applied to Radiation Treatment Planning,
Radiology, **91,** 686-693.

Barth, N.H. (1990):
An Inverse Problem in Radiation Therapy,
Int. J. Radiat. Oncol. Biol. Phys., **18,** 425-431.

Becker, G., Lohrum, R., Werner, T., Bürkelbach, J., Nemeth, G., Boesecke, R., Schlegel, W., Lorenz, W.J. (1989):
Presentation and Evaluation of 3D Dose Distributions in Radiotherapy Planning,
CAR 89, Proceedings of the International Symposium, 254-261.

Becker, G. (1990):
persönliche Mitteilung.

Bertsekas, D. und Tsitsiklis, J. (1989):
Parallel and Distributed Processing – Numerical Methods,
Prentice-Hall Int., USA.

Blum, E. and Oettli, W. (1975):
Mathematical optimization,
Springer-Verlag, Berlin-Heidelberg-New York.

Bortfeld, T., Boesecke, R., Schlegel, W., Bohsung, J., (1990):
3-D Dose Calculation Using 2-D Convolutions and Ray – Tracing Methods, in: Proceedings of the 10th International Conference on the Use of Computers in Radiation Therapy (ICCR), im Druck.

Bortfeld, T., Bürkelbach, J., Boesecke, R., Schlegel, W. (1990a): Methods of Image Reconstruction from Projections Applied to Conformation Radiotherapy,
Phys. Med. Biol., im Druck.

Boyer, A. und Mok, E. (1985):
A Photon Dose Distribution Model Employing Convolution Calculations.
Med. Phys., **12,** 169-177.

Bracewell, R.N. und Riddle, A.C. (1967):
Inversion of Fan-Beam Scans in Radio Astronomy,
Astrophys. J., 150, 427-434.

Brahme, A. (1987):
Design Principles and Clinical Possibilities with a new Generation of Radiation Therapy Equipment,
Acta Oncologica, **26,** 403-411.

Brahme, A. (1988):
Optimization of Stationary and Moving Beam Radiation Therapy Techniques,
Radiotherapy and Oncology, **12,** 129-140.

Brigham, E.O. (1987):
FFT - Fast Fourier Transformation,
Oldenbourg Verlag, Munich.

Brooks, R.A. und Di Chiro, G. (1976):
Principles of Computer Assisted Tomography (CAT) in Radiographic and Radioisotopic Imaging,
Phys. Med. Biol., **21,** 689-732.

Bürkelbach, J. (1990):
Optimization of dose distribution in percutaneous radiotherapy by modulation of the radiation field,
Dissertation, University of Heidelberg.

Bürkelbach, J., Bortfeld, T., Becker, G., Boesecke, R. Schlegel, W., Lorenz, W.J. (1990a):
Optimization of Radiation Dose Distributions by Modulated Irradiation Fields, in: Proceedings of the 10th International Conference on the Use of Computers in Radiation Therapy (ICCR), in print.

Chesler, D.A. und Riederer, S.J. (1975):
Ripple Suppression During Reconstruction in Transverse Tomography,
Phys. Med. Biol., **20,** 632-636.

Chin, L.M., Kijewski, P.K., Svensson, G.K., Chaffey, J.T., Levene, M.B., Bjärngard, B.E. (1981):
A Computer-Controlled Radiation Therapy Machine for Pelvic and Para-aortic Nodal Areas,
Int. J. Radiation Oncology Biol. Phys., **7,** 61-70.

Clarkson, J.R. (1941):
A Note on Depth Doses in Fields of Irregular Shape,
Br. J. Radiol., **14,** 265.

Cormack, A. (1987):
A Problem in Rotation Therapy with X-Rays,
Int. J. Radiat. Oncol. Biol. Phys., **13,** 623-630.

Cunningham, J.R. (1972):
Scatter-Air Ratios,
Phys. Med. Biol., **17,** 42-51.

Cunningham, J.R., Shrivastava, P.N., Wilkinson, J.M. (1972a):
Program IRREG – Calculation of Dose from Irregularly Shaped Radiation Beams,
Comput. Progr. Biomed., **2,** 192-199.

Dinter, W. (1990):
personal communication.

Düchting, W., Lehrig, G., Rademacher, G., Ulmer, W. (1989):
Computer Simulation of Clinical Irradiation Schemes Applied to In Vitro Tumor Spheroids,
Strahlenther. Onkol., **165,** 873-878.

Ende, G. (1990):
Transfer of anatomical structures between three-dimensional medical images,
Diploma thesis, University of Heidelberg.

Evans, R.D. (1955):
The Atomic Nucleus,
McGraw-Hill, USA.

Goitein, M. (1990):
The Inverse Problem,
Int. J. Radiat. Oncol. Biol. Phys., **18,** 489-491.

Holthusen, H. (1936):
Experiences on the tolerance limit for X-rays and their useful application for the prevention of damage,
Strahlentherapie [Radiotherapy], **57,** 254-269.

Hope, C.S., Laurie, J., Orr, J.S., Hainan, K.E. (1967):
Optimization of X-Ray Treatment Planning by Computer Judgement,
Phys. Med. Biol., **12,** 531-542.

Hope, C.S. und Cain, O. (1972):
A Computer Program for Optimised Stationary Beam Treatment Planning Using Score Functions,
Comput. Progr. Biomed., **2,** 221-231.

ICRU Report 24 (1976):
Determination of Absorbed! Dose in a Patient Irradiated by Beams of X or Gamma Rays in Radiotherapy Procedures,
International Commission on Radiation Units and Measurements, Washington, D.C., USA.

ICRU Report 33 (1980):
Radiation Quantifies and Units,
International Commission on Radiation Units and Measurements, Washington, D.C., USA.

ICRU Report 42 (1987):
Use of Computers in External Beam Radiotherapy – Procedures with High-Energy Photons and Electrons,
International Commission on Radiation Units and Measurements, Bethesda, Maryland, USA.

Iglesias, J.R., Esparza, J., Tönnsen, K., Aruffo, C., Brinnel, Ch., Maier-Hauff, K. (1989):
Computer Assisted Diagnosis of Brain Tumours in CT-Scan Imaging,
CAR 89, Proceedings of the International Symposium, 423-429.

Jähne, B. (1989):
Digitale Bildverarbeitung,
Springer-Verlag, Berlin-Heidelberg.

Johns, H.E. und Cunningham, J.R. (1983):
The Physics of Radiology,
Charles C. Thomas, Illinois, USA.

Kooy, M.H. und Barth, N.H. (1990):
The Verification of an Inverse Problem in Radiation Therapy,
Int. J. Radiation Oncology Biol. Phys., **18,** 433-439.

Künzi, H.P. and Oettli, W. (1969):
Nonlinear optimization - recent methods and bibliography,
Springer-Verlag, Berlin-Heidelberg-New York.

Legras, J., Legras, B., Lambert, J.P., Aletti, P. (1986):
The Use of a Microcomputer for Non-Linear Optimisation of Doses in External Radiotherapy,
Phys. Med. Biol., **31,** 1353-1359.

Lind, B.K. und Källman, P. (1990):
Experimental Verification of an Algorithm for Inverse Radiation Therapy Planning,
Radiotherapy and Oncology, **17,** 359-368.

Lohrum, R. (1989):
Computer-aided assessment of three-dimensional radiotherapy plans, Dissertation, University of Heidelberg.

Lyman, J.T. (1989):
Complication Probability as Assessed from Dose-Volume Histograms,
Radiation Research, **104,** 13-19.

Mackie, T.R., Scrimger, J.W., Battista, J.J. (1985):
A Convolution Method of Calculating Dose for 15-MV X Ray,
Med. Phys. **12,** 188-196.

McDonald, S.C. und Rubin, P. (1977):
Optimization of External Beam Radiation Therapy,
Int. J. Radiat. Oncol. Biol. Phys., 2, 307-317.

Mohan, R. und Chui, C. (1987):
Use of Fast Fourier Transforms in Calculating Dose Distributions for Irregularly Shaped
Fields for Three-Dimensional Treatment Planning,
Med. Phys., **14,** 70-77.

Morita, K., Kimura, C., Takahashi, K., Ueda, T. (1974):
Improving dose distribution in conformational irradiation of collum carcinoma,
Strahlentherapie, **147,** 487-497.

Nemeth, G. und Schlegel, W. (1987):
Radiation Therapy of Intrathoracic Paraaortic Lymph Node Metastases,
Acta Oncologica, **26,** 203-206.

Pastyr, O., Schlegel, W., Boesecke, R., Alandt, K., Meenenga, D.,
Maier-Borst, W., Lorenz, W.J. (1987):
A computer controlled lamella collimator for conformational radiotherapy,
in: Medical Physics 1987 (ed. H. Bergmann), 665-669.

Pastyr, O. (1989):
Stereotactically Guided Convergent Beam Irradiation with a Linear Accelerator: Localization-
Technique,
Acta Neurochir. **99,** 61-64.

Paul, J.M., Koch, R.F., Khan, F.R., Devi, B.S. (1983):
Characteristics of Mevatron 77 15-MV Photon Beam,
Med. Phys., **10,** 237-242.

Quast, U. und Krause, K. (1978):
New Individual Tissue Compensators for High-Energetic Photons,
Strahlentherapie, **154,** 333-341.

Raeside, D.E. (1976):
Monte Carlo Principles and Applications,
Phys. Med. Biol., **21,** 181-197.

Redpath, A.T., Vickery, B.L., Wright, D.H. (1976):
A New Technique for Radiotherapy Planning using Quadratic Programming, Phys. Med.
Biol., **21,** 781-791.

Rosenfeld, A. und Kak, A. (1982):
Digital Picture Processing, 2nd. ed.,
London: Academic Press.

Rossmann, K. (1955):
The tangential pendulum irradiation as a special method of motion irradiation,
Fortschr. Röntgenstr., **82,** 625-637.

Schafer, R.W., Mersereau, R.M., Richards, M.A. (1981):
Constrained Iterative Restoration Algorithms,
in: Proceedings of the IEEE, **69,** 432-450.

Scherer, E. (ed.) (1987):
Strahlentherapie, 3rd Edition,
Springer-Verlag Berlin-Heidelberg.

Schlegel, W., Scharfenberg, H., Bader, R., Hartmann, G., Schnabel, K., Lorenz, W.J. (1981):
Computer Algorithms for Calculation of Isodose Distributions from CT Matrices,
in: Computerized Tomographic Scanners in Europe, British Journal of Radiology. Supplement 15, 118-121.

Schlegel, W., Scharfenberg, H., Doll, J., Hartmann, G.H., Sturm, V., Lorenz, W.J. (1984):
Three Dimensional Dose Planning Using Tomographic Data,
in: Proceedings of the Eighth International Conference on the Use of Computers in Radiation Therapy, Toronto Canada, IEEE Computer Society Press, 191.

Schoknecht, G. (1968):
The description of radiation fields by separating primary and scattered radiation,
Strahlentherapie, **136,** 24-32.

Siddon, R.L. (1981):
Solution to Treatment Planning Problems Using Coordinate Transforms,
Med. Phys., **8**, 766-774.

Spencer, L.V. und Fano, V. (1951):
Penetration and Diffusion of X-Rays. Calculation of Spatial Distributions by Polynomial Expansion,
Phys. Rev., **81**, 464.

Starkschall, G. (1984):
A Constrained Least-Squares Optimization Method for External Beam Radiation Therapy Treatment Planning,
Med. Phys., **11**, 659-665.

Takahashi, K., Purdy, J.A., Liu, Y. (1983):
Treatment Planning System for Conformation Radiotherapy,
Radiology, **147,** 567-573.

Takahashi, S., Kitabatake, T., Morita, K. et al. (1961):
Conformation Radiotherapy Applied to Cancer of Uterus,
Nippon Acta Radiol., **20,** 2746-2753.

Takai, M., Nishimura, T., Kaneko, M. (1987):
Optimization of the Conformation Radiotherapy,
in: The Use of Computers in Radiation Therapy, I.A.D. Bruinvis et al. (Editors), Elsevier Science Publishers B.V. (North-Holland), 231-234.

Treuer, H., Boesecke, R., Hartmann, G.H., Schlegel, W., Lorenz, W.J. (1987):
Dosimetric determination of the primary fluence and the focal size of a 15-MeV linear accelerator,
in: Medical Physics 1987 (ed. H. Bergmann), 375-380.

Webb, S. (1989):
Optimisation of Conformai Radiotherapy Dose Distributions by Simulated Annealing,
Phys. Med. Biol., **34,** 1349-1369.

Webb, S. (1990):
Inverse Tomograph,
Nature, **344,** 284.

Webb, S. und Fox, R.A. (1980):
Verification by Monte Carlo Methods of a Power Law Tissue-Air Ratio Algorithm for Inhomogeneity Corrections in Photon Beam Dose Calculations, Phys. Med. Biol., **25,** 225-240.

zum Winkel, K. (ed.) (1987):
Enhancing the efficacy of radiotherapy of malignant tumors,
Springer-Verlag, Berlin-Heidelberg.

Wolf, M., Ziegengeist, S., Bornholdt, F., Michalik, S., Michalik, M. (1989):
Classification of Brain Tumours by CT-Image Walsh Spectra,
CAR 89, Proceedings of the International Symposium, 86.

Youla, D.C. und Webb, H. (1982):
Image Restoration by the Method of Convex Projections,
IEEE Trans. Med. Imaging, **1**, 81-94.

Curriculum vitae

Name	Thomas Bortfeld
Date of birth	03/15/ 1962
Place of birth	Hannover
Nationality	German
Marital status	single
Parents	Monika Bortfeld, née Stute
	Prof. Dr. Reinhard Bortfeld, Geophysicist

Education

1968 – 1972	Primary school Peter-Petersen-School Hanover
1972 – 1981	Gymnasium Tellkampfschule Hannover [German college preparatory secondary school]
05/22/ 1981	Abitur [German school-leaving examination]
07/01/ 1981 – 09/30/ 1982	Basic military service in Stade and Munster

Study

WS 1982/83 – SS 1983	Study of physics in Hannover
WS 1983/84 – WS 1984/85	Studied geophysics in Kiel, graduated: Intermediate diploma
SS 1985 – SS 1988	Study of physics in Heidelberg
11/01/ 1986 – 01/31/ 1988	Diploma thesis at the Institute for Applied Physics I of the University of Heidelberg
01/07/ 1988	Physics degree

Graduation

since 11/01/ 1988	Doctoral thesis at the Institute for Applied Physics at the University of Heidelberg
since 03/01/ 1989	research assistant at the Institute of Radiology and Pathophysiology of the German Cancer Research Center Heidelberg

TRANSPERFECT

SUBMISSION ID:	2488240
DATE OF TRANSLATION:	15-Apr-2021
ELECTRONIC FILE NAME:	Bortfeld thesis.pdf
SOURCE LANGUAGE:	German (Germany)
TARGET LANGUAGE:	English (United States)
TRANSPERFECT JOB ID:	US0944113

TransPerfect is globally certified under the standards ISO 9001:2015, ISO 17100:2015, and ISO 18587:2017. This Translation Certificate confirms the included documents have been completed in conformance with the Quality Management System documented in its ISO process maps and are, to the best knowledge and belief of all TransPerfect employees engaged on the project, full and accurate translations of the source material.

TRANSPERFECT TRANSLATIONS INTERNATIONAL, INC.
TRANSPERFECT GLOBAL HQ
1250 BROADWAY, 7TH FLOOR, NEW YORK, NY 10001

TCert v. 4.0